Development and Applications of *In Vitro*-Microdialysis: A Sampling Platform for Fast Analysis of Non-Electroactive Analytes

A THESIS
SUBMITTED TO THE FACULTY OF
UNIVERSITY OF MINNESOTA
BY

Amy Louise Stading

IN PARTIAL FULFILLMENT OF THE REQUIREMENTS
FOR THE DEGREE OF
DOCTOR OF PHILOSOPHY

Michael T. Bowser, Advisor

April 2016

Acknowledgements

There are so many people and organizations who have helped me on my path towards (and through) graduate school. This thesis is a result of their input, support, and collaboration. I'd like to thank them now, in a mostly chronological fashion.

I first discovered my proclivity for the sciences in an 11th grade introductory chemistry course. I didn't take the advanced class because I was convinced that I would hate and/or be terrible at chemistry. I was wrong. My teacher, Mr. Mostad, helped me to identify my skills in and appreciation for science. His encouragement is what led me to continue studies in chemistry. I would not have found myself sitting in AP chemistry the very next year had it not been for Mr. Mostad's class, and I certainly would not have entered college as a declared chemistry major.

My college years were incredibly formative both in my education and personal life. There are a number of faculty members whose support, encouragement, and extra efforts were essential in my development as a person and as a scientist. Thank you, Dr. McKenna, for your always open door and helping me through several tough spots. Thank you, Dr. White, for your humor, availability, and somehow getting me to pass thermodynamics. Thank you, Dr. Ross, for introducing me to analytical chemistry, a class made all the more interesting by your dry sarcasm and my inability to properly solder anything together.

Though I didn't plan on pursuing graduate studies until my final years of college, I found myself at the University of Minnesota and in the lab of Dr. Michael Bowser. Mike, you've been an exceptional advisor to me. I can't thank you enough for all of the guidance and support you've given me throughout this process. Thank you for believing

in me, for pushing me to do and be my best, and for fostering an incredibly positive, healthy, and enjoyable work environment. Joining your research group was the best decision I could have made upon entering graduate school and I am incredibly thankful for how you have shaped my graduate career. Thank you.

I'd also like to thank the members of the Bowser group (both past and present) who have contributed to my successes and joys as a graduate student: Nic Frost, Thane Taylor, Matt Geiger, Megan Weisenberger, Anne Mohns, Renee Cline, Alex Johnson, Rachel Harstad, Sarah Anciaux, Kailey Soller, and Sean Dembowski. I enjoyed working with each of you. Thank you for maintaining a fun and productive work space.

With regards to the production of this work, there are several groups at the University of Minnesota who deserve acknowledgement for their assistance and support. Thank you to the labs of Dr. Edgar Arriaga and Dr. Christy Haynes for your assistance and collaboration on some of the cell work. Thank you to the University Imaging Center for providing the equipment and expertise used to produce the 3D composite fluorescent images in this work.

On a more personal note, there are a number of people who have played a significant role in my development and happiness as a person: Jess, Mikaela, Alyse, Laura, J-Fer, Ryan, Pam & Glenn, Jenny & Doug, Leesa, Christy, and Karla. Thank you for the unique joys, insights, and support each of you have brought to my life. To my parents: Thank you for instilling in me a curiosity of our world and for always supporting my education. It's looking like the childhood lessons of straw-pipetting in restaurants have finally paid off...

Lastly, the dearest of these: my husband, Jason. It astounds me that you came into my life only 3.5 years ago. I'm not sure where I'd be without your boundless love and support. Sharing my life with you is such an honor and a joy. Thank you for always making me laugh (even when I take a ceiling shot), for your adventurous spirit, your listening ear, and for talking with me about this thesis for SO many hours. You're my best friend and I love you entirely.

Dedicated to my husband, Jason, for his support, humor, and unconditional love.

~

And to our baby on the way,
whose kicks have kept me both
entertained and highly motivated.
I can't wait to meet you in a few weeks.

Abstract

When considering the measurement of release events from cells, it can be done at levels as small as the single cell and performed in systems increasingly larger and more complex up to *in vivo* studies. Though *in vitro* systems lack the physiological relevance of *in vivo*, their simple and controlled environment is highly advantageous in preliminary mechanistic studies. In spite of this, there exists a serious gap in our ability to perform *in vitro* measurements on a wide array of analytes within a meaningful time frame. While electrochemical techniques are unparalleled in their ability to temporally resolve minute signals in biological systems, there is only a small class of targets which are suitable for this type of analysis. When analyzing non-electroactive analytes, measurements are often plagued by slow temporal responses (5+ minutes). Fluorescent imaging offers opportunities to monitor faster dynamics of non-electroactive analytes, but the target analyte must be either natively fluorescent or labeled, which can result in nonspecific binding and cytotoxicity. In both of these cases fast dynamics can be observed, but the array of analytes is small and only a few can be monitored simultaneously.

In this work, a novel *in vitro* sampling platform is described which is capable of simultaneously monitoring approximately 15 non-electroactive analytes with 20 second temporal resolution. Cells were cultured on the surface of a microdialysis probe coupled with an analytical system for analysis. Small molecules released from the cells upon stimulation diffuse across the porous membrane because of the close proximity. A high-speed CE, built in house, enabled analysis of the collected dialysate. The ability of our platform to detect basal and stimulated release of amines was confirmed by transferring the probe between artificial cerebrospinal fluid (aCSF) and a potassium-spiked (100 mM

K^+-aCSF) stimulant solution. A variety of cell models were tested for compatibility with the *in vitro*-microdialysis platform, both single cell type and co-cultures were initiated. Adherence of viable cells was confirmed by labeling cells with either fluorescein diacetate (FDA) or specific antibody labelling, followed by imaging under a microscope. As a step towards continuously monitoring the change of non-electroactive analytes released from cultured cells, microdialysis was coupled directly to micro free flow electrophoresis (μFFE) device instead of the high-speed CE instrument.

Table of Contents

List of Figures

List of Tables

List of Abbreviations

µFFE	Micro Free Flow Electrophoresis
µFFIEF	Micro Free Flow Isoelectric Focusing
µFFZE	Micro Free Flow Zone Electrophoresis
aCSF	Artificial Cerebrospinal Fluid
ADME	Adsorption, distribution, metabolism, and excretion
ASM	Airway Smooth Muscle
ATCC	American Type Culture Collection
BME	Basal Medium Eagle
BSA	Bovine Serum Albumin
Ca^{+}	Calcium
CAPS	N-Cyclohexyl-3-Aminopropanesulfonic Acid
CCD	Charge Coupled Device
CE	Capillary Electrophoresis
CNS	Central Nervous System
CZE	Capillary Zone Electrophoresis
DAAO	D-Amino Acid Oxidase
DAPI	4’,6-Diamidino-2-Phenylindole
DI	Deionized
DMEM	Dulbecco’s Modified Eagle Medium
DSU	Disk Scanning Unit
EDTA	Ethylenediaminetetraacetate
FBS	Fetal Bovine Serum
FDA	Fluorescein Diacetate
FFE	Free Flow Electrophoresis

FITC	Fluorescein Isothiocyanate
FMOC	Fluorenylmethyloxycarbonyl
GFAP	Glial Fibrillary Acidic Protein
GFP	Green Fluorescent Protein
HEPES	4-(2-Hydroxyethyl)-1-Piperazineethanesulfonic Acid
HP-β-CD	Hydroxypropyl-β-cyclodextrin
HPLC	High Performance Liquid Chromatography
HRP	Horse Radish Peroxidase
IEF	Isoelectric Focusing
IgE	Immunoglobulin E
K^+	Potassium
LC	Liquid Chromatography
LIF	Laser Induced Fluorescence
LOD	Limit of Detection
MS	Mass Spectrometry
MWCO	Molecular Weight Cutoff
NBD-F	7-Fluoro-4-Nitrobenzo-2-Oxa-1,3-Diazole
NDA	2,3-Naphthalenedicarboxaldehyde
OPA	O-Phthalaldehyde
PBS	Phosphate-Buffered Saline
PMT	Photomultiplier Tube
PTFE	Polytetrafluoroethylene
RFU	Relative Fluorescence Units
SEC	Size Exclusion Chromatography
T25	Tissue Culture Flasks sized 25 cm^2

TRIS	2-Amino-2-hydroxymethyl-propane-1,3-diol
VRAC	Volume Regulated Anion Channels

Chapter 1

Introduction

1.1 Introduction to Microdialysis Sampling

1.1.1 Traditional Applications

Microdialysis is one of the most commonly employed sampling techniques for *in vivo* analysis, and has been used to sample chemicals in the brain for several decades. A Web of Science search indicated that nearly 600 articles were published in 2014 alone with microdialysis in the title, keyword, or abstract. Although microdialysis has found widespread application, it is particularly useful in the neurosciences for monitoring chemical changes in the brain and has been applied in studies ranging from but not limited to pharmacology[1, 2], pharmacokinetics of absorption, distribution, metabolism, excretion (ADME)[3-5], toxicology[6, 7], and drug delivery[8-10].

Traditionally, microdialysis samples are collected by fractions and followed by offline analysis, giving rise to temporal resolutions on the order of 10-30 minutes. Temporal resolution can be dramatically improved by coupling probes directly with an online analytical separation.[11] The improved temporal resolution of online analysis is necessary to monitor chemical events which occur on fast time scales.[12] When microdialysis is coupled directly to an analytical separation, the temporal resolution is primarily determined by the analysis time, sample volume requirements, and detection limits of the instrument as well as lateral diffusion through system tubing. The small sample volume requirement and fast analysis times of capillary electrophoresis (CE) make it an ideal analytical separation for online analysis with microdialysis sampling. Coupling microdialysis with CE has achieved sampling rates as fast as 5-10 seconds and temporal resolutions on the order of 10-30 seconds.[13, 14] The ability to monitor such a diverse field of analytes at these time scales is unparalleled and has allowed

neuroscientists to monitor chemical changes in the brain caused by both pharmacological and sensory inputs, gaining new insights into brain function.[15]

Despite the success of microdialysis for *in vivo* analysis it has rarely been adopted for *in vitro* sampling. When employed *in vitro,* microdialysis is often used merely to calibrate *in vivo* results, not to make unique biological measurements. There have been previous reports of *in vitro* microdialysis methods which describe either insertion of probes into a fluid containing cell suspensions[16] or into a small volume chamber containing tissue slices[17-19]. In both cases, dilution of the analytes into the bulk fluid resulted in relatively long sampling times with temporal resolutions ranging from 10-20 minutes.[16, 17, 20]

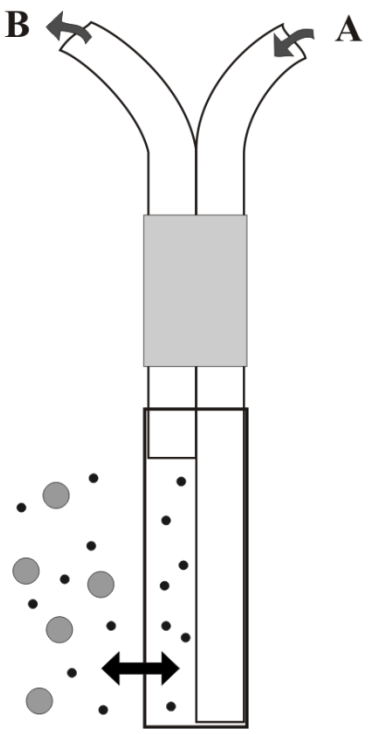

Figure 1.1. Schematic of a microdialysis probe. Perfusate flows through the inlet capillary (A) into the dialysis tubing. Analytes diffuse across membrane and exits the probe through the outlet capillary (B) as a continuous stream of dialysate.

1.1.2 Design and Function

A microdialysis probe (Figure 1.1) is comprised of three basic components: an inlet capillary, an outlet capillary, and a piece of hollow fiber dialysis tubing. The dialysis tubing is porous and acts as a membrane across which small molecules can diffuse. Tubing with different molecular weight cutoff (MWCO) values can be selected based on the application. Fluid, referred to as the perfusate, is pushed through the inlet capillary into the dialysis tubing. Small molecules diffuse across a defined area of the membrane known as the sampling region. The flow of perfusate drives solution to exit

the probe membrane through the outlet capillary. This outlet stream, which now contains analyte, is referred to as dialysate. Small molecule analytes diffuse across the membrane according to a concentration gradient. Continuous recovery and/or delivery of small molecules is possible without removal of fluid from the extracellular space. This unique property enables microdialysis to continuously monitor chemical dynamics in nearly any tissue, organ, or biological matrix.[21]

1.1.3 Recovery, Resolution, and Limitations

The suitability of microdialysis for nearly any aqueous sample has led to its widespread use in the field. However, the inability to achieve absolute quantification of analytes has continued to be a fundamental limitation of the technique. Microdialysis probes are typically perfused at flow rates between 0.1-1 μL/min. At these rates, equilibrium is not established across the membrane and the concentration of the collected analyte ends up being some fraction of the actual concentration in the surrounding extracellular matrix.[11] Thus, careful distinction must be made with respect to what the measured signal actually represents.

Assuming the concentration of analyte outside the probe lumen is proportional to the concentration in the dialysate, the external concentration can be determined based on the recovery for a particular set of experimental parameters. This recovery may be used as absolute recovery, defined as the total amount of analyte that enters the perfusion medium per unit time, or as relative recovery, defined as the concentration of analyte in the perfusion medium relative to the extracellular concentration.[22] These recoveries are particularly sensitive to the flow rate of the perfusion fluid through the microdialysis

probe such that the absolute recovery increases with higher flow rates, while relative recovery decreases. This relationship is depicted in Figure 1.2.[21]

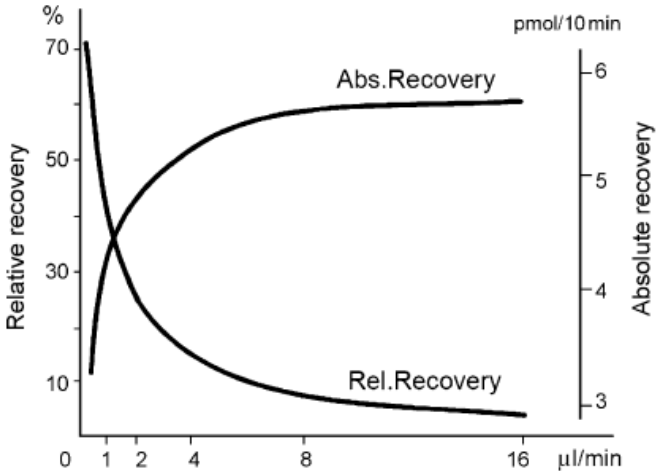

Figure 1.2. Relative and absolute recoveries for a microdialysis probe, plotted as a function of flow rate. Adapted from Reference 21.

Several mathematical expressions have been developed to better explain the dynamics of microdialysis recovery. Though extraction efficiency and relative recovery are often used interchangeably, they present a subtle difference. The extraction efficiency is defined as the ratio between gain of analyte in a dialysate and the loss of analyte from the surrounding matrix:

$$EE = \frac{C_d - C_i}{C_e - C_i} \qquad (1.1)$$

where C_d is the concentration of analyte in the dialysate, C_i is the concentration in the perfusion fluid, C_e is the concentration in the surrounding matrix. When performing microdialysis in the recovery mode, essentially C_i=0, the extraction efficiency becomes identical to the relative recovery. A widely accepted mathematical expression for relative recovery as a function of resistance to solute movement at a steady state was developed by Bungay *et al.*, [23]

$$\mathrm{RR} = \frac{\mathrm{C}_d}{\mathrm{C}_e} = 1 - \exp^{\left(\frac{1}{Q_d(R_d+R_m+R_e)}\right)} \qquad (1.2)$$

where Q_d is the perfusion flow rate, and $R_{d,m,e}$ is the resistance to solute movement in the dialysate, membrane, and tissue/solution, respectively. R_e is dependent on diffusion through the sample matrix to the probe and will become almost negligible *in vitro* due both to a decrease in diffusional barriers and the possibility of increased convective motion by stirring.[24] R_d and R_m are independent of the environment surrounding the probe and depend, rather, on the properties of the probe and dialysate. Variables affecting these parameters include membrane radius, length, and material; diffusion coefficient of analyte across the membrane; diffusion of analyte within the dialysis membrane; flow properties of dialysate through the membrane; and chemical interactions between the analyte and membrane.[24, 25] Under the conditions of our *in vitro*-microdialysis model, these variables will remain essentially unchanged over time and a steady state will be reached. This allows extraction and recovery ratios of microdialysis probes to be measured directly when experiments are carried out in solution.[26-28]

When quantitation of the analyte is desired, the relative recovery of the probe must be determined. For *in vitro* studies, the probe can be calibrated by immersing the membrane in various solutions with known concentrations of analyte and comparing the obtained signal to that resulting from direct introduction of the same concentration of analytes into an analysis system, sans microdialysis.[29-31] However, due to the fact that *in vitro* relative recovery differs significantly from those obtained *in vivo*, this style of calibration is inadequate for the majority of microdialysis studies.[32, 33] Probe recoveries *in vivo* are characteristically lower than those obtained *in vitro*. This is likely due to a

variety of mechanisms regarding the complexity of the tissue and extracellular matrix including an undefined and tortuous path that the analyte travels to reach the probe membrane, as well as the existence of release/uptake mechanisms along the way.[34]

In an attempt to address the difficulties described above, several methods have been developed and employed for *in vivo* probe calibration including variation of perfusion flow rate[33] (also referred to as "zero flow"),[35] no-net-flux,[36] and retrodialysis.[37, 38] The method of no-net-flux relies on altering the concentration gradient between the probe lumen and the extracellular matrix by varying the concentration of the analyte present in the perfusion fluid. A change in the concentration perfusing the membrane will result in a corresponding change in net increase of the concentration of the dialysate.[36] Though this is the most often employed method of *in vivo* probe calibration,[21] it is not always of practical utility due to the extended period of time it takes to reach steady-state conditions.

Despite the many advances in methodology to address the difficulties with quantitation of microdialysis sampling, factors remain which further limit the capabilities of this technique. The most often cited drawbacks to microdialysis sampling are the spatial and temporal resolutions that can be achieved. Spatial resolution is only a serious factor for *in vivo* microdialysis studies when, due to implantation of the probe, damage is done to surrounding tissue.[39] Furthermore, the specificity for which the probe samples from a particular region is limited by the size of the sampling region (1-5 mm). When probes are operated at slightly higher flower rates to accommodate increased absolute recovery (1-10 μL/min), compounds from an area directly around the probe are removed

at a more rapid rate inducing a concentration gradient that can extend for several millimeters away from the probe, further decreasing spatial resolution.[32]

Temporal resolution is a factor for both *in vitro* and *in vivo* studies, as well as for both online and offline coupling of microdialysis to an analytical system. The overall temporal resolution is determined by a number of factors pertaining to both the rate of perfusion through the microdialysis probe and the capabilities of the analytical system. With regards to the analytical system, if analysis can be performed faster than the observed dynamics take to entirely change, it is possible to detect a change in abundance as a function of time. In this case, the temporal resolution corresponds to the time it takes to go from 10-90% of maximum signal intensity; for fast changes, this resolution depends on the rate of diffusion across the membrane.[21] With regards to the microdialysis probe, using a slower perfusion rate increases the efficiency of the probe but results in longer sampling times. Longer sampling times correspond to decreasing temporal resolution. Ultimately, the trade-offs between flow rate of the perfusion fluid, the concentration detection limit and sample volume requirement of the analytical system will most strongly dictate the temporal resolution that can be achieved for the experiment.[11] An additional factor contributing to the temporal resolution of the system is longitudinal diffusion.[40] This can occur within extended pieces of tubing connecting the probe with the analytical system. In a system where there must be additional tubing (to perform online derivatization, for example), the speed at which dialysate is carried through the tubing must be considered. Shorter tubing lengths and faster speeds will both minimize the effect of longitudinal diffusion, so balancing these with the physical requirements of the system is important in enhancing temporal resolution.

1.2 Microdialysis Analysis

1.2.1 Coupling to an Analytical System

An article search demonstrated that upwards of one thousand or more papers employing microdialysis are cited each year, in spite of the limitations described above. This is indicative of the utility of this sampling technique and demonstrates the continuing need to develop methods which improve the capabilities of microdialysis analysis. The most critical factor in analysis of microdialysis samples is coupling the probe to an appropriate analytical system such as CE,[32] LC,[5, 41, 42] MS,[43, 44] biosensors,[45-47] immunoassays,[48] and microchip electrophoresis.[49, 50] Coupling the probe to an appropriate system can be accomplished using either offline fraction collection or online analysis. Performing a separation on an analytical system requires discrete sample injections but microdialysis is a continuous sampling technique. Consequently, an interface must be employed which collects dialysate for a specified period of time to produce a sample plug. Early studies relied on offline methods since effective interface schemes were only beginning to be developed.[51-53]

Jorgenson and Lemmo presented a transverse flow gating interface using steel plates in the early 1990s. Briefly, screws held the steel plates in place with a polytetrafluoroethylene (PTFE) spacer between them, forming a flow channel. Fused silica connection tubing was introduced into the interface and aligned opposite the CE separation capillary by a distance defined by the spacer (typically 50-75μm). Two additional ports allowed electrophoresis buffer to flow through the channel during a separation. Though the interface was originally developed for the coupling of size exclusion chromatography (SEC) with capillary zone electrophoresis (CZE), it

demonstrated the utility of using low microdialysis flow rates (~80nl/min) while retaining sampling times around one minute.[32, 54] Shortly after the development of the steel plate interface, the Kennedy lab employed this design to couple microdialysis and CZE.[32] This early design was successful in coupling microdialysis to high-speed online analysis, but the design suffered from operational difficulties and lack of reproducibility.

In 1997, Jorgenson and Hooker designed a more routine and reproducible interface for micro-HPLC and CZE.[55] This new flow gating model (Figure 1.3) was constructed from a chemically inert, clear, polycarbonate polymer allowing for visualization of the region between the capillaries. Alignment of the capillaries was more routine than with the steel plate design and the interface was relatively easy to machine. The utility of this design for coupling microdialysis with high-speed analytical techniques, particularly CE, was demonstrated by its immediate and widespread application.[11, 14, 56, 57]

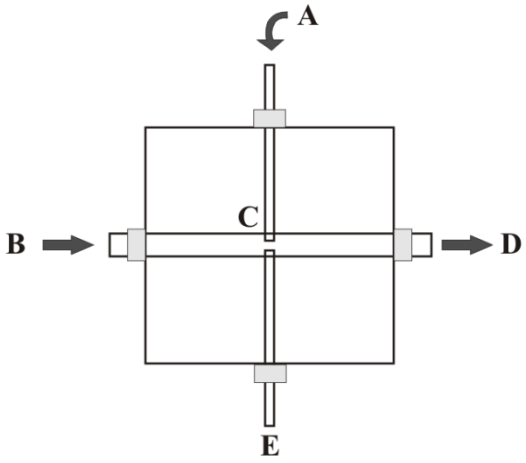

Figure 1.3. Cross-sectional view of polycarbonate flow gate interface. Continuous dialysate flow enters through the reaction capillary (A) which is aligned with the CE separation capillary (E). Buffer flows across the alignment cross (C) from a buffer reservoir (B) into waste (D). When this crossflow is stopped, sample accumulates in the gap space prior to a voltage-controlled injection.

The inception of efficient interfacing schemes for coupling microdialysis sampling to analysis systems brought an increase in studies employing online analysis versus offline fraction collection. Online analysis allows data output to be collected in

near-real time which is highly advantageous when monitoring events which occur on fast time scales.[12] Furthermore, when microdialysis is coupled online to an analytical system, the temporal resolution is primarily determined by the analysis time, sample volume requirements, and detection limits of the instrument. Thus, using high-speed techniques with small sample volume requirements permits sampling rates as fast as 5-10 seconds and temporal resolutions on the order of 10-30 seconds.[13, 14] When offline fraction collection is employed, the temporal resolution becomes dependent on the time required to collect enough volume for analysis. This can be on the order of 5-10 minutes and is considered to be a fundamental limitation to the method.[21] Additionally, the handling of such small sample volumes for offline analysis can be difficult.

Despite the apparent advantages of online coupling over offline fraction collection, there are situations where a specific method is more appropriate. For example, if a technique requiring longer analysis times must be employed, such as LC, the temporal resolution would be limited to the chromatographic analysis time.[58] In this case, an offline approach would be advantageous. Physical constraints to an online method may also contribute to complicated set-ups, unsatisfactory levels of diffusion through system tubing, and/or a temporal resolution better than 20 seconds is needed to see a particular signal. For these reasons, labs have recently began developing methods to segment the dialysate stream into a series of aqueous "plugs" created when mixed with immiscible oil. As the analyte travels from the probe membrane to an offline fraction collector[12] or online analysis system,[59] the effects of zone broadening caused by flow and diffusion of analyte are limited. Improvements of temporal resolutions down to 2 seconds were reported.[59]

The development of flow gated technology has provided a mechanism for converting the continuous stream of dialysate into discrete sample plugs of finite volume and demonstrated the utility of pairing microdialysis with CE. The small sample volume requirement and fast analysis times of CE make it an ideal analytical system for online coupling with microdialysis sampling. Furthermore, probe efficiency can be increased by employing lower flow rates of dialysate which maintain compatibility with CE injection volumes (1-10nL).[11] A further advantage of online analysis is that it allows for online derivatization of analytes, making them amenable to sensitive detection methods such as LIF.[14, 57, 60, 61]

1.2.2 Derivatization and Detection of Analytes

Sampling from a biological matrix using microdialysis inherently results in a small mass recovery of the analyte. Thus, the sensitivity requirements of the detection scheme become extremely important. The limit of detection corresponds to the smallest amount of analyte that produces a signal significantly different than the blank. In practice, this is three times the standard deviation in the baseline. The most sensitive detection limits for CE separations, while maintaining applicability to a wide array of analytes, are achieved using LIF.[62] Most of the analytes analyzed by microdialysis-CE are not natively fluorescent, so they must be derivatized to be made detectable. A fluorescent labeling reagent can be chosen to selectively form a covalent bond with a particular moiety for the analyte(s) of interest. This both reduces possible interferences from unwanted signals and generates a single, fully-tagged class of analytes resulting in

sharper peaks with improved efficiencies, higher plate counts, and lower limits of detection.[63]

The fluorescence labeling reagents o-phthalaldehyde (OPA) and 2,3-naphthalenedicarboxaldehyde (NDA) are particularly well suited for use with a microdialysis-CE assay because they are compatible with the system conditions; both react efficiently within 1 minute, at room temperature, under basic conditions, and in an aqueous environment.[64] Originally, OPA was the most commonly used and most frequently referred to labeling reagent for microdialysis-CE methods.[65] However, derivatization with OPA is prone to instability and photobleaching and has poorer limits of detection than other common reagents.[66] Early work in our lab sought to identify alternative reagents that could replace OPA for detection of neuroamines using microdialysis-CE. 7-Fluoro-4-Nitrobenzo-2-Oxa-1,3-Diazole (NBD-F) was selected as a viable labeling reagent for our analyses because it reacts efficiently with primary and secondary amines, has an optimum excitation wavelength compatible with common 488 nm lasers, and has been previously used in similar assays.[67]

The reaction of NBD-F with the primary amine of an amino acid is depicted in Figure 1.4. Despite the advances made in both ease and efficiency of fluorescent derivatization, it is not without difficulties. For example, a significant drawback to the NBD-F labeling scheme is the formation of large amounts of hydrolysis product. Others have reported significant falls in temporal resolution due to band broadening which occurs during the derivatization process.[14, 28, 60]

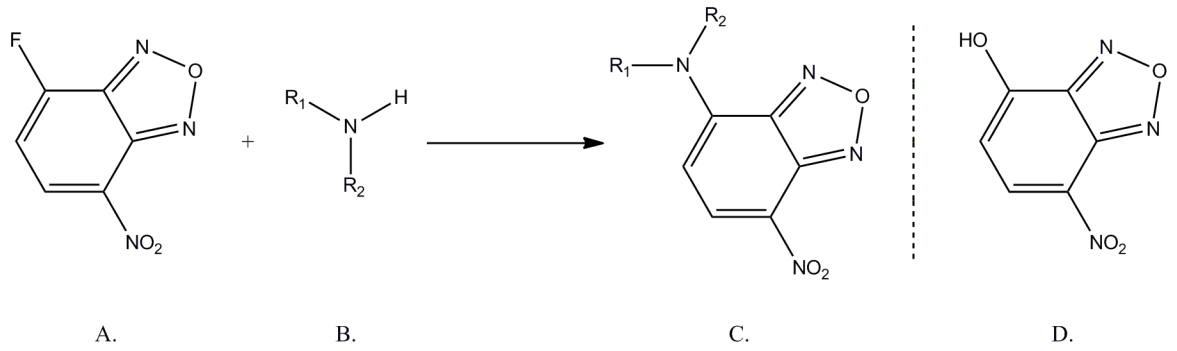

Figure 1.4. The nucleophilic reaction of NBD-F (A) with amines (B). The fluorescent amine derivatives (C) are detectable using our LIF detection scheme with 488 nm excitation. A by-product (D) is produced by hydrolysis of NBD-F.

Derivatization can be accomplished at several positions within the analytical setup and is classified by whether the reaction occurs before (pre-column), during (on-column), or after (post-column) the separation. On-column and post-column derivatization methods are inevitably conducted online.[64] Online derivatization methods are most frequently employed when the analytical system is coupled to microdialysis sampling. The low flow rates used with microdialysis-CE requires a derivatization procedure suitable for small sample volumes, high sensitivity, and short analysis time.[65] Online derivatization occurs by mixing the dialysate stream with the labeling reagent using a reaction cross or T-junction prior to sample injection for CE analysis. The speed with which this derivatization can be executed and its small volume compatibility make it an ideal method with respect to the requirements above.

The detection limits of microdialysis-CE-LIF systems have been further improved using a sheath-flow cuvette. In this setup, off-column detection is achieved as a buffer stream is used to ensheath the analyte upon elution from the capillary.[68] The optical properties of the sheath-flow cause a dramatic decrease in background signal due to a

reduction in the contributions from both scattered excitation light and fluorescence of impurities found in fused silica capillaries. It has been demonstrated that on-column detection results in a 100 fold increase in background when compared to detection with a sheath-flow cuvette.[69]

1.3 Astrocytes

1.3.1 Physiological Model

Astrocytes were originally believed to be support cells in the brain, not involved in brain function, but over the past several decades research has shown that they play a much more significant role. Studies have implicated astrocyte involvement in blood flow regulation,[70] pathogenesis of Alzheimer's disease,[71] maintaining ionic and metabolic stability in CNS,[72] glial-neuronal communication,[73] and synaptic modulation.[74] In light of the conclusive evidence for astrocytic functionality, major debates have ignited within the neuroscience community regarding the interpretation of results, the underlying mechanisms, and the relevance to normal brain activity. Of particular interest is if and how astrocytes engage with neurons by the Ca^{2+}-dependent release of glutamate through exocytosis.

In the early 1990s, it was demonstrated that cultured astrocytes were capable of propagating glutamate-induced waves of Ca^{2+} between adjacent cells, suggesting that astrocytes could be involved in a functionally relevant signaling system in the brain.[75] Shortly thereafter, Parpura *et al.* used several stimuli (bradykinin, micropipettes, photostimulation) to raise the internal Ca^{2+} levels of cultured astrocytes. Upon stimulation, an increase in glutamate release was observed, demonstrating the ability of

astrocytes to release glutamate through a Ca^{2+}-dependent mechanism.[76] Astrocyte-neuron co-cultures were also investigated to determine whether the triggered release of glutamate then communicated with neurons. Increases in the Ca^{2+} levels of adjacent neurons were observed and inhibited by D-glutamylglycine, an antagonist for excitatory amino acid receptors. The authors were the first to conclusively state that astrocytes demonstrated the ability to regulate neuronal Ca^{2+} levels through the Ca^{2+}-dependent release of glutamate.

These pioneering experiments provided the first insights to individual release events in astrocytes and were a turning point in research pertaining to astrocytic functionality, fueling a series of responding studies. It is important to note that early experiments were performed in cell culture and the physiological relevance of the results has long been in question. Often the results obtained *in vitro* did not correspond to what was observed in comparable studies performed *in vivo*. Porter and McCarthy were the first to discover similar signaling phenomena *in situ* when they used immunocytochemistry to demonstrate astrocytic responses to glutamate released from neuronal terminals in tissue slices.[77] The observation of glial-neuronal signaling in non-cultured cells provided a compelling physiological context for previously obtained *in vitro* results. Within the last decade several more studies conducted *in vivo* have indicated direct evidence for astrocytic Ca^{2+}-elevations in response to triggered neuronal activity.[78] The suggestion of Ca^{2+} transients in astrocytes following transmitter release from nearby nerve terminals, and the ability of these fluctuations to trigger the release of glutamate, implies that astrocytes do play an active role in synaptic modulation.[74]

Despite the fact that *in situ* models can produce results which differ significantly from what is observed *in vivo*, astrocytic function has primarily been studied using tissue

slices and cell cultures. Consequently, many findings pertaining to astrocytic function are attacked for physiological irrelevance. One such finding is that astrocytes, which are relatively inactive in an intact brain, display dynamic activity in culture. Similarly, the potentiation of long-range Ca^{2+} waves has been reported in many other cultured cell types. Taken together these results imply that the observed events are more a property of cells in culture than physiologically relevant astrocytes.[79] Though the benefit of using tissue slices as a more physiologically relevant model seems obvious, the validity of these models is also debated. *In situ* models lack the characteristics of intact circuits such as normal synaptic activity, metabolic functionality, and long range modulatory signals.[70]

1.3.2 Techniques Used to Study Astrocytes

Studies pertaining to astrocytic function in the brain have been primarily conducted using fluorescence microscopy,[80-82] electrochemical/physiological techniques,[72, 83-85] and immuno-cytochemistry.[86, 87] The discrepancies detailed above are primarily due to the limitations of these techniques. Though very high spatial and temporal resolutions have been reported for electrochemical methods, the number of molecules which are suitable for analysis is hugely limited. Furthermore, these techniques have been criticized for difficulties in simultaneously monitoring multiple compounds and causing electrical interferences which alter the signal.[88] While imaging techniques afford the ability to monitor analytes simultaneously with high temporal resolution (averaging of collected frames allows visualization at sampling frequencies around 1 Hz), the field of suitable analytes is again limited and spatial resolution is

sacrificed due to light diffraction and optical distortions in the excitation and detection modes.[89]

The gold standard in characterizing uptake/release events of neuroactive molecules in astrocytes requires the introduction of radiolabeled amino acids into cultured cells, stimulating a release event, and detecting the signal released into the bulk culture medium. Typically, fractions of medium are collected and analyzed every 1-10 minutes. Despite claims that these techniques have effectively characterized the mechanisms of release, there are still gaps in understanding the events. The temporal resolution is limited by the frequency of fraction collection, so only gradual increases in released analyte are able to be monitored. Mechanistic information regarding fast release events is lost. Furthermore, the magnitude of the signal is decreased upon dilution into the bulk medium.

Recently, more desirable temporal resolution has been achieved with enzymatic bioassays. For example, the exocytotic release of D-serine was characterized using a D-amino acid oxidase (DAAO) and horseradish peroxidase (HRP)/luminol assay where emitted photons were counted on a 32-ms-interval and detection down to pM concentrations was reported.[90] Though enzymatic assays offer powerful detection on fast timescales, the utility of these methods is limited to a small subset of particular analytes which are proper substrates for the enzyme. Additionally, the reactions are technically difficult and can be easily complicated by coupling reactions.

1.4 Scope of Thesis

When considering a highly dynamic process, such as release events from cells, the speed at which chemical changes can be monitored is of great importance. While fluorescent imaging offers impressive spatiotemporal resolution with high contrast images, the target analyte must be either natively fluorescent or labeled, which can result in nonspecific binding and cytotoxicity.[91] Similarly, electrochemical techniques are unparalleled in their ability to temporally resolve minute signals in biological systems, but there is only a small class of targets which are suitable for this type of analysis.[92] In both of these cases fast dynamics can be observed, but the array of analytes is small and only a few can be monitored simultaneously. In this work, we describe a novel technique, *in vitro*-microdialysis, capable of monitoring fast release events of a wide array of non-electroactive analytes from cultured cells.

Chapter 2 describes the development of our technique, *in vitro*-microdialysis, which when coupled with high-speed CE is capable of resolving a wide array of non-electroactive analytes with a temporal resolution of 20 seconds. This demonstrated a proof of concept for the technique. Chapter 3 discusses further characterization of the developed technique, illustrating if and how the observed signal intensity is dependent on or independent of a variety of parameters. Chapter 4 presents a variety of alternative physiological models to demonstrate the wide-spread applicability of this technique as an *in vitro* sampling platform. Chapter 5 describes progress towards coupling *in vitro*-microdialysis probes to a microfluidic device capable of continuous separations. Chapter 6 gives a summary of the work and presents opportunities for future direction of *in vitro*-microdialysis.

Chapter 2

Monitoring Neurochemical Release from Astrocytes Using *in Vitro*-Microdialysis Coupled with CE

"Hogerton, A.L and M. T. Bowser. *Anal. Chem.* **2013**, *85* (19), 9070–9077."

Reproduced with permission

2.1 Summary

Cell-based assays have long been used to obtain biochemical information while avoiding the inherent complications of *in vivo* systems such as metabolism, transport, uptake/release mechanisms, tortuosity, and interferences. Though many advances to classic *in vitro* methods have been made, analysis is still primarily limited to either fast detection of electrochemically active events or time-delayed measurements of non-electroactive species with poor temporal resolution. Thus, there remains an analytical challenge in monitoring fast dynamics of non-electroactive molecules *in vitro*. We have developed an alternative *in vitro* sampling platform by culturing astrocyte cells directly onto a microdialysis probe coupled with an online high-speed capillary electrophoresis (CE) instrument. This model offers an alternative *in vitro* approach to conventional cell culture, capable of measuring the fast release events of small non-electroactive neurochemicals from astrocyte cells. Immortalized astrocytic cell clones, C8-D1A, were cultured in direct contact with the porous membrane of a microdialysis probe. Small molecules released from the cells upon stimulation diffuse across the porous membrane because of the close proximity. A high-speed CE, built in house, enabled near-real time analysis of the collected dialysate. Dynamic changes in the relative abundance of analytes in response to stimulation were monitored with 20 second temporal resolution. The ability of our platform to detect basal and stimulated release of amines was confirmed by transferring the probe between artificial cerebrospinal fluid (aCSF) and a potassium-spiked (100 mM K^+-aCSF) stimulant solution. Upon stimulation, there are marked and varied increases in the relative abundance of several analytes. Glycine demonstrated the largest percent increase in relative abundance (700%), followed by taurine (185%) and

serine (215%). Amino acids such as phenylalanine, which are not known to have any participation in cellular swelling mechanisms, were unaffected by the stimulation. To the best of our knowledge, release events of non-electroactive compounds in culture have not previously been observed on this time scale.

2.2 Introduction

The traditional approach for measuring release from cells is by making ensemble biochemical measurements from a large cell population and analyzing them with an analytical technique such as high-performance liquid chromatography (HPLC) or CE. Sampling from the bulk medium results in low temporal resolution and an inability to resolve the fast kinetics of cell secretion, detect trace amounts of released molecules, or reveal functions of cell membrane domains.[93] The emergence of micro- and nanotechnologies holds promise in resolving fast cell dynamics, but the current platforms still depend almost exclusively on electrochemical detection. There remains a gap between *in vitro* techniques that are able to make fast measurements but only with a limited set of analytes and techniques that are compatible with a larger range of analytes but are limited to slower time scales. In this work, an alternative *in vitro* sampling method was developed by culturing cells in direct contact with a microdialysis probe. The proximity of cells to the porous dialysis membrane enables diffusion of small molecules released from the cells across the membrane. These analytes, now present in the dialysate fluid, can be analyzed by directly coupling the microdialysis probe to a high-speed CE for fast analysis and sensitive LIF detection.

As a test case, a line of immortalized astrocyte cells were selected for their robustness, adherent properties, well-documented release responses to stimuli, and current interest in the neuroscience community. Astrocytes are the most abundant glial cell in the central nervous system (CNS) and they have been increasingly implicated in involvement with blood flow regulation[70], pathogenesis of Alzheimer's disease[71], maintaining ionic and metabolic stability in CNS[72], glial-neuronal communication[73], and

synaptic modulation[74]. A series of studies in the late 1990s were the foundation for a new model of synaptic function, one in which astrocytes affect activity at the synapse by the calcium-dependent release of small neuroactive molecules known as "gliotransmitters." Over the past twelve years, hundreds of publications have reported on astrocytic influence in synaptic communication, and at present many neuroscience textbooks now include sections on glial-neuronal signaling.[94] Though the idea that astrocytes play an active role in brain function is ubiquitously accepted, there is still plenty of debate and skepticism regarding astrocytic transmitter release.[95, 96] In large part, the inability to reconcile these observations is attributable to a lack of experimental techniques, and further demonstrates the need for an analytical method capable of monitoring fast release dynamics for a wide array of analytes that are non-electroactive.

This work reports the successful development of a novel *in vitro* sampling technique capable of resolving non-electroactive analytes on a sub-minute time scale. Astrocyte cells were cultured on the surface of a microdialysis probe and analyte release was monitored with online high-speed CE. A high-potassium stimulation was administered to depolarize the cells and changes in the relative abundances of nearly a dozen amino acids were observed with 20 second temporal resolution. Imaging was used to confirm that a confluent monolayer of cells was achieved over the sampling region. This platform is well-suited as a model for studying fast dynamics in cell-based systems and offers utility in diagnostic, pharmacological, and drug discovery studies pertaining to neurological and metabolic diseases.

2.3 Materials and Methods

2.3.1 Chemicals and Reagents

Reagents. Dulbecco's modified Eagle medium (DMEM) and fetal bovine serum (FBS) were purchased from Invitrogen Molecular Probes (Eugene, OR). Trypsin solution (10×, 5 g/L trypsin, 2 g/L EDTA·4NA, 8.5 g/L NaCl), phosphate-buffered saline (PBS), and all amino acid standards were purchased from Sigma-Aldrich (St. Louis, MO). Sodium tetraborate decahydrate was purchased from Fisher Scientific (Pittsburgh, PA).

Buffers and Solutions. All solutions were prepared in deionized water (Milli-Q, 18.2 MΩ; Millipore, Bedford, MA) and filtered (0.22 μm) unless otherwise described. Sheath flow buffer contained 100 mM borate adjusted to pH 10.5. CE Separation buffer contained 100 mM borate/20 mM hydroxypropyl-β-cyclodextrin (HP-β-CD, pharmaceutical grade, 5.5 degree substitution, lot H4F110P, Cargill, Cedar Rapids, IA) and was also adjusted to pH 10.5. Artificial cerebral spinal fluid (aCSF) was prepared with NaCl (145 mM), KCl (2.7 mM), $MgSO_4$ (1.0 mM), and $CaCl_2$ (1.2 mM). High-K^+ aCSF solutions were prepared with NaCl (45 mM), KCl (102.7 mM), $MgSO_4$ (1.0 mM), and $CaCl_2$ (1.2 mM). Derivatization solution was prepared fresh daily by dissolving 40 mM NBD-F (TCI America, Portland, OR) in methanol and diluting 1:1 with 500 μM HCl yielding a final solution of 20 mM NBD-F/250 μM HCl in 50% methanol which was degassed under vacuum for 2 minutes. Fluorescein diacetate (FDA; Sigma-Aldrich Co, St. Louis, MO) stock solution was prepared by dissolving 1 mg/mL in fresh acetone and was stored in a glass culture tube, covered with tinfoil, in a refrigerator.

2.3.2 *In Vitro*-Microdialysis

Microdialysis probes were built in-house according to the side-by-side geometry[97]. Briefly, were inserted into a 200 µm i.d. piece of hollow fiber dialysis tubing made from regenerated cellulose (13 kD MWCO, Spectrum Laboratories, Rancho Dominiquez, CA), a stretchy material allowing both capillaries to fit snugly inside. The capillaries were staggered by 1 cm to create a sampling region which was sealed using polyimide resin (Alltech, Deerfield, IL). Prior to introduction into cell culture, probes were conditioned by perfusion of ethanol (60 µL/hr for 30 min) then aCSF (60 µL/hr for 45 min) and sprayed with a 70% ethanol solution.

Type-1 astrocyte cell clones, C8-D1A, were obtained (CRL-2541, ATCC, Manassas, VA) in a 1 mL frozen vial. These astrocytic clones were originally collected from 8 day old mouse cerebella after spontaneous transformation (no addition of carcinogens or oncogenic viruses) and are considered to be an immortalized line since they were maintained for more than 100 generations after cloning.[98] Confluent monolayer cultures were sustained in 25 cm^2 tissue culture flasks (T25) containing 9 mL of high glucose DMEM supplemented with 10% fetal bovine serum and 110 µL gentamicin. Cultures were kept at 37°C in an incubator and were passaged using a ratio of 1:6 every 3-4 days with 0.25% trypsin/0.03% EDTA solution.

Monolayers of cells were grown directly on the surface of microdialysis membranes by serially seeding suspensions of cells into a flask containing several probes. To accelerate the time it takes for cells to differentiate across the entire sampling region, this process is performed with 5 passages of cells, resulting in an in-culture time of approximately 2-3 weeks.

2.3.3 Online CE-LIF Instrumentation

A schematic of the *in vitro*-microdialysis sampling platform coupled online to a high-speed CE-LIF instrument is shown in Figure 2.1. The labeling assay has been previously reported[67] and here is presented with slight modifications.

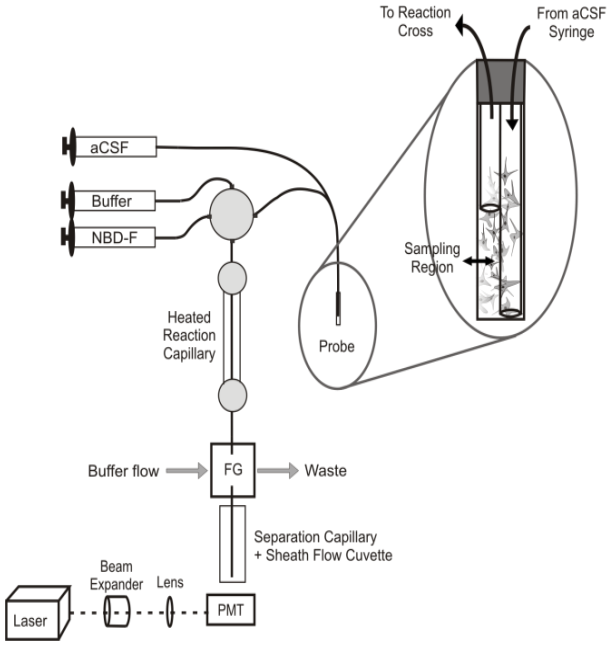

Figure 2.1. Schematic of online CE system coupled to the *in vitro*-microdialysis platform. Either aCSF or stimulant-spiked aCSF can be perfused into the probe. Cells are cultured onto the surface of the microdialysis membrane. Small molecules released by the cells will diffuse across the sampling region of the dialysis membrane and be transported to the reaction cross in the dialysate. 7-Fluoro-4-Nitrobenzo-2-Oxa-1,3-Diazole (NBD-F) is used to fluorescently label primary and secondary amines. Injections onto the separation capillary are made by stopping buffer flow through the flow gate (FG) interface. Analytes are excited by the 488 line of diode pumped solid-state laser and detected with a PMT.

Derivatization Reaction. Microdialysis probes were perfused with aCSF at a rate of 25 µL/hr with a microsyringe pump (Harvard Apparatus Inc., Holliston, MA, USA). Dialysate was transported in a 40 µm i.d. × 360 µm o.d. fused silica capillary to a 250 µm i.d. stainless steel cross (Valco Instruments Co. Inc, Houston, TX) where it was mixed with a 5 uL/hr stream of borate buffer and a 5 uL/hr stream of derivitization solution. The labeling reaction progressed as it traveled through a 90 cm capillary of 75 µm i.d. × 360 µm o.d. dimensions. The rate of the reaction was accelerated by heating a 66 cm portion of this capillary to 80ºC by passing the capillary through tubing that was circulated with

water from a heating bath (NESLAB EX-7 Digital one heating bath circulator, Thermo, Newington, NH). The length of the reaction capillary and flow rates of solutions resulted in a 5 minute reaction time allowing the reaction to go to completion.

High-Speed Capillary Electrophoresis. A flow gated interface[55] was used to segment the continuous stream of labeled dialysate into discrete injection plugs onto a 6.5 cm CE separation capillary with 5 µm i.d. × 360 µm o.d. The reaction and separation capillaries were coaxially aligned in the vertical channels of the flow gate with a 50 µm gap between them. A syringe pump (Pump 22 syringe pump, Harvard Apparatus, Holliston, MA) flowing at 40 mL/hr was used to push separation buffer across the gap between capillaries in the horizontal channels of the flow gate or into a waste reservoir. The flow stream was controlled using a pneumatically actuated 10 port valve (C2-3000A, Valco Instruments Co. Inc., Houston, TX). Injections were performed by stopping buffer flow through the flow gate while no voltage was applied, allowing a sample plug to form. Sample was drawn into the capillary by applying a voltage of 16-18 kV. Separations were conducted by increasing the voltage to 18-20 kV and resuming buffer flow through the flow gate. Injections were controlled using a LabView program designed in house.

Detection Scheme. LIF detection was achieved using the 488 nm line of a diode pumped solid-state laser (Coherent, Santa Clara, CA) at a power of 60 mW. The laser beam was in line with a 10× beam expander (Edmund Optica, Barrington, NJ) and a 1× lens used to focus the beam just below the tip of the separation capillary in the sheath flow cuvette. Fluorescence emission was collected at 90° with a photomultiplier tube (PMT R1477, Hamamatsu Corp., Bridgewater, NJ) after being filtered through spatial and bandpass filters (543.5 ± 10 nm). Current was amplified, filtered with a 10 ms rise

time, and recorded using a data acquisition card (National instruments Corp., Austin, TX). Cutter Analysis 7.0[99] was used to analyze data.

Measuring Release Dynamics from Astrocytes. Microdialysis probes cultured with a monolayer of astrocytes were transferred from culture flasks to 1.5 mL eppendorf tubes containing aCSF held at 37ºC using a dry bath incubator (Fisher Scientific, Pittsburgh, PA). Probes were perfused with aCSF for 10 minutes prior to online coupling with CE, allowing interferences from the cell growth medium to be cleared from the interior lumen of the probe prior to analysis. Basal amino acid levels were recorded while the probe remained in a solution of aCSF. Amino acid release was stimulated by transferring the probe to a solution of high-K^+ aCSF for a duration of 2 minutes followed by returning the probe to the original aCSF solution. Several stimulations could be performed on a single probe at intervals of at least 20 minutes, allowing for stimulated release to return to basal levels before subsequent stimulations.

Bulk Measurements. Stimulation experiments were performed on cells cultured in bulk as a point of comparison. Briefly, cells were cultured in a T25 flask until a confluency of approximately 75%. Cells were then washed with PBS (3× 5mL) and aCSF was added to the flask (10 mL). After 10 minutes, an aliquot was removed and analyzed using microdialysis-CE. aCSF was then removed and replaced with high-K^+ aCSF. Again, an aliquot was removed after 10 minutes and the stimulation solution was replaced with aCSF. Process was then repeated.

2.3.4 Imaging

Medium was removed from the culture flask and cells were rinsed three times with PBS. The final PBS rinse was left in the flask. 2 µL of FDA stock solution was added for each 1 mL of PBS for a final amount of 2 ug/mL FDA. The solution was incubated for 15 minutes at 37ºC. Cells were imaged immediately on a Nikon A1R-MP multi-photon confocal microscope connected to an upright FN1 microscope with a PlanApo LWD 25× water-immersion objective (Nikon Instruments Inc, Melville, NY).

2.4 Results and Discussion

2.4.1 Cell Coverage on Probe Surface

Two key issues that must be addressed with the *in vitro*-microdialysis platform is the extent of surface cell coverage across the sampling region and the viability of the cells growing on the probe. To determine if a significant number of active cells were present, viable cells were labeled with FDA and imaged over the sampling region of a microdialysis probe using confocal microscopy (see Figure 2.2). As a non-fluorescent precursor, FDA, is often used for assessing cell viability since it only generates a fluorescent signal once it has been taken up by mammalian cells and the acetate groups are removed by active intracellular enzymes.[100]

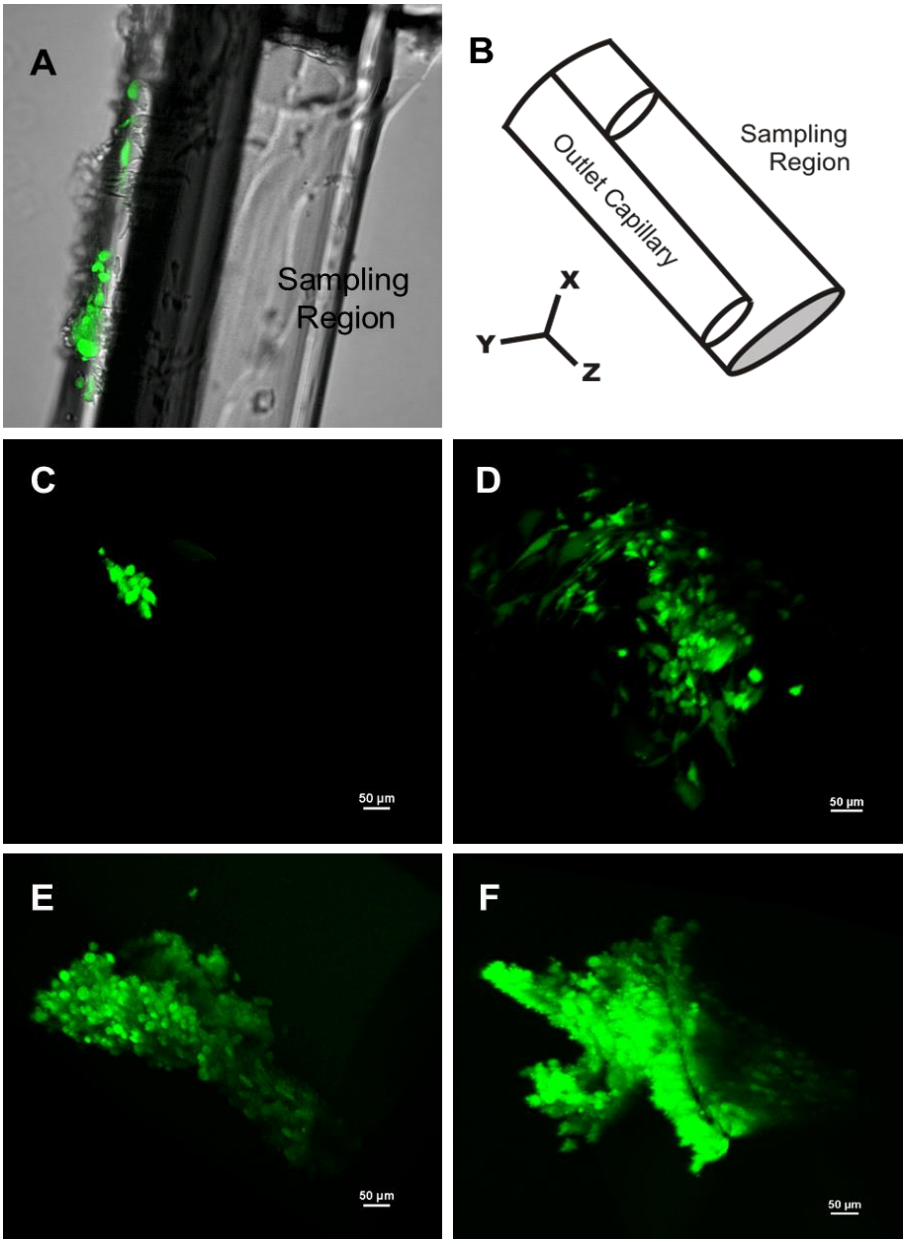

Figure 2.2. Astrocyte clones (C8-D1A) were cultured in direct contact with the porous membrane of microdialysis probes. Viable cells were labeled with FDA and imaged over the surface of the sampling region **(A)**. To visualize how surface coverage increased with time and number of passages, probes were oriented according to **(B)** and imaged using confocal microscopy. After 3 days in culture and with 1 passage of cells seeded onto the membrane surface **(C)** only a small patch of cells was observed. A second passage of cells was seeded and imaged after 1 week in culture **(D)**, resulting in a noticeable increase in cell coverage. The serial-seeding of cell passages continued and images were collected after 2 weeks in culture with 4 passages of cells **(E)** and 3 weeks in culture with 5 passages of cells **(F)**.

The C8-D1A astrocytic clones adhered easily to the regenerated cellulose membrane, with no special surface treatment or handling necessary to incorporate cells onto the probe. Although transfer was straightforward it was noticed that the astrocytes did propagate at a slower rate on the probe surface than in bulk culture. To increase the rate of cell incorporation onto the surface, multiple passages of cells were sequentially seeded onto a probe over several weeks. A confluent monolayer of cells was reproducibly achieved when 5 passages of cells were seeded over a three week time period. A time-progression series of images were collected by imaging probes at four time points during the culture process: 3 days in culture with 1 passage of cells seeded on (Figure 2.2 C), 1 week in culture with 2 passages of cells (2.2 D), 2 weeks in culture with 4 passages of cells (2.2 E), and 3 weeks in culture with 5 passages of cells (2.2 F). Probe surfaces for each of the presented images are oriented in the same axial direction, as demonstrated in Figure 2.2 B.

As shown in the time-progression images presented in Figures 2.2 C-F, the surface area of cell coverage increased as more passages of cells were seeded onto the probe. After a few days in culture with one passage of cells (2.2 C) only a small patch of cells adhered to the membrane. Though these cells demonstrated some propagation, it was at a slower rate than in the culture flask. After an additional week in culture and two more passages, cell coverage over the membrane began to spread, reaching approximately 50-60% confluency (2.2 D). The trend of increased coverage further passages continued (2.2 D-E) and complete coverage was achieved at approximately 3 weeks in culture. At this point, cells began to form a thick monolayer over the sampling region resulting in a tissue-like surface visible to the naked eye.

Fibrous astrocytes are characterized by processes which extend out from the cell body. At low density there are typically 2-4 processes which are short and thick. As the cells become more confluent, processes become longer, thinner, and more numerous.[98] This trend can be visualized in Figure 2. At lower densities, the cell bodies appeared prominently with only a few processes extending out. As more cells adhered to the surface of the probe membrane, individual cell bodies became difficult to visualize under the reach of neighboring projections. Observed cell bodies were typically 30 μm in diameter, with processes ranging from 50-80 μm in length. The size and morphology of the observed cells were consistent with previous descriptions[98], suggesting that culturing cells on the surface of the membrane did not alter cell physiology and function.

Careful attention was necessary to prevent bacterial contamination of the probes during their preparation. In particular, the glue and resin used in probe construction are not able to withstand autoclaving. To limit contamination, newly fabricated probes were sprayed with ethanol (70%) and stored in a clean hood. Prior to use probes were conditioned with autoclaved aCSF using autoclaved syringes and capillaries. These steps successfully minimized bacteria growth and enabled probes to be kept in cell cultures for several weeks.

2.4.2 High-Speed CE Analysis

Analyte peaks were visually identifiable at concentrations as low as 500 nM (see Figure 2.3A). At this concentration, several amino acids including glycine and taurine were still easily distinguished from baseline levels. A calibration was performed daily before stimulation experiments by preparing serially diluted amino acid standards ranging

in concentration from 10 uM to 100 nM. Actual limits of detection varied from 100-250 nM. Figure 2.3B plots the area of a glycine peak against time as the probe was moved between standard solutions of known concentrations. This plot shows how the signal

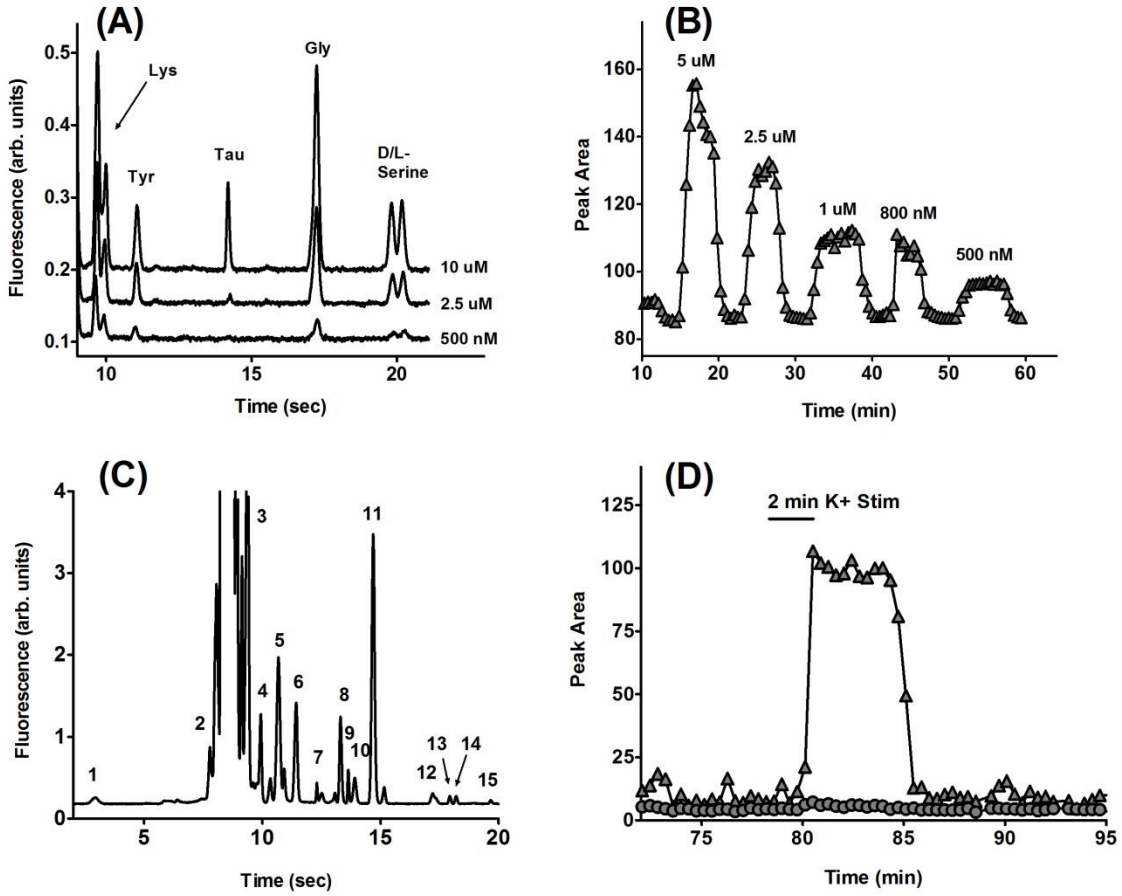

Figure 2.3. **(A)** Electropherograms from the online microdialysis-CE analysis of a series of amino acid standards. Detection limits were typically between 100-250 nM. **(B)** Change in intensity of the glycine peak as the probe is moved between standard solutions of different concentrations. Note that the probe was returned to aCSF between each standard solution. **(C)** Electropherogram from an online microdialysis-CE analysis of K^+ stimulated release from a probe cultured with astrocytes. Identified peaks include: (1) glutamate, (2) arginine, (3) lysine, (4) tyrosine/phenylalanine,(5) leucine/isoleucine, (6) valine, (7) histidine/methionine, (8) taurine, (9) alanine, (10) threonine/glutamine, (11) glycine, (12) asparagine, (13) L-serine, (14) D-serine, and (15)PEA. **(D)** The temporal response of the *in vitro*-microdialysis CE instrument during a 2 min. stimulation of astrocytes cultured onto the probe surface with high K^+ aCSF. Injections were made every 20 seconds, and in this time the signal increased from 10-90% of intensity. Glycine (▲) and phenylalanine (●) are presented to contrast the rapid increase in abundance of glycine in response to a depolarizing stimulation, with the insignificant change observed for phenylalanine.

responds to analyte concentration as well as the temporal response of the instrument. Note that probe was returned to aCSF between standard solutions to allow the signal to return to baseline. Concentrations reached their highest values within 1-2 CE separations corresponding to a temporal response of 20-40 seconds.

Figure 2.3C shows an electropherogram from the online CE analysis of potassium-stimulated release from a confluent layer of C8-D1A astrocyte cells cultured on the surface of a microdialysis probe. The astrocytes released many small molecule amines at concentrations well above the limits of detection of the CE-LIF instrument. Peaks were identified using the double-dialysis method,[101] where 10 µL of dialysate was collected over a 15 minute period from a probe coated with cells placed in a high-K^+ aCSF solution. A second, bare surface microdialysis probe was moved between the collected dialysate (diluted to 300 µL with DI water) and solutions containing small molecule amine standards to confirm the CE migration times of individual analytes. A hydrolysis byproduct of the NBD-F labeling reaction was observed from 8-9 seconds. Despite this interference, 15 small molecule amines released from the astrocytes were resolved and identified in a 20 second separation window. Among the identified analytes, several are of particular importance to astrocyte physiology including: glycine, taurine, D- and L-serine, alanine, and glutamate. Significant drift in analytes with longer migration times prevented reliable measurement of glutamate in several probes. It should be noted that C8-D1A astrocytic cell clones do not contain GABA[102], so it is not included in this analysis.

Figure 2.3D demonstrates the temporal response of the instrument when using a cell coated probe. In this experiment a cell coated probe is moved from aCSF to high-K^+

aCSF, stimulating a rapid increase in glycine release. Note that the observed temporal response of the instrument is even faster than when bare surface probes are moved between standard solutions (Figure 2.3B). It is hypothesized that the close proximity of the cells to the probe enhances diffusion to the membrane surface, resulting in the observed improvement in temporal resolution. Overall the temporal resolution of the *in vitro*-microdialysis CE system was determined to be 20 seconds and limited by the CE separation time.

2.4.3 Dynamics of Small Molecule Amine Release from Astrocytes

Astrocytes are known to have a high K^+ permeability, which is important in regulating extracellular K^+, a necessary action for maintaining neuronal excitability.[103] A physiologically interesting consequence of this permeability is that an abundance of extracellular potassium, typically a consequence of action potential generation in nearby neurons, can elicit a number of responses in astrocyte cells. Two release mechanisms are expected to be triggered by excess extracellular potassium: cellular swelling and transport reversal. Cellular swelling via volume regulated anion channels (VRACs) is induced by the entrance of extracellular K^+ and Cl^- ions. To recover, the cell opens VRACs which release amino acid transmitters such as glutamate, glycine, GABA, aspartate, and taurine into the extracellular region.[104, 105] Transport reversal is second K^+-dependent release event observed in astrocytes. To control the abundance of excitatory amino acids in the extracellular space, astrocytes express Na^+-dependent amino acid transporters. Under normal conditions, these transporters rely on Na^+ and K^+ gradients to uptake amino acids into the cell. Raising extracellular levels of K^+, perturbs this gradient and causes a

reversal of these transporters.[106, 107] Triggering either of these mechanisms is expected to induce in an increased release of small molecule amino acids from astrocytes.

To demonstrate the ability of the online *in vitro*-microdialysis CE platform to detect fast release events, we exposed astrocyte cells cultured onto the surface of a microdialysis probe to high-K^+ levels. Stimulations were administered for 2 minutes and were performed by simply transferring the probe from an aCSF solution to a vial containing high-K^+ aCSF. As demonstrated in Figure 2.4 A, electropherograms collected during high-K^+ exposure (red) show a noticeable increase in the abundance of amino acids when compared to those collected during basal release (black). Figure 2.4 B demonstrates the time course of the stimulations and the

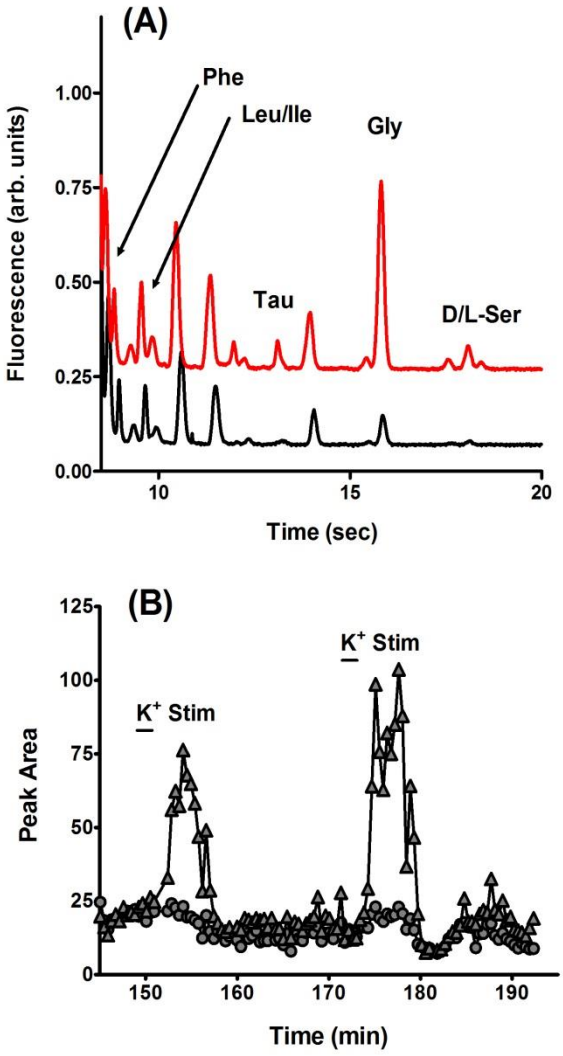

Figure 2.4. Online microdialysis-CE analysis of fluorescently labeled small molecule amines released from C8-D1A astrocyte cells. Electropherograms **(A)** were collected both before (black) and during (red) a 2 minute K+ stimulation. Traces have been offset for clarity. Peak area was plotted as a function of time to demonstrate the time-course of stimulation experiments **(B)**. For the experiment presented here, the percent increase in the relative abundance of amino acids ranged from 11 percent (phenylalanine, ●) to 370 percent (glycine, ▲).

subsequent increases in the relative abundance of monitored amino acids. While glycine increases rapidly in response to high-K^+, many amino acids were unperturbed. Phenylalanine is shown as a point of comparison. It should be noted that levels quickly returned to baseline after clearance of the high-K^+ aCSF. Astrocytes responded to multiple stimulations with high-K^+ (see Figure 2.4 B), suggesting continued viability of the cells on the probe over periods of several hours. The increased response of amino acid release to the second stimulation in Figure 2.4 B is attributed to biological variability. In other experiments, the first stimulation demonstrated a larger response than later stimulations (data not shown) which indicates that the increased effect seen here is not a result of previously released analyte accumulated in or near the probe membrane.

Astrocytes cultured onto three different probes were each administered two high K^+ stimulations to assess reproducibility. The average percent increase in the relative abundance of several key amino acids is plotted in Figure 2.5. It is important to note that several amino acids were much more responsive to the potassium stimulation than others. Glycine demonstrated the largest percent increase in relative abundance (700%), followed by taurine (185%) and serine (215%). Instrumental variability day-to-day prevented us from reproducibly achieving complete resolution between D- and L- serine, so the areas were taken together for this analysis. Our results are in agreement with a previous study which reported a 94% increase in the evoked release of taurine from Type 1 astrocytes with a 50 mM high-K^+ stimulation.[108]

To demonstrate the utility of the developed method, a comparable stimulation experiment was performed in a bulk cell culture (Figure 2.5, black). Here, aliquots of aCSF were removed at 10 minute intervals before, during, and after exposure to high-K^+ aCSF. Dilution of the analyte into the bulk fluid both prevented collection at increased frequency and caused several analytes to fall below the LOD of the instrument (*). This result illustrates the advantages that *in vitro*-microdialysis offers over traditional methods. Changes in the relative abundance of analytes can be observed for more analytes at lower concentrations with significantly improved temporal resolution.

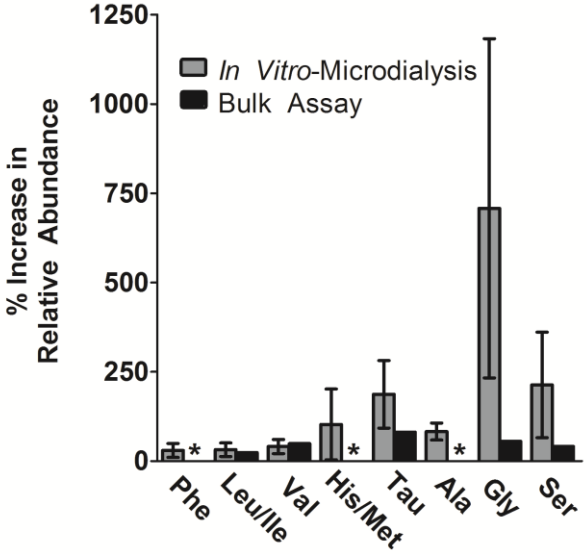

Figure 2.5. The increase in the relative abundance of amino acids after a 2 minute K+ stimulation using both the developed *in vitro*-microdialysis platform (gray, n=4) and a traditional bulk assay (black, n=1) for a control. When monitoring changes with *in vitro*-microdialysis, glycine consistently demonstrates the largest increase in abundance with response to the stimulus, though marked increases are also observed for taurine, serine, alanine, and histidine/methionine. Observed changes during bulk analysis were significantly lower, due to dilution, with several analytes below the LOD (denoted with *).

The large, yet variable responses among analytes is exciting for several reasons. First, the non-uniform increases across the different analytes supports the premise that the observed changes are biological in origin, not artifacts of the instrument. Second, the amino acids which are more greatly affected by exposure to high-K^+ are in agreement with previous reports on astrocyte physiology. Several different studies have concluded

that depolarized astrocytes release taurine[109] and serine[110] from VRACs, while glycine release may be occur via transport reversal[111]. Amino acids such as phenylalanine, which are not known to have any participation in cellular swelling mechanisms, were unaffected by the stimulation.

There are several factors which likely contribute to the dramatic responses observed using our system. First, the cell line was chosen to induce a large signal. C8-D1A astrocyte clones are a designated Type 1 astrocytic cell line. This type of cell has higher concentrations of glutamine and alanine (4×) and glutamate, asparagine, serine, and threonine (2×) when compared to Type 2 astrocytes.[108] It has also been demonstrated that these cell clones synthesize taurine and glycine, resulting in high endogenous levels of these particular amino acids.[102] Furthermore, both the close proximity of the cells to the microdialysis membrane and the high temporal resolution of the online CE instrument allow us to more efficiently capture and analyze released analytes in comparison to bulk methods. Lastly, a strong stimulation was administered. Depolarization of astrocyte cells is often performed by exposing cells to a hypoosmotic medium containing depleted NaCl concentrations, as opposed to increased potassium.[105, 109] It has been reported that hypoosmotic media induces less intense release patterns than a similar isosmotic medium in which an K^+ is used to replace an equimolar amount of Na^+.[112] It is likely that the 100 mM K^+ isosmotic stimulation evoked a significantly larger response due to strength and osmolality. Again, this stimulation was intended to induce a dramatic and predictable response as a means of validating the online *in vitro*-microdialysis CE method.

2.5 Conclusions

The model proposed here offers an alternative microdialysis approach where cells are cultured directly onto the surface of the porous membrane. Culturing cells directly onto the probe surface allowed efficient recovery of released analytes, eliminating the dilution that limits the sensitivity and temporal response of traditional bulk *in vitro* assays. Integration with online, high-speed CE allowed the benefits of this efficient recovery to be realized, resulting in low nM detection limits and a 20 second temporal response for a number of important neurochemicals. Detection of cellular release was demonstrated using immortalized C8-D1A astrocyte cells. Dynamic changes in release were stimulated by exposure to extracellular potassium. Depolarization induced an increase in the overall relative abundance of several amino acids; most notably, glycine, but also taurine, serine, alanine, and histidine/methionine. These results are in agreement with previous reports of astrocyte physiology and serve as a validation for this method.

Chapter 3

Characterization of the *in Vitro*-Microdialysis Sampling Platform

3.1 Summary

In this work, a variety of parameters affecting the efficacy and accuracy of *in vitro*-microdialysis were investigated. Cell medium used to maintain cells prior to analysis, was fully perfused from the probe after a duration of 10 minutes, minimizing any effects on the intensity and duration of the observed signal. Upon removal from cell medium, it was initially unclear whether the cells were properly sustained in the solution of artificial cerebrospinal fluid (aCSF) previously used to analyze basal release. A study was performed characterizing cell survival in several buffered-aCSF solutions. No significant increase in cell death was observed in a simple aCSF solution, when compared with the buffered systems, for up to two hours. Several parameters influencing the microdialysis environment, specifically temperature and size of the containment, were also investigated. Both were found to have a substantial effect on signal intensity and release dynamics. When compared to basal and release levels collected at 37ºC, transferring a probe to a solution maintained at room temperature lowered the signal intensity, demonstrating a need to perform experiments at biological temperatures. Microdialysis was performed in several sized containments: 0.7 and 1.5 mL eppendorf tubes as well as a 150 mL beaker. Signal intensity appeared larger in the smaller environments, indicating that diffusion back towards the probe may be occurring, a finding further supported by a prolonged duration of stimulated release in smaller containers. However, sample-to-sample variability and high standard deviations contribute to a lack of statistical significance for this result.

3.2 Introduction

The widespread application of microdialysis for *in vivo* sampling has been established. The relatively small size of the probe limits disruption to surrounding tissue while the molecular weight cut-off (MWCO) serves as a built-in cleanup of the sample.[113] Aqueous perfusate is pushed through the probe continuously, resulting in no net-loss of fluid across the membrane. This allows microdialysis to be performed within living biological systems. In Chapter 2, a new sampling platform was discussed detailing the use of microdialysis as an *in vitro* technique by culturing cells on the surface of the microdialysis probe. High-K^+ stimulations were performed on cell-cultured probes to demonstrate the ability to monitor dynamic analyte changes with temporal resolution of 20 seconds. While initial work proved promising, further characterization of the parameters influencing both the well-being of the cells during experimentation and the sampling process was required.

Cultured cells must be maintained under a common set of conditions to ensure health. Though these conditions can vary depending on the cell line, several parameters remain fairly constant. For example, mammalian cells are often kept in an incubator set to 37ºC and 5% CO_2. In addition to the temperature and gas composition of their environment, the health and longevity of cultured cells is heavily dependent on the composition of the fluid (termed "cell growth medium") in which they live. The recommended medium for maintaining the C8-D1A cultured astrocyte cells initially used for *in vitro*-microdialysis is Dulbecco's Modified Eagle's Medium (DMEM), a variation of Basal Medium Eagle (BME) that contains a four-fold higher concentration of amino acids and vitamins. In the process of culturing cells on the microdialysis membrane,

probes were subsequently immersed in this fluid for approximately 3 weeks. Since this medium contains high concentrations of analytes of interest, the extent to which cell growth medium can influence the observed amino acid levels during experimentation must be identified. Of additional interest is how long cells could survive (and maintain physiological functions) once removed from their life sustaining medium.

In addition to determining the effects of the fluid in and around the probe, it is necessary to better understand how the sampling dynamics are influenced by the cell barrier at the sampling surface. Long-standing difficulties with accurately determining recovery, and the inability to effectively perform calibrations, continue to complicate the interpretation of microdialysis experiments. Through the early 90's, *in vitro* microdialysis was often used to calibrate *in vivo* results; however, this was found to inaccurately represent the results because (i) the diffusion resistance encountered in tissue is not the same as that found in an *in vitro* reference medium and (ii) in tissue the various active and passive clearance processes, which are absent *in vitro*, bring another uncontrollable factor when comparing *in vitro* with *in vivo* microdialysis.[114] Essentially, the added complexities of *in vivo* systems (including analyte metabolism, uptake and release, and tissue tortuosity) has too much of an effect on the observed signal to be compared with results obtained in the absence of these factors.

Because our experiments aren't performed *in vivo*, variables that we previously didn't have access to are now available. Specifically, we're interested in variables that are easy to manipulate and control: temperature and size of environment. By identifying the effects of these new parameters at our disposable, we will be able to better understand the

dynamics of *in vitro*-microdialysis sampling and design more specific and biologically-relevant experiments in the future.

3.3 Materials and Methods

3.3.1 Chemicals and Reagents

Reagents. Dulbecco's modified Eagle medium (DMEM) and fetal bovine serum (FBS) were purchased from Invitrogen Molecular Probes (Eugene, OR). Trypsin solution (10×, 5 g/L trypsin, 2 g/L EDTA·4NA, 8.5 g/L NaCl), phosphate-buffered saline (PBS), and all amino acid standards were purchased from Sigma-Aldrich (St. Louis, MO). Sodium tetraborate decahydrate was purchased from Fisher Scientific (Pittsburgh, PA).

Buffers and Solutions. All solutions were prepared in deionized water (Milli-Q, 18.2 MΩ; Millipore, Bedford, MA) and filtered (0.22 μm) unless otherwise described. Sheath flow buffer contained 100 mM borate adjusted to pH 10.5. CE Separation buffer contained 100 mM borate/20 mM hydroxypropyl-β-cyclodextrin (HP-β-CD, pharmaceutical grade, 5.5 degree substitution, lot H4F110P, Cargill, Cedar Rapids, IA) and was also adjusted to pH 10.5. TRIS buffer contained TRIS (12.5 mM), glucose (5.6 mM), $CaCl_2$ (1.5 mM), $MgCl_2$ (1.4 mM), NaCl (150 mM), KCl (4.2 mM) and was pH adjusted to between 7.0-7.5. Artificial cerebral spinal fluid (aCSF) was prepared with NaCl (145 mM), KCl (2.7 mM), $MgSO_4$ (1.0 mM), and $CaCl_2$ (1.2 mM). High-K^+ aCSF solutions were prepared with NaCl (45 mM), KCl (102.7 mM), $MgSO_4$ (1.0 mM), and $CaCl_2$ (1.2 mM). Phosphate-buffered aCSF was prepared with KH_2PO_4 (1.5 mM), Na_2HPO_4 (8.1 mM), and glucose (10 mM) in aCSF and pH adjusted to between 7.0-7.5. HEPES (Alfa Aesar, Heysham, Lancashire, UK) –buffered aCSF was prepared with Na_2HPO_4 (1.25 mM), glucose (10 mM), and HEPES (10 mM) in aCSF and pH adjusted

to between 7.0-7.5. Derivatization solution was prepared fresh daily by dissolving 40 mM NBD-F (TCI America, Portland, OR) in methanol and diluting 1:1 with 500 µM HCl yielding a final solution of 20 mM NBD-F/250 µM HCl in 50% methanol which was degassed under vacuum for 2 minutes. Trypan Blue (Thermo Scientific, Waltham, MA) was prepared to 0.4% in PBS.

3.3.2 Cell Viability in Buffer Systems

Cells in suspension. Confluent monolayer cultures of C8-D1A astrocyte clones (CRL-2541, ATCC, Manassas, VA) were sustained in 25 cm^2 tissue culture flasks (T25) containing 9 mL of high glucose DMEM supplemented with 10% fetal bovine serum and 110 µL gentamicin. Cultures were kept at 37°C in an incubator and were cleaved from the flask wall using 0.25% trypsin/0.03% EDTA solution. A 1:1 solution of trypsin cell suspension and cell medium (DMEM) was centrifuged (Sorvall ST 16R, Thermo Scientific, Waltham, MA) for 10 minutes at 1000 relative centrifugal force (rcf). The solution was decanted and the resulting cell pellet re-suspended in PBS (4 mL) and split into 4× 1mL aliquots in 1.5 mL eppendorf tubes. Eppendorf tubes were centrifuged using the same parameters (10 minutes, 1000 rcf) and the resulting pellets re-suspended in the desired buffer system (1 mL): 1) aCSF, 2) TRIS, 3) PO_4-buffered aCSF, or 4) HEPES-buffered aCSF.

Immediately upon addition of the buffer, (time, T=0), 100 µL of cell suspension was removed from each eppendorf tube and mixed with 100 µL of Trypan Blue. The resulting mixture was then carefully pipetted into a hemocytometer. Cells were counted under magnification. After 30 minutes had passed, T=30, 100 µL of cell suspension was again removed from each tube and mixed with 100 µL of Trypan Blue. Each of the

solutions were counted under magnification with a hemocytometer. This process was repeated again at 60 and 120 minute intervals (T=60 & T=120).

Adhered monolayer of cells. Confluent monolayer cultures of C8-D1A astrocyte clones were sustained in 25 cm^2 tissue culture flasks (T25) containing 9 mL of high glucose DMEM supplemented with 10% fetal bovine serum and 110 µL gentamicin. Cultures were cleaved from the flask wall using 0.25% trypsin/0.03% EDTA solution. Cells were plated onto a 96-well plate (Corning Inc., Corning, New York) to measure cell survival in different buffer systems while adhered to a surface. Cells were sustained in DMEM for several days until they grew to confluency. At that point, DMEM was removed and replaced with a buffer of interest. The buffer systems investigated were: 1) aCSF, 2) TRIS, 3) PO_4-buffered aCSF, 4) HEPES-buffered aCSF, 5) control – cell medium, and 6) negative control- no cells present. At T=0, immediately after the medium was replaced with buffer, 100 µL of Trypan Blue was added. These wells were then imaged with an inverted confocal microscope (Olympus IX81 inverted microscope equipped with an Olympus DSU confocal unit). This process was repeated at T=30, T=60, and T=120 time intervals. Cells were plated and counted in triplicate for each condition and time point. Cell counting was performed by counting cells in a manufactured grid over the image similar to a hemocytometer.

3.3.3 Online CE-LIF Assays for Varying Parameters

The instrumentation for all online CE-LIF experiments is identical to that described in Section 2.3.3. The following variations describe different experimental approaches performed on the same instrument.

Temperature Dependence. Microdialysis probes cultured with a monolayer of astrocytes were transferred from culture flasks to a 1.5 mL eppendorf tube containing aCSF held at 37ºC using a dry bath incubator. Probes were perfused with aCSF for 10 minutes prior to online coupling with CE, allowing interferences from the cell growth medium to be cleared from the interior lumen of the probe prior to analysis. Basal amino acid levels were recorded while the probe remained in a solution of aCSF. Amino acid release was stimulated by transferring the probe to a solution of high-K^+ aCSF (also maintained at 37ºC) for a duration of 2 minutes followed by returning the probe to the original 37ºC aCSF solution. The probe remained in this solution for 5 minutes allowing the stimulated release levels to return to baseline. At this point, the probe was transferred to a 1.5 mL eppendorf tube containing aCSF held at room temperature. The probe remained in this solution for 5 minutes allowing the cells to adjust prior to administering another 2 minute high-K^+ aCSF (maintained at room temperature). The probe was then transferred back to the room temperature aCSF for 5 minutes. This cycle can be repeated once per probe.

Sampling Environment. Microdialysis probes cultured with a monolayer of astrocytes were transferred from culture flasks to either a 0.7 mL eppendorf tube, 1.5 mL eppendorf tube, or 150 mL glass beaker containing aCSF held at 37ºC. For eppendorf tubes, this was achieved using a dry bath incubator. The beaker temperature was maintained using a carefully controlled hotplate. Probes were perfused with aCSF for 10 minutes prior to online coupling with CE, allowing interferences from the cell growth medium to be cleared from the interior lumen of the probe prior to analysis. Basal amino acid levels were recorded while the probe remained in a solution of aCSF. Amino acid

release was stimulated by transferring the probe to a solution of high-K^+ aCSF for a duration of 2 minutes followed by returning the probe to the original aCSF solution. Several stimulations could be performed on a single probe at intervals of at least 20 minutes, allowing for stimulated release to return to basal levels before subsequent stimulations.

3.4 Results and Discussion

3.4.1 Cell Survival in Buffer Systems

The methodology described to perform *in vitro*-microdialysis in Chapter 2 incorporated the use of artificial cerebrospinal fluid (aCSF) for all stimulation experiments. Basal measurements were collected in aCSF and stimulations were performed in a potassium-spiked aCSF variant. The performed experiments varied in length from approximately 30-120 minutes, at which point the cells typically appeared to become exhausted, indicated by a decrease in the basal release of amino acids. In an attempt to prolong the viability of cells in *in vitro*-microdialysis experiments, several aCSF buffer systems were investigated: aCSF, PO_4-buffered aCSF, HEPES-buffered aCSF, and TRIS.

Initially, the viability of cells in the different buffer systems was tested over a two hour period using a Trypan Blue assay in a suspension of cells. Trypan Blue is a dye-exclusion viability assay in which live cells (with intact cell membranes) are impenetrable to the dye and appear normal, whereas dead cells are penetrated and appear dark blue. After exposing cells to Trypan Blue, dead cells can be easily visualized and counted under magnification using a hemocytometer. Figure 3.1 illustrates cell survival (in suspension) for the different buffer systems over a two hour time period. After two

hours had passed, cell survival in every buffer system appeared to have dropped significantly. Half-life calculations were performed, and aCSF was found to have the shortest half-life (32.7 minutes) while HEPES-buffered aCSF was found to have the longest (119.5 minutes). Phosphate-buffered aCSF and TRIS had nearly identical half-lives around 95 minutes. This was a surprising result since other reports demonstrate prolonged cell health in similar buffered systems.[8] It was hypothesized that the cells were adsorbing to the interior surface of the eppendorf tubes, leading to decreased numbers of viable cells remaining in suspension. The experiment was redesigned to investigate to the longevity of cells in each buffer system while adhered to a well plate surface. Figure 3.2 (A) and (B) shows cells survival in aCSF after 30 and 120 minutes, respectively. Again, Trypan Blue was used to visualize the ratio of live to dead cells. Live cells appear to have

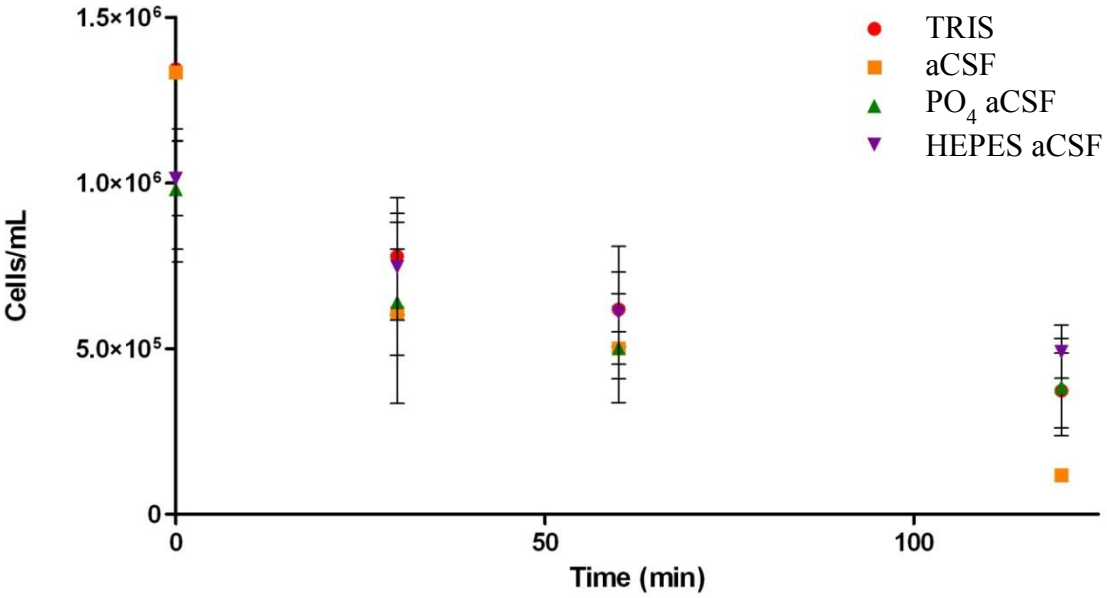

Figure 3.1. Cell survival in various buffer systems is shown by plotting cell count from a suspension of cells (cells/mL) as a function of time. HEPES- and PO_4-buffered aCSF solutions demonstrate the smallest degree of change over the course of the experiment. Initial cell counts were lower than in TRIS and aCSF solutions (insignificant) yet they contained higher counts than aCSF after 2 hours had elapsed. Standard deviation error bars are included.

white/translucent cell bodies whereas dead cells appear as dark circles or debris. For both buffer systems, there is only a small amount of cell death occurring between 30 and 120 minutes. A one-tailed, unpaired statistical p-test was used to determine whether the degree of cell death was significant. P-values of 0.146 and 0.246 were obtained for the aCSF (A,B) and PO_4-buffered aCSF (C,D) systems, respectively. These values indicate that even when employing a confidence interval as low as 90%, the difference in cell abundance between the two time points is insignificant. Data is not shown for the other buffered systems as they all demonstrated the same trend: there was no significant change in the ratio of live to dead cells after two hours had elapsed. For remaining experiments, aCSF was used exclusively as the basal-condition sampling matrix.

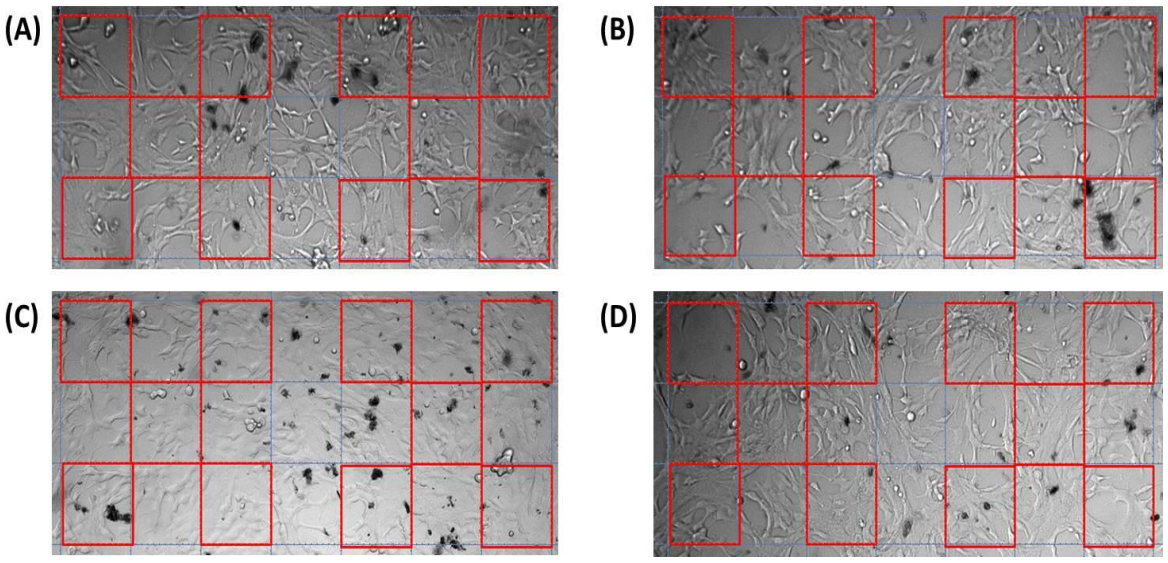

Figure 3.2. Cell survival in aCSF after **(A)** 30 minutes and **(B)** 120 minutes and in PO_4-buffered aCSF after **(C)** 30 minutes and **(D)** 120 minutes. Cell counting was performed by manufacturing a hemocytometer-like grid which was placed over images collected on an Olympus IX81 inverted microscope. There was no significant degree of cell death (indicated by an increase in dark debris) in aCSF after 2 hours when compared with cells sustained in the other buffer systems.

3.4.2 Effects of Cell Media on CE Analysis

In order to maintain healthy cell cultures, cell medium contains a large quantity of amino acids in addition to other small molecules, biomolecules, and antibiotics. The permeability of the membrane, combined with the extended time the probes spent in culture, enables diffusion of small molecules from the medium into the probe lumen. When probes were removed from culture to be used in an experiment, cell medium remained in the probe. It was unknown whether medium could simply be pumped from the probe or if small molecules adsorbed to the interior surface. It was important to determine if the peaks observed in the electropherograms were the result of analyte release from cells or merely contamination from the

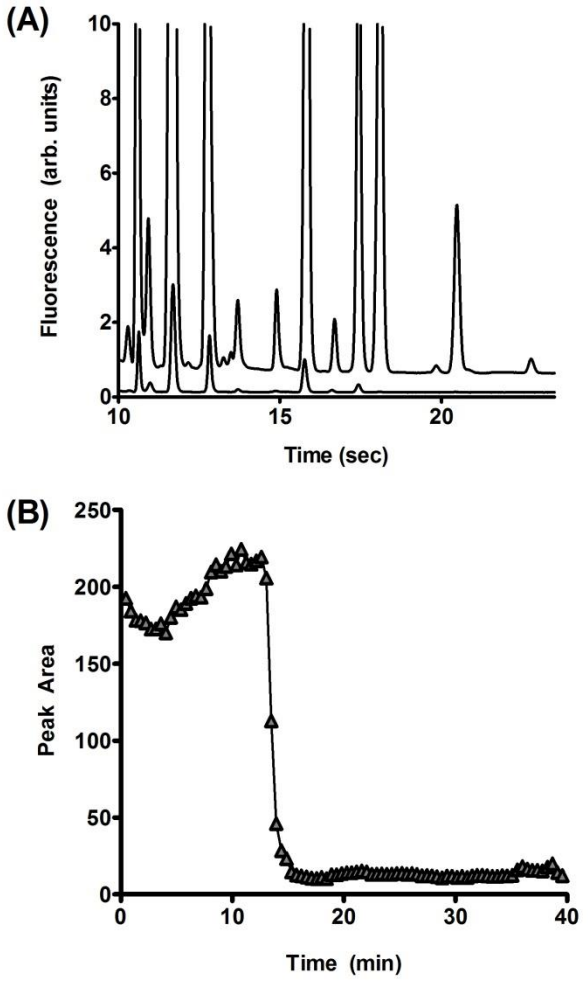

Figure 3.3. **(A)** Electropherograms collected immediately after an astrocyte cultured probe was removed from the medium (top) and after 30 minutes of perfusion with aCSF (bottom). Top trace was offset for clarity. **(B)** Peak area of glycine (▲) plotted as a function of time to demonstrate the time course of medium clearance from the astrocyte coated probe after removal from culture. Medium is cleared and baseline values are established after approximately 10 minutes. All subsequent experiments were performed after 30 minutes of perfusion with aCSF to minimize medium interference.

medium. To determine the influence of the medium on signal intensity, probes (with cells cultured onto the surface) were connected to the online CE system immediately after removal from the culture flask and electropherograms were recorded from the onset of perfusion. The speed at which the intense medium signal clears provides important information regarding how small molecules within the medium interact with the probe. A fast and dramatic drop in signal intensity is expected if medium can be quickly pumped out of the probe, whereas an extended decrease would be expected if small molecules adsorbed to the surface were slowly desorbed.

Figure 3.3A compares electropherograms recorded during initial perfusion (top trace) of the probe with those recorded after 30 minutes (bottom trace). The magnitude of signal is extremely high during initial perfusion, suggesting significant medium contamination. Figure 3.3B plots the area of the glycine peak over time to demonstrate the time course of medium effects. Elevated levels are present for approximately 10 minutes before falling rapidly and stabilizing to baseline levels. This trend was monitored daily and was highly reproducible. The fast and dramatic change implies there is little to no adsorption of small molecules to the probe surface that remains after 10 minutes. All subsequent experiments involving astrocytes were conducted after the probe had been perfused for 30 minutes, allowing for elimination of medium contamination.

3.4.3 Temperature Dependence of Stimulation Response

Several studies investigating the release of amino acid neurotransmitters *in vivo* have found that, depending on the brain region, the rate and magnitude of release is a temperature dependent process.[115-117] The temperature dependent release of taurine, for

example, was attributed to its hypothalamic location. In this region, taurine is thought to be released from intracellular stores through transporters and voltage sensitive channels, as opposed to exocytosis.[118, 119] However, a study investigating hypothalamaic and cerebellar astrocytes found that both cell types demonstrated a temperature-dependence efflux model under basal and stimulated conditions.[120] Some have hypothesized that a decreased release observed at low temperatures may serve to protect astrocytes from thermally induced osmotic changes, while others argue that it may occur in response to changes in the fluidity of membrane constituents thereby affecting diffusion processes.[120, 121]

Our initial interest was simply to determine whether or not it's necessary to perform experiments at 37ºC. If no difference was observed between basal and stimulated levels collected at 37ºC and room temperature, experiments could be performed with more ease and simplicity at room temperature without jeopardizing physiology of the cells. Figure 3.4 shows the peak areas of two amino acids (glycine and phenylalanine) throughout the time course of a temperature-dependence experiment. Shaded areas (B&D) denote when the probe was in room-temperature solutions while other areas (A, C, and D) were maintained at 37ºC. Red bars near the top of the graph denote administration of a 100 mM K^+ stimulation by transferring the probe to a K^+-spiked solution of aCSF (also held at the corresponding temperature). Note that for both of the observed amino acids, the basal release drops almost instantaneously to being placed in a room temperature solution (A to B and C to D).

Likewise, an almost instantaneous increase in basal release is observed with transfer back into a 37ºC environment (B to C). One possible explanation for this fast and

dramatic change is that the metabolism of the cell is extremely temperature dependent.[122-124] By lowering the temperature of the surrounding environment, metabolism is suppressed, and a drop in the release of amino acids is observed. After four stimulations and three temperature transfers, cells become unresponsive to the K^+ stimulation. This is attributed to an exhaustion of the cells (D and E).

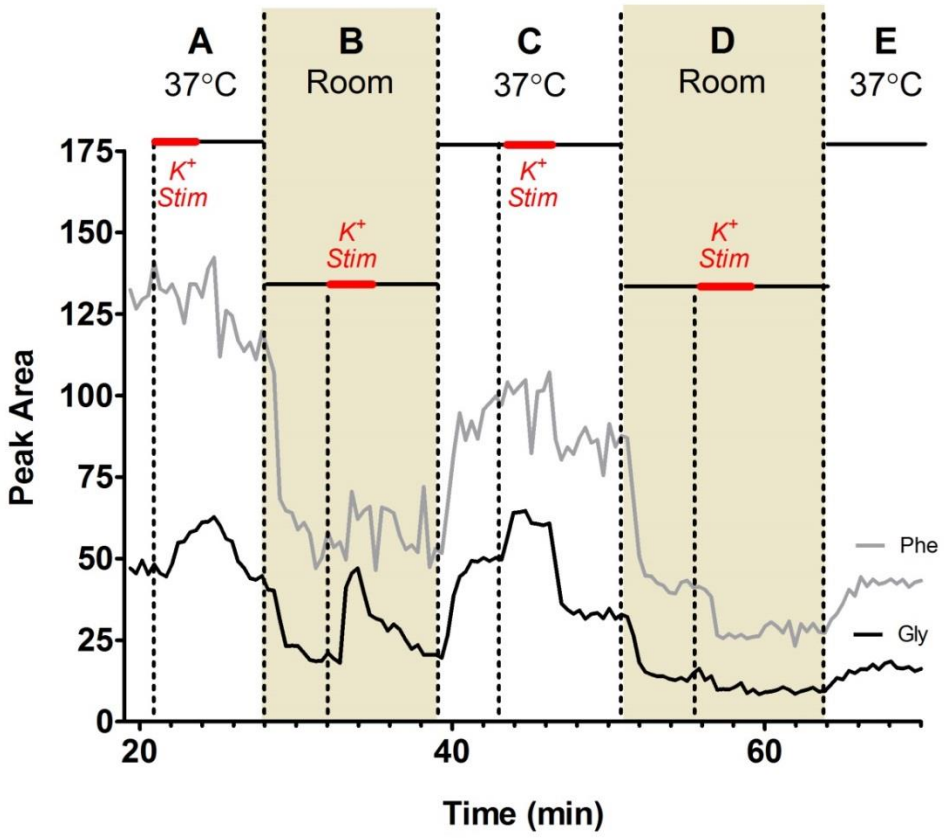

Figure 3.4. Peak areas for phenylalanine (gray) and glycine (black) plotted as a function of time during a temperature-changing experiment. Probes were initially in a solution of aCSF maintained at 37ºC (A) and given a K^+-stim (red bar). After allowing elevated levels to return to baseline, the probe was moved to a room-temperature solution of aCSF (B). Another K^+-spike was administered. This process was repeated, thus, shaded areas (B&D) represent when the probe was at room-temperature while other areas (A, C, & D) were maintained at 37ºC. Red bars denote when the probe was exposed to a K^+-spiked solution of aCSF. The subsequent response of phenylalanine and glycine can be traced at the bottom. Phenylalanine demonstrates no increase in abundance with response to the K^+-stimulation, whereas glycine shows a repeated response in sections A, B, and C. The lack of response from either amino acid in section D signifies exhaustion of the cells.

The dependence of amino acid release on temperature observed in Figure 3.4 was an anticipated result. More surprising is how the magnitude of the stimulated release was influenced. It was previously discussed that at lower temperatures, release of amino acids tends to be suppressed in cerebellar astrocytes.[120] We found that while this is true with regards to the amount of amino acid released at basal levels, there is actually an increase in the magnitude of release stimulated by high K^+. Figure 3.5 shows the peak area responses for serine (A) and taurine (B) to a K^+-stimulation at both room (◊) temperature and 37ºC (▲). With regards to the temporal dynamics of release, there does not appear to be a significant dependence on temperature. Under both conditions, stimulated release reaches maximum magnitude within 1-2 separations and declines after approximately the same time. The primary difference lies in the magnitude of release. At room temperature, there is a greater increase in the abundance of amino acid in response to the K^+-

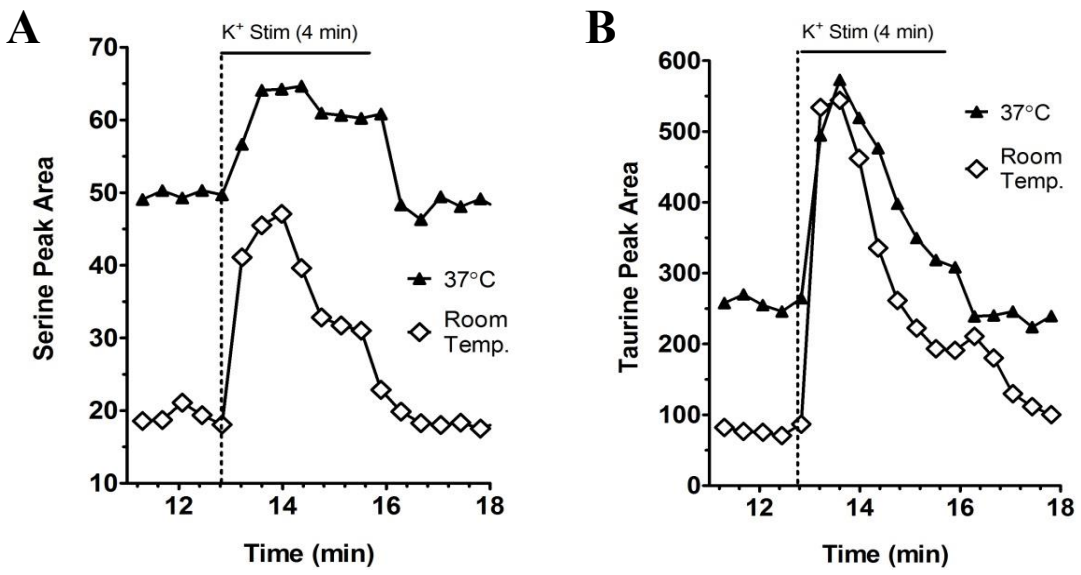

Figure 3.5. Peak area versus time for serine (A) and taurine (B) in response to a K^+-stimulation at both room (◊) temperature and 37ºC (▲).

stimulation. Our primary theory is that though basal release is significantly suppressed at the lower temperature, the stimulation response is not. Therefore, the magnitude of release appears larger though the overall amount of analyte is still much lower at room temperature.

3.4.4 Sampling Environment

The recovery, resolution, and limitations of microdialysis sampling were introduced in Section 1.1.3. In a recent review, several neuroscience researchers identified key limitations of microdialysis: the limited time resolution capabilities (identified as an absolute minimum of approximately 1 minute, though often closer to 10), the invasive nature of the technique which will ultimately always damage the tissue to some extent, and the generation of a depletion zone in which all solutes capable of crossing the probe membrane fall in concentration disproportionately to the surrounding area as they are sampled.[23, 125] The depletion zone is generated *in vivo* by removal of low molecular weight analytes from the area immediately surrounding the microdialysis probe, diffusing across the membrane barrier and being transported away in the dialysate. Figure 3.6A illustrates this depletion by plotting the approximate analyte concentration as a function of distance away from the *in vivo* probe. If a depletion zone exists while conducting experiments *in vivo*, it could have ramifications influencing the physiological dynamics of the target mechanism. Some have argued that by perfusing the brain with artificial cerebrospinal fluid (aCSF), which is free of neurotransmitters, an artificial neurotransmitter concentration gradient is formed which enables the detection of neurotransmitter changes in the implanted area.[110] Others believe there is little to no

effect brought about by this depletion zone. In one study, the effect of a microdialysis-induced depletion of all low molecular weight materials around the microdialysis probe was found not to effect the estimation of extracellular dopamine.[126]

Unlike the depletion zone formed during *in vivo* experimentation, it is likely that the opposite occurs *in vitro*. As a result of culturing cells immediately on the probe surface, the concentration of released analytes will be high in the area immediately surrounding the probe and drop in abundance as distance away from the probe increases (Figure 3.6B). It is hypothesized that this enrichment zone around the *in vitro* probe increases the observed signal in smaller containers –where random motion of analytes will result in diffusion back towards the probe as opposed to diffusing away.

Figure 3.7 illustrates the empirical relationship between the size of the sampling environment and the magnitude of observed release. In the largest environment, a 150

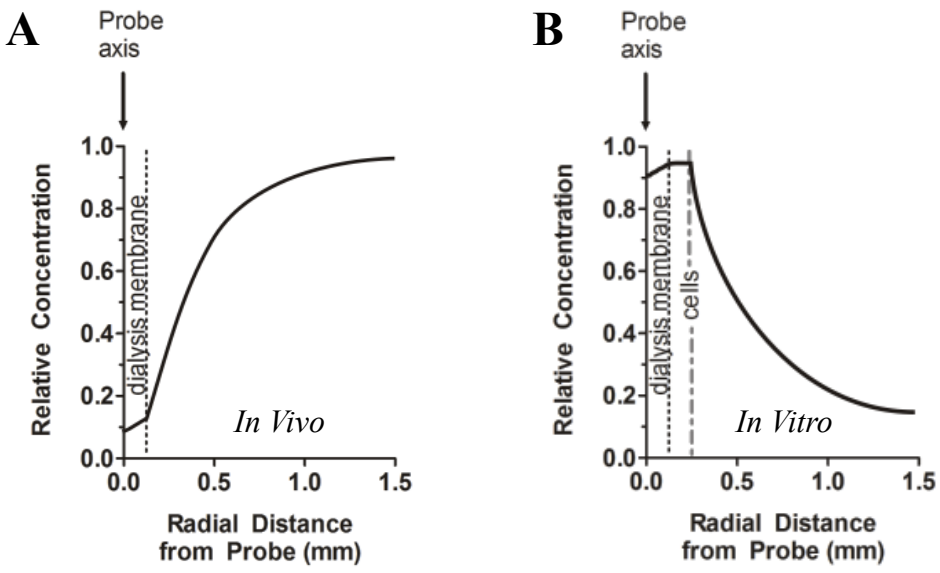

Figure 3.6. Approximate analyte concentration plotted as a function of distance away from an *in vivo* probe (A). Adapted from reference 23. Hypothesized analyte concentration plotted as a function of distance away from an *in vitro* probe with cells cultured on the membrane surface (B).

mL beaker (grey), the magnitude of release appears much lower for all of the amino acids. This phenomena is likely not due to an actual decrease in stimulation response, but rather to a more complete dissipation of released analytes into the bulk surrounding fluid. The opposite is true in the smaller environment, 0.7 mL eppendorf tube (white). The increase in abundance of analyte in response to the K^+ stimulation appears dramatically higher in the smaller environment for all amino acids except taurine, where there is no significant difference between the 0.7 mL and 1.5 mL sized environments. This observed increase in smaller environments is attributable to a containment of the enrichment zone depicted in Figure 3.6B, an effect in which analytes that would normally dissipate into the surrounding matrix are ultimately sampled due to the close proximity to the probe. It should be noted that with both glycine and taurine, there are large standard deviations. Though it cannot be said for certain why this is, it likely stems from biological variability between the probes. A one-tailed,

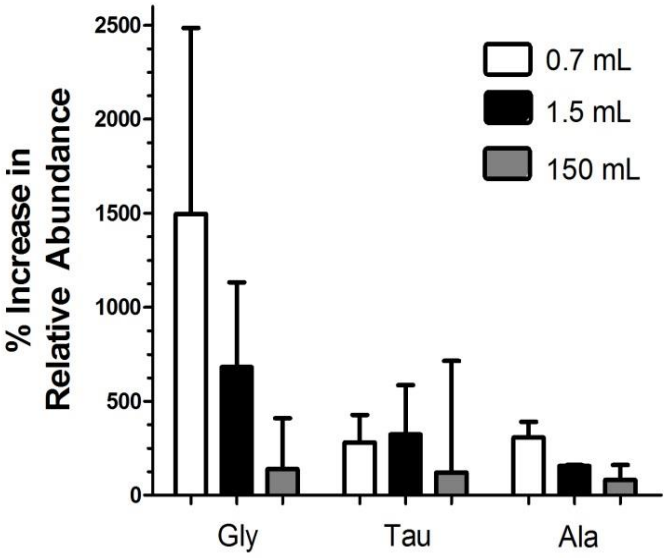

Figure 3.7. K^+ stimulations were performed on *in vitro*-microdialysis probes in three different sized environments: 0.7 mL eppendorf tube (white), 1.5 mL eppendorf tube (black), and a 150 mL beaker (grey). For the majority of released analytes, the percent increase in relative abundance after a stimulation was much higher in smaller containers and dropped dramatically as the size of the environment was increased. The only amino acid which did not follow this trend was Taurine. Standard deviation error bars are included. Experiment was performed in triplicate (N=3).

unpaired, p-test was performed on each of the data sets to determine whether the large percent increase in relative abundance depicted in the smaller containers was significantly higher than those obtained in 150 mL. The high standard deviations in glycine and taurine contributed to an overall insignificance of the change (p-values of 0.151 and 0.407, respectively). A p-value of less than 0.05 is necessary to claim the difference is significant with a 95% confidence interval and less than 0.1 with a 90% confidence interval. The decrease in alanine, which follows the same trend but exhibits smaller variability between trials, is a statistically significant change with a p-value of 0.061.

To illustrate how the size of the sampling matrix influences the temporal dynamics of sampling, the baselines of 3 different stimulations (each performed in a different size container) are plotted for Alanine (Figure 3.8). As the volume gets larger the observed magnitude of release is diminished when compared to the smaller volume. The duration of stimulated release

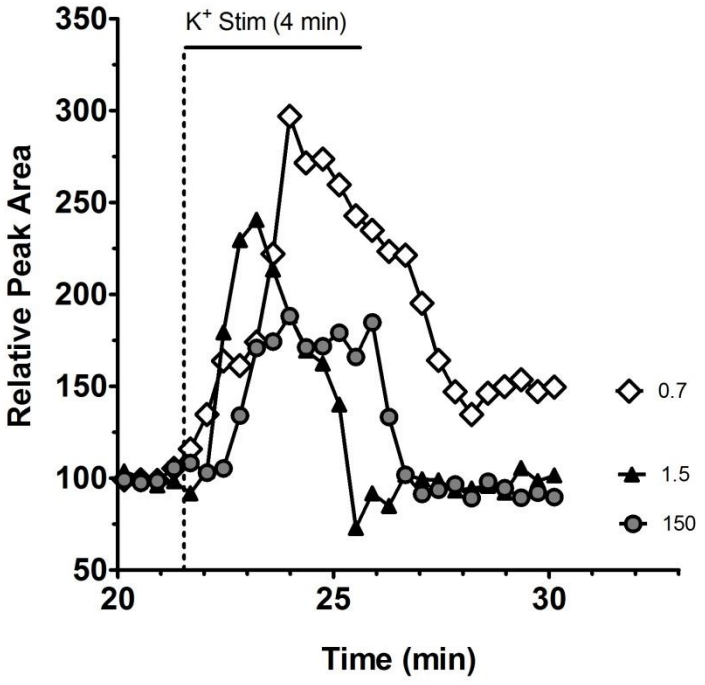

Figure 3.8. Baseline plots for the peak area of Alanine in response to a K^+ stimulation performed in a 0.7 mL eppendorf tube (white), 1.5 mL eppendorf tube (black), and 150 mL beaker (grey). Peak areas have been normalized to an initial basal value of 100.

also demonstrates a dependence on container size, increasing with decreasing volume of the container. In the smaller environment (white) the stimulation evokes a much wider span of release than in the larger environment (gray). This trend is supports the hypothesis that there is some degree of diffusion back towards the probe in smaller containers that would dissipate in larger environments. This causes a perceived increase in the span over which analytes are being released at elevated levels.

3.5 Conclusions

Variables affecting the performance and accuracy of *in vitro*-microdialysis have been investigated. To confirm that cells were maintaining maximum viability over the longest period of time, they were exposed to several buffer systems and analyzed using Trypan Blue viability assay. Both cell suspensions and adhered monolayers were used, demonstrating that aCSF was suitable for keeping the cells alive for several hours. Effects of the cell-sustaining media were ruled out as influencing the signal intensity during stimulation experiments. Technique parameters, such as temperature dependence and size of the sampling environment, were also studied to determine their impact on signal intensity and duration. It was found that high-K^+ stimulated release of amino acids from the cultured astrocytes was a temperature dependent process, with significantly larger basal and stimulated release levels at 37ºC when compared to room temperature. The size of the container also had a marked influence on signal dynamics. In smaller environments, diffusion of analytes back towards the probe results in heightened signal intensity and prolonged release patterns under stimulation. Through these dynamics, Taurine seemed to behave differently than the other amino acids indicating perhaps a

different mechanism of release. Future work could focus on probing these more specific biological pathways.

Chapter 4

Biological Models for *in Vitro*-Microdialysis

4.1 Summary

In this work, a variety of new cell models were tested for compatibility with *in-vitro* microdialysis. Though immortalized astrocyte cells were employed in initial studies to develop and characterize this new sampling platform, it was believed that the model would be amenable to nearly any other adherent cell line of interest. Three types of cell lines have been successfully cultured over the sampling region of the microdialysis probe: 3T3 fibroblasts (ATCC CCL-92), RBL-2HC fibroblasts (ATCC CRL-2256), and C8-D1A astrocytes (ATCC CRL-2541). These cell types were individually cultured and confirmed with imaging after a viability assay employing fluorescein diacetate (FDA).

Several co-cultures were also established on the probe. These include: 3T3-RBL, RBL-astrocyte, and astrocyte-neuron models. Presence of both cell types was confirmed using specific antibody labeling in conjunction with fluorescence confocal microscopy. Efforts to initiate a co-culture across the membrane barrier (one cell type internal, the other external), so that cells could be in chemical, but not physical, contact, were unsuccessful. Thus, co-cultures were established as two cell-types in physical contact on the external probe surface. One cell type that was unable to adhere to the microdialysis probe was a line of primary adipocyte cells obtained from human fat tissue. It is believed that these cells failed to adhere because of the large cell body size. Release of analytes from one cell type, mast cell model RBLs, were analyzed by coupling the *in vitro*-microdialysis probe online to a high-speed CE instrument (data not shown). The analyte fingerprint was different than those previously obtained with astrocytes, demonstrating the utility of *in vitro*-microdialysis for studying a variety of models.

4.2 Introduction

Chapters 2 and 3 described the development and characterization of *in vitro*-microdialysis coupled with high-speed capillary electrophoresis (CE) for the fast analysis of non-electroactive analytes released from cells in culture. In these initial stages, the platform was exclusively used to analyze release events from astrocyte cells, a central nervous system (CNS) cell primarily selected for its robustness and ease of handling. Astrocytes also proved to be an interesting model from a physiological stand-point because, as described in Section 1.3, though they are now believed to play a significant role in brain function, there is still relatively little known about them. The literature gaps surrounding astrocytes are largely due to the fact that they communicate primarily with non-electroactive molecules which are more difficult to measure on small and fast scales. The ability of *in vitro*-microdialysis to monitor non-electroactive analytes with sub-minute temporal resolution makes it a useful tool to identify fast release dynamics that are lost with previous techniques.

Though we have, until now, focused on the utility of *in vitro*-microdialysis with the astrocyte model, it is amenable to a wide variety of other physiological models. Mast cells, basophil granule-containing cells found in connective tissue, are important in allergic and inflammatory responses such as asthma, mastocytosis, and autoimmune diseases.[127] Because of difficulties stemming from isolation and culture of degranulating cells, many mast cell studies employ an immortalized cell line that closely resembles mast cells to represent the inflammation response. Among the most common is a continuous rat cell line, RBL-2H3. Like mast cells, RBLs have high affinity immunoglobulin E (IgE) receptors and, as a result, these cells have been extensively used

for studying IgE and receptor interactions, signaling pathways for degranulation, and to test mast cell stabilizers.[128] Additionally, one of the primary analytes released from RBL cells in the inflammation response is histamine, an amino acid neurotransmitter, making this cell type another physiologically interesting model for *in vitro*-microdialysis analysis.

The goal of this work was to identify additional cell models, such as RBLs, that are compatible with the *in vitro*-microdialysis sampling platform. Compatibility was assessed based on two primary factors: adherence to the probe membrane and propagation across the sampling region surface, both of which were confirmed by imaging viable cells across sampling region. For single cell type models, the fluorescein diacetate (FDA) viability assay was used, while co-cultures required specific antibody labeling. Each of the explored models have unanswered questions regarding release pathways and/or communication mechanisms that *in vitro*-microdialysis could possibly elucidate. However, these biological experiments are beyond the scope of this work so they are presented only as a basis for experimental design and offered as a route for future study.

4.3 Materials and Methods

4.3.1 Chemicals and Reagents

Reagents. Dulbecco's modified Eagle medium (DMEM), alpha-MEM, fetal bovine serum (FBS), penicillin-streptomycin (10,000 U/mL), and gentamicin (10 mg/ml liquid) were purchased from Invitrogen Molecular Probes (Eugene, OR). Trypsin solution (10×, 5 g/L trypsin, 2 g/L EDTA·4NA, 8.5 g/L NaCl), phosphate-buffered saline (PBS), bovine serum albumin (BSA), and Triton X-100 were purchased from Sigma-Aldrich (St.

Louis, MO). Neurofilament-L Rabbit mAb Alexa Fluor 594 conjugate (Product #8743), GFAP Mouse mAb Alexa Fluor 488 conjugate (Product #3655), DAPI (Product #4083), and normal goat serum were purchased from Cell Signaling Technology (Danvers, MA). Formaldehyde (16%, methanol free) was purchased from Polysciences, Inc. (Warrington, PA).

Buffers and Solutions. Fluorescein diacetate (FDA; Sigma-Aldrich Co, St. Louis, MO) stock solution was prepared by dissolving 1 mg/mL in fresh acetone and was stored in a glass culture tube, covered with tinfoil, in a refrigerator. All solutions were prepared in deionized water (Milli-Q, 18.2 MΩ; Millipore, Bedford, MA) and filtered (0.22 μm) unless otherwise described.

4.3.2 Cell Line Establishment and Culturing

Type-1 astrocyte cell clones, C8-D1A, were obtained (CRL-2541, ATCC, Manassas, VA) in a 1 mL frozen vial. These astrocytic clones were originally collected from 8 day old mouse cerebella after spontaneous transformation (no addition of carcinogens or oncogenic viruses) and are considered to be an immortalized line since they were maintained for more than 100 generations after cloning.[98] Confluent monolayer cultures were sustained in 25 cm^2 tissue culture flasks (T25) containing 9 mL of high glucose DMEM supplemented with 10% fetal bovine serum and 110 μL gentamicin. Cultures were kept at 37°C in an incubator and were passaged using a ratio of 1:6 every 3-4 days with 0.25% trypsin/0.03% EDTA solution.

A line of contact inhibited fibroblasts, 3T3, had been previously purchased (CCL-92, ATCC, Manassas, VA) and established by colleagues in the lab of Dr. Christy Haynes. Cultures were initiated from a vial of cryopreserved cells (1×10^6 cells/mL, in

DMEM + 10% DMSO). Confluent monolayers were sustained in T25 culture flasks containing 9 mL of high glucose DMEM supplemented with 10% fetal bovine serum and 110 μL gentamicin. Cultures were kept at 37°C in an incubator and were passaged using a ratio of 1:6 every 2 days with 0.25% trypsin/0.03% EDTA solution.

A line of basophil fibroblasts, RBL-2HC, had been previously purchased (CRL-2256, ATCC, Manassas, VA) and established by colleagues in the lab of Dr. Christy Haynes. Cultures were initiated from a vial of cryopreserved cells (1×10^6 cells/mL, in DMEM + 10% DMSO). Confluent monolayers were sustained in T25 culture flasks containing 9 mL of high glucose DMEM supplemented with 10% fetal bovine serum and 110 μL gentamicin. Cultures were kept at 37°C in an incubator and were passaged using a ratio of 1:6 every 3-4 days with 0.25% trypsin/0.03% EDTA solution.

Neuronal cells, HCN-1A, were purchased (CRL-10442, ATCC, Manassas, VA) and received in a 1 mL frozen vial. The neuronal clones were originally obtained from the cortical tissue of an 18-month-old female suffering from unilateral megalencephaly, a condition characterized by the overgrowth of all or part of the cerebral hemispheres.[129] Confluent monolayer cultures were sustained in T25 culture flasks containing 9 mL of high glucose DMEM supplemented with 10% fetal bovine serum and 110 μL gentamicin. Cultures were kept at 37°C in an incubator. HCN-1A cells are reported to double every 96-120 hours and will need to be passaged every 3-4 days at a ratio of 1:3.[130] Cells only remain viable for up to 2 passages after cryo-preservation.

Human pre-adipocytes were obtained by the Kirkland lab (Mayo clinic, Rochester, MN) from patients undergoing gastric bypass surgery. Confluent monolayers were sustained in T25 culture flasks containing 9 mL of alpha-MEM supplemented with

fetal bovine serum (10%) and penicillin-streptomycin (1%). Cultures were kept at 37°C in an incubator and were passaged using a ratio of 1:4 every 3-4 days with 1× trypsin.

4.3.3 Co-Culture Propagation on Probe Surface

Exterior surface. Monolayers of cells were grown directly on the surface of microdialysis membranes by serially seeding suspensions of cells into a flask containing several probes. To accelerate the time it takes for cells to propagate across the entire sampling region, this process was performed with 5 passages of cells, resulting in a culturing time of approximately 2-3 weeks. If only one cell type was desired, probes were removed at this stage for imaging analysis. To initiate a co-culture, a second cell type was seeded directly onto probes already containing a confluent monolayer of the base cell type. This second cell layer was seeded on 3 times, so the probes remained in culture an additional 1-2 weeks. Base cell type for each co-culture model was determined by preferential adherence to the probe and/or physiological properties (i.e. astrocytes outnumber neurons 9:1 in the brain[131], therefore, astrocytes were used as the base cell).

Flow-through injection method for interior co-culture. Two syringes (500 µL, Hamilton, Reno, NV) were equipped with unions and 40 µm i.d. × 360 µm o.d. fused silica capillaries (Polymicro Technologies, Phoenix, AZ). One contained TRIS and the other a 3T3 cell suspension (1×10^5 cells/mL in DMEM). The probe was perfused with TRIS at a rate of 40 µL/hr for approximately 10 minutes using a microsyringe pump (Harvard Apparatus Inc., Holliston, MA, USA). At this point, the inlet of the probe was switched to the cell suspension (also flowing at 40 µL/hr) for a 2 minute duration, after which TRIS was reconnected. The cell-containing probe was then transferred

immediately to a T25 culture flask with DMEM and placed in an incubator held at 37ºC until ready for imaging.

4.3.4 Imaging

Single cell type. Medium was removed from the culture flask and cells were rinsed three times with PBS. The final PBS rinse was left in the flask. 2 µL of FDA stock solution was added for each 1 mL of PBS for a final amount of 2 ug/mL FDA. The solution was incubated for 15 minutes at 37ºC. Cells were imaged immediately on an Olympus IX81 inverted microscope equipped with a DSU confocal unit (Olympus, Allentown, PA).

Co-Culture. Probes with an established co-culture on the exterior of the probe surface were removed from medium and fixed in a solution of formaldehyde (4% in PBS) for 15 minutes. Fixative was aspirated and the probes were rinsed three times in PBS for 5 minutes. After the final PBS rinse was aspirated, nonspecific binding was blocked by incubation in a blocking buffer (1× PBS/ 5% normal goat serum / 0.3% Triton X-100) for 60 minutes. While probes were incubating in blocking buffer, primary antibody was prepared in antibody dilution buffer (1× PBS / 1% BSA / 0.3% Triton X-100). Primary antibody (100 µL aliquot) and DAPI (2.5 µL of 5 mg/mL stock) were added to 10 mL of antibody dilution buffer. Blocking solution was aspirated, the prepared antibody dilution buffer was added, and probes were incubated overnight at 4ºC. Cells were rinsed three times with PBS (5 min) to remove antibody buffer. The final rinse was left in the flask for imaging. Cells were imaged on a Nikon A1R-MP multi-photon confocal microscope connected to an upright FN1 microscope with a PlanApo LWD 25× water-immersion objective (Nikon Instruments Inc, Melville, NY).

4.4 Results and Discussion

4.4.1 Cell Line Models for *In Vitro*-Microdialysis

The utility of *in vitro*-microdialysis as tool for monitoring release of non-electroactive analytes from cell culture is contingent on the ability to culture cells on the surface of the microdialysis membrane. Initial work, presented in Chapters 2 & 3, focused exclusively on culturing an immortalized line of astrocytic cell clones, C8-D1A. In order to prove that cells were adhering to the probe, covering the surface area of the sampling region, and retaining physiological viability, a series of images was collected over 3 weeks using a fluorescence confocal microscope depicting an increase in cell density across the membrane (Figure 2.2). *In vitro*-microdialysis probes produced by culturing cells on the membrane surface were then successfully used to monitor release of amino acids in response to a K^+-stimulation with 20 second temporal resolution.

To establish that *in vitro*-microdialysis is amenable to a variety of additional physiological models, several different cell lines were cultured on the surface of the probe. When cells adhered, probes were subjected to the same viability imaging experiments previously performed on C8-D1A cells. Information for the types of cells cultured on microdialysis probes can be found in Table 4.1. The first three cell types (3T3, RBL-2HC, and C8-D1A) were employed both as single cell-type cultures on the microdialysis surface and in co-culture models. The human neuron line (HCN-1A) was *only* employed as the second cell-type in a co-culture model. Independent growth on the probe was never attempted due to the inability to propagate and the fragility of the cells. Recent findings suggest that neuron cultures are actually more stable and present

enhanced synaptic function when co-cultured with glia cells as opposed to individually.[132]

Table 4.1. Summary of cell information for models employed with in vitro-microdialysis.

Cell Name	Organism	Tissue	Type	Morphology	Properties
3T3	Mouse	Embryo	Fibroblast	Fibroblast	Adherent
RBL-2HC	Rat	Peripheral Blood	Basophil	Fibroblast	Adherent
C8-D1A	Mouse	Brain, cerebellum	Astrocyte	Neuronal	Adherent
HCN-1A	Human	Brain, cortical	Neuron	Neuronal	Adherent
---	Human	Fat	Adipocyte	Pre-differentiated	Adherent

The last cell type in Table 4.1, human adipocytes, were a primary line of cells obtained during human gastric bypass by Dr. James Kirkland's lab at the Mayo Clinic in Rochester, MN. Rachel Harstad, a colleague in the lab of Dr. Michael Bowser, attempted to culture these cells on microdialysis probes as an alternate model for *in vitro*-microdialysis. Of all the cells described above, this was the only cell line which failed to be cultured on the membrane surface of the probe (unpublished data). It's believed that the incompatibility of these cells with the *in vitro*-microdialysis model is due to the large size of the cell body. Even in the pre-differentiated state, prior to accumulation of lipids, the cell body is approximately 100 µm in diameter. This is significantly larger than the cell body size of other attempted models (which range from 20-30 µm) and is half the

diameter of the probe membrane (200 μm). This line of human adipocytes was successfully cultured on a flat membrane surface of the same material, regenerated cellulose, which is further evidence that the failure of adipocytes to adhere to the microdialysis probe was a size-based issue (unpublished data). Currently, size is the only determinant influencing whether a line of adherent cells can be cultured on the surface of the microdialysis probe.

For the three cell-types that did adhere to the microdialysis probe (3T3, RBL-2HC, and C8-D1A) initial experiments sought to assess whether cells on the membrane surface were not only adhered but retained physiological viability. To test this, an FDA imaging assay was used. As discussed in Chapter 2, FDA is a non-fluorescent precursor and is often used for assessing cell viability since it only generates a fluorescent signal once it has been taken up by mammalian cells and the acetate groups are removed by active intracellular enzymes.[100]

Figure 4.1 shows a series of images depicting three cell types adhered to the microdialysis membrane surface. All three cell types, 3T3 (A-B), RBL-2HC (C-D), and C8-D1A (E-F), exhibit fluorescence on the membrane surface, indicating the presence of live-cells.

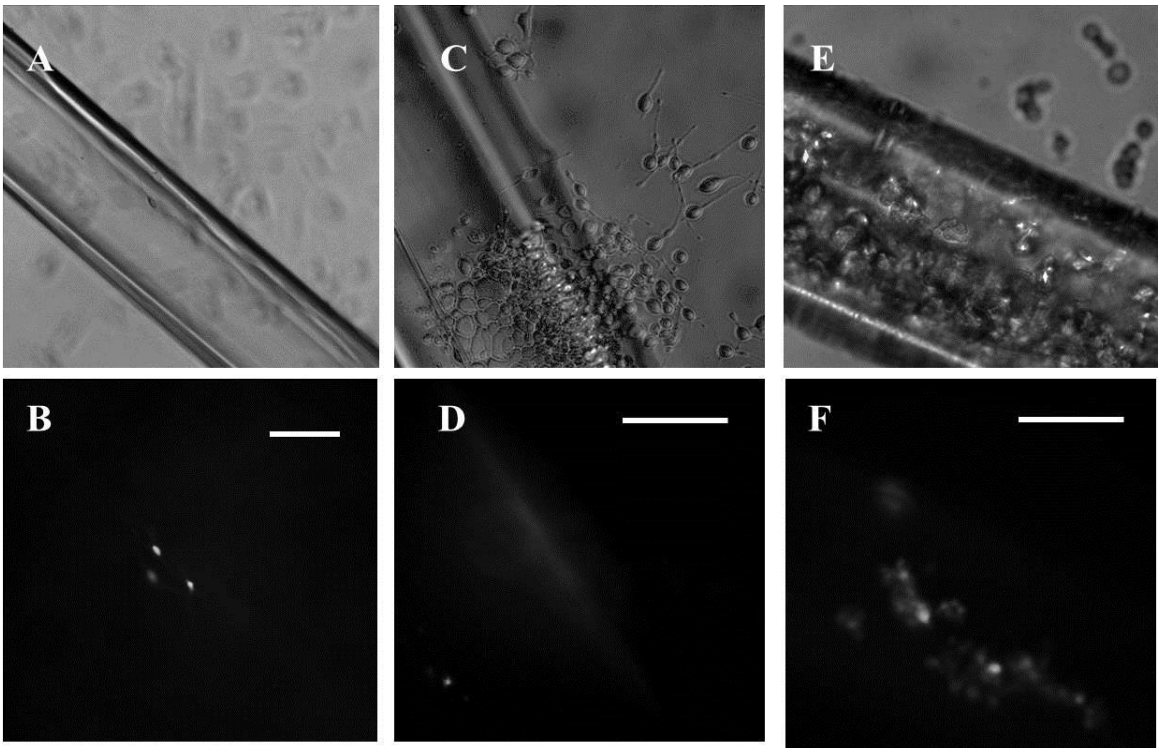

Figure 4.1. Images depicting 3T3 (A-B), RBL-2HC (C-D), and C8-D1A (E-F) cells on the surface of microdialysis probe membranes. Grayscale images on the left were collected in brightfield, while black-and-white images on the right were collected through a green fluorescence filter cube (ex. filter: 460-500 nm with 505 nm dichroic; em. filter: 520-600 nm). Fluorescent cells indicate viability via uptake of FDA. White scale bars are sized to 100 μm.

Adherence to the membrane, as opposed to the flask wall, was confirmed by varying the focal point at the time of imaging. This is more clearly illustrated in Figure 4.2, which uses a brightfield image and two fluorescent images of the same RBL-2HC cells at different focal planes. Here, a brightfield image exposes cells both on the

membrane surface and flask wall (A) while fluorescent images are collected in varying focal planes between the top of the membrane surface (B) and the flask wall (C). It is using this method that cells were initially confirmed to be adhering to the probe.

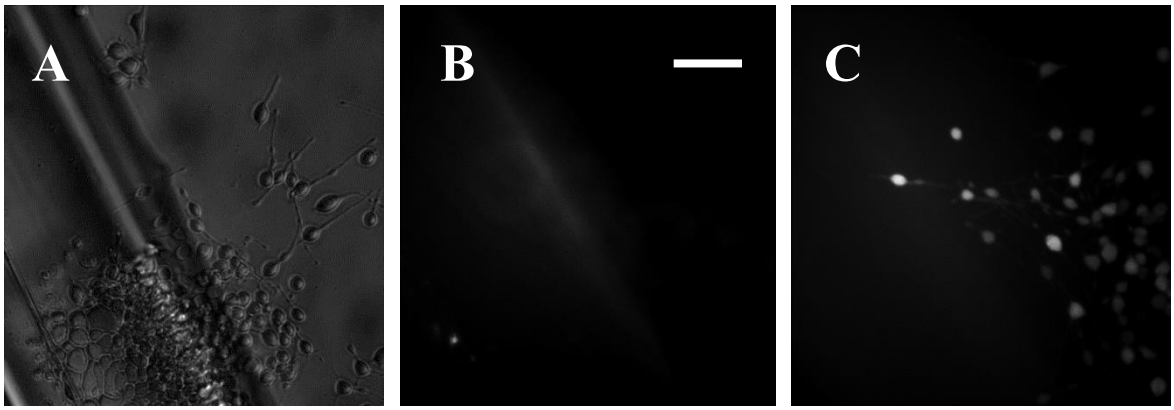

Figure 4.2. Series of images depicting RBL-2HC adhered to both the flask wall and the microdialysis probe. All cells, despite location of adherence, can be visualized using brightfield filter settings (A). In green fluorescence settings, the focal point was varied to focus on cells adhered to the top surface of the membrane (B) and down to the flask wall (C). White scale bar is representative of 100 μm.

It should be noted that while these initial imaging experiments were important in establishing the ability of a cell line to adhere to the microdialysis probe, they were not designed to illustrate coverage across the sampling region. These probes were imaged after approximately 1 week in culture on a basic microscope. The purpose was to determine whether or not a cell line simply appeared to adhere to the surface, upon which further experimentation could progress.

To more clearly illustrate coverage cross the sampling region, probes with RBL-2HC and C8-D1A cells were imaged by collecting z-stack images with GFP filter settings on a confocal fluorescence microscope. Combining these images into a 3D composite allows cells to be visualized around the curvature of the sampling region (Figure 4.3).

Both RBL-2HC (A) and C8-D1A (B) cells demonstrate the ability of healthy, viable cells to grow around the membrane surface of a microdialysis probe. Complete coverage of the sampling region (with approximately 80% confluency and higher) can be achieved by serially seeding the cells onto the probes in culture over a span of 3 weeks. The successful propagation of both cell types across the probe surface is an important finding because it implies the applicability of this platform for a variety cell models.

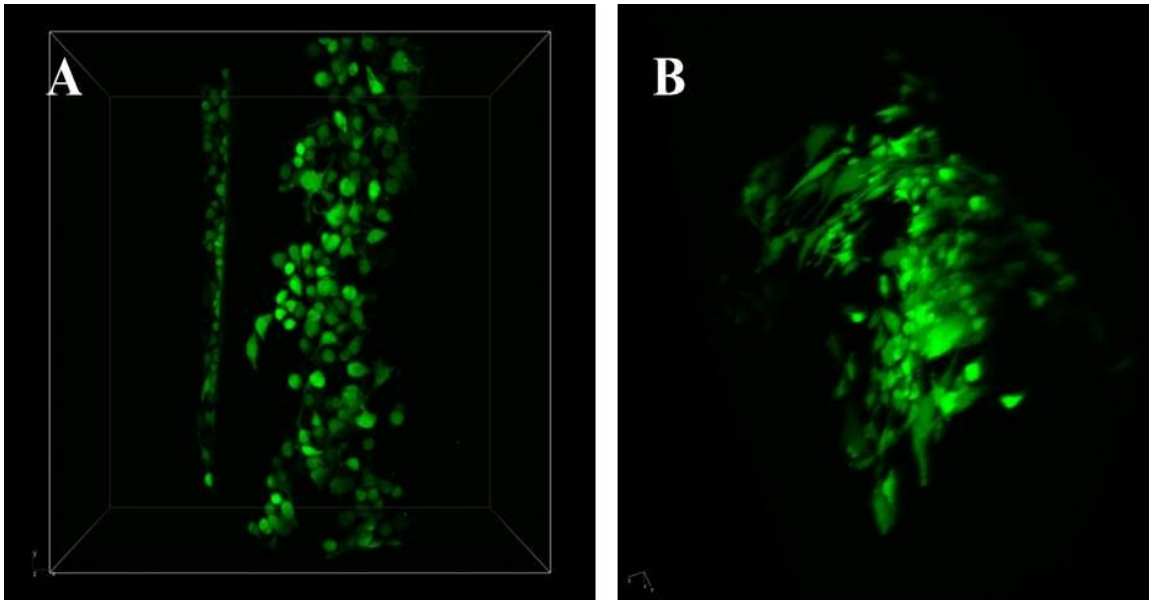

Figure 4.3. 3D composite images of RBL-2HC (A) and C8-D1A (B) cells across the curved microdialysis membrane surface. Composites were created from z-stack images collected under GFP filter settings with a confocal fluorescence microscope.

4.4.2 Mast Cell Co-Culture Models

Two co-culture models employing RBL cells as a model for mast cell physiology were explored: RBL-3T3 co-culture and RBL-astrocyte co-culture. Both models, given further experimentation, could provide biological insights not currently observable with alternative techniques. Though these biological implications will be discussed as

evidence for why certain models were selected, the biological questions they are structured to answer are beyond the scope of this work which was to identify a method for establishing and characterizing different types of co-cultures on microdialysis probe surfaces.

RBL-3T3 Fibroblast. Asthma is a chronic lung disease that causes inflammation and narrowing of airways. Mast cells are known to play an important role in the immunopathology of asthma through the release of cytokines and proteases.[133] Mast cells are able to permeate structures in asthmatic airways, such as the airway smooth muscle (ASM), where they reside in a highly activated state.[134] In this way, there is interaction between mast cells and airway smooth muscles in an asthmatic state. There are several ways researchers have hypothesized that this cell-cell interaction between ASM and mast cells influences asthmatic events. One explanation is that ASM provides the correct microenvironment for the differentiation and activation of mast cells.[135] It has also been discovered that mast-cells produce histamine, prostaglandin D_2, and cysteinyl leukotrienes, all of which are spasmogens of airway smooth muscle.[136] Taken together, these studies demonstrate that the infiltration of mast cells into ASM is a functionally important process, though specific mechanisms remain unclear.

One fundamental question still unanswered is whether physical contact between ASM and mast cells is a necessary component of this interaction, or if chemical contact is all that is required for the interactions to take place. *In vitro*-microdialysis offers a unique approach to address this question. In addition to culturing a single cell type monolayer on the exterior surface of the probe membrane, an alternate cell type could be cultured on the interior surface of the membrane. This design would allow the cells to be in chemical

contact, via the porous dialysis membrane, while remaining physically separated by the barrier (Figure 4.4).

Due to the inherent difficulties of establishing a cell culture on the interior of a microdialysis probe, the initial model for a physically-separated co-culture model required simplicity. 3T3 fibroblasts (ATCC, CCL-92) were used as a simplified model for ASM physiology. It has been demonstrated that when cultured with ASM cells, 3T3's improve the survival rate of ASM in culture and promote the physiology of ASM models. Recent studies confirm that ASM-3T3 microtissues behave in a highly physiological manner and compare favorably to other models of ASM contraction.[137] They are, thus, a suitable platform for assessing ASM function in health and disease. In a similar manner, RBL-2H3 cells which are a very robust and easy cell line to work with were employed as a mast cell model.

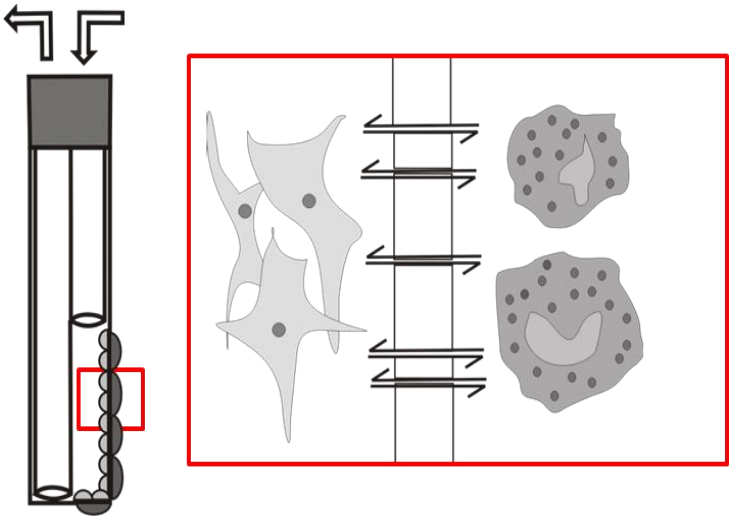

Figure 4.4. *In vitro*-microdialysis schematic for physically barricaded co-culture models. Here, the interior cell (light grey) represents 3T3 fibroblasts and the exterior cell (dark grey) represents RBL-2HC cells. Cells are able to communicate chemically due to transport of small molecules through the porous membrane, which simultaneously serves to block the cell types from physical contact.

The cell body size of 3T3s is slightly smaller than RBLs so they were selected as the interior cell. Since both cell types had already previously been cultured on the surface

of a microdialysis probe, the difficulty with this approach was establishing a monolayer of 3T3s adhered on the interior surface of the membrane. A flow-through method was developed where a suspension of 3T3 cells was pumped into the inlet of an already constructed and conditioned probe. In an attempt to prevent cells from adhering in the inlet and outlet of the probe, a segmented flow-injection was performed whereby TRIS was pumped through the probe before and after the cell suspension (Section 4.3.3). Probes were imaged after 24 hours using the FDA viability assay to look for live-cells adhered to the interior probe membrane (Figure 4.5). An intense background fluorescent signal from scatter across the capillary made it difficult to distinguish any cells adhered to the surface. However, cells that would have adhered to the membrane surface should still have been visualized and they were not.

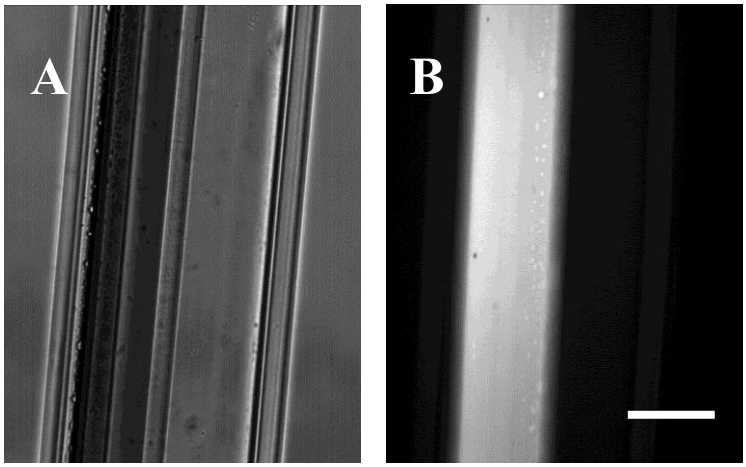

Figure 4.5. Brightfield (A) and fluorescent (B) images collected 24 hours after a 3T3 cell suspension was perfused through a microdialysis probe. Due to the intense background fluorescence of the capillary, it is difficult to distinguish any cells on the surface. White scale bar is representative of 100 μm.

To test whether viable cells could successfully be introduced into the probe lumen via the syringe pump, a solution of FDA labeled cells in suspension was pumped into a probe while under a microscope. The stream of cell-containing perfusate could then be visualized in real time as it exited the inlet capillary within the membrane interior.

Several time-progressed images from this experiment were compiled and are presented in Figure 4.6. Prior to the cell suspension reaching the probe lumen (A) no cells and/or debris are visible. Within a minute of the suspension reaching the probe (B) a small number of particles could be visualized exiting the capillary and sticking to the lower edge of it. Within several minutes (C) a large cloud of particles was seen entering the probe lumen. With reference to the scale bar (100 μm) the observed particles are too small to be considered intact cells. Though the interior diameter of the union and capillary (40 μm) is large enough to accommodate intact cell bodies, it is believed that cells are ruptured during the process of forcing the suspension out of the syringe and into the union.

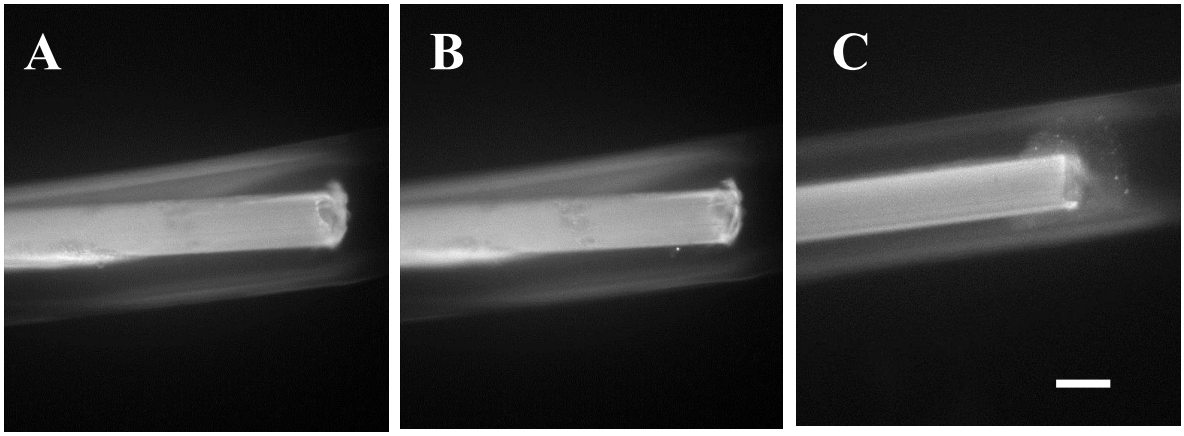

Figure 4.6. Series of images captured before (A) and during (B-C) the flow-through injection of FDA labeled 3T3 cells into a microdialysis probe. Within a minute of pumping the cell suspension into the probe (B) a few small particles were visualized exiting the capillary. Within several minutes (C) a large cloud of cell debris could be seen entering the probe lumen. White scale bar represents 100 μm.

An alternative approach to flowing cells into the interior surface of a microdialysis membrane would be to grow cells inside the probe membrane *prior* to final construction of the probe. This is in contrast to the flow-through method which involved pushing cells into a completed and conditioned probe. There are several hurdles with this

approach that need to be addressed such as bacteria prevention during the post-cell-growth probe construction and ensuring cells do not also get on the exterior of the membrane during the culture phase. Though this route has not yet been attempted, it offers potential and is proposed here as an option for future work.

The inherent difficulties of producing a physically barricaded co-culture, with one cell-type on the interior surface of a microdialysis probe, prevented further pursuit of this model. Instead, an alternative RBL co-culture model was explored with astrocytes. Here, the cells would not need to be physically separated from each other in order to answer biologically relevant questions, so a simpler co-culture scheme could be employed.

RBL-Astrocyte. It has been reported that the viability of mast cells *in vitro* can actually be supported, if not improved, by co-culturing with astrocytes.[138] Recent findings reported that when co-cultured in the presence of astrocytes, mast cells demonstrated time-dependent increases in the release of histamine and leukotrienes as well as intracellular Ca^{2+} levels and cytokine production.[139] The release of these mediators is believed to result in the activation of both mast cells and astrocytes, leading to a cascade of inflammatory agents exchanged between the cells. The initialization of this process appears to be dependent on activation through CD40-CD40L, a process requiring physical contact.[17] For this reason, a mast cell-astrocyte co-culture model where both cell types were cultured on the exterior of the probe could be useful in further elucidating the mechanism of communication and activation between these cells.

To establish the co-culture on the microdialysis probe, a confluent monolayer of astrocytes was grown as the base layer prior to seeding RBL-2HC basophils onto them as a mast cell alternative. It is currently unclear whether or not using RBLs as the base layer

would influence the physiology of the model. The co-activation between these cells has been reported in both the thalamus and perivascular sites, but it is unclear which cell type predominates.[17] It would be beneficial for future experiments, focusing on targeting biological pathways, to investigate the co-culture in both orientations. For our purposes, astrocytes were selected as the base cell because of their tendency to reach greater confluency across the sampling region.

After several weeks in culture, a specific antibody labeling scheme was developed to illustrate the presence/coverage of both cells. DAPI (4', 6-diamidino-2-phenylindole) was selected as a generic nucleus stain, allowing the cell body of any cell type to be visualized. An astrocyte-specific antibody label targeting glial fibrillary acidic protein (GFAP) was employed to aid in the exclusive visualization of astrocytic cell membranes. Cells were fixed and labeled directly on the microdialysis probe and imaged with confocal microscopy (Figure 4.7). By using these two labels in conjunction with one another, astrocytes could be identified by locating areas where a DAPI stained nucleus was surrounded by a green-stained membrane (4.7 A.i) while mast cells could be identified by locating areas where a DAPI stained-nucleus was not surrounded by green-strained membranes (4.7 A.ii). Coverage of cells across the sampling region was confirmed by overlaying the fluorescent images with a brightfield scan (4.7 B) and by rotating a 3D composite image in space (4.7 C-D) to visualize adherence of cells around the curvature of the membrane.

Though coverage of the cells is high (100% confluency) it was difficult to conclusively identify which cells were astrocytes and which cells were RBLs. There was a high amount of green fluorescence present along the probe surface either because there

were too many astrocytes, the layer of astrocytes was too thick, or the green signal had too much noise. This, in combination with no specific antibody label for the RBL cells, makes it nearly impossible to articulate the ratio/distribution of cell types. To better determine the ratio of cells in the co-culture a better labeling scheme would need to be employed that enables the specific labeling of RBLs as well as astrocytes. Additionally, probes could be removed from astrocyte culture and a smaller amount of GFAP antibody could be used to reduce background noise in the green fluorescence channel. Lastly, the experiment could be repeated with RBLs as the base cell to see if and how the cell coverage of each cell is dependent on the layering.

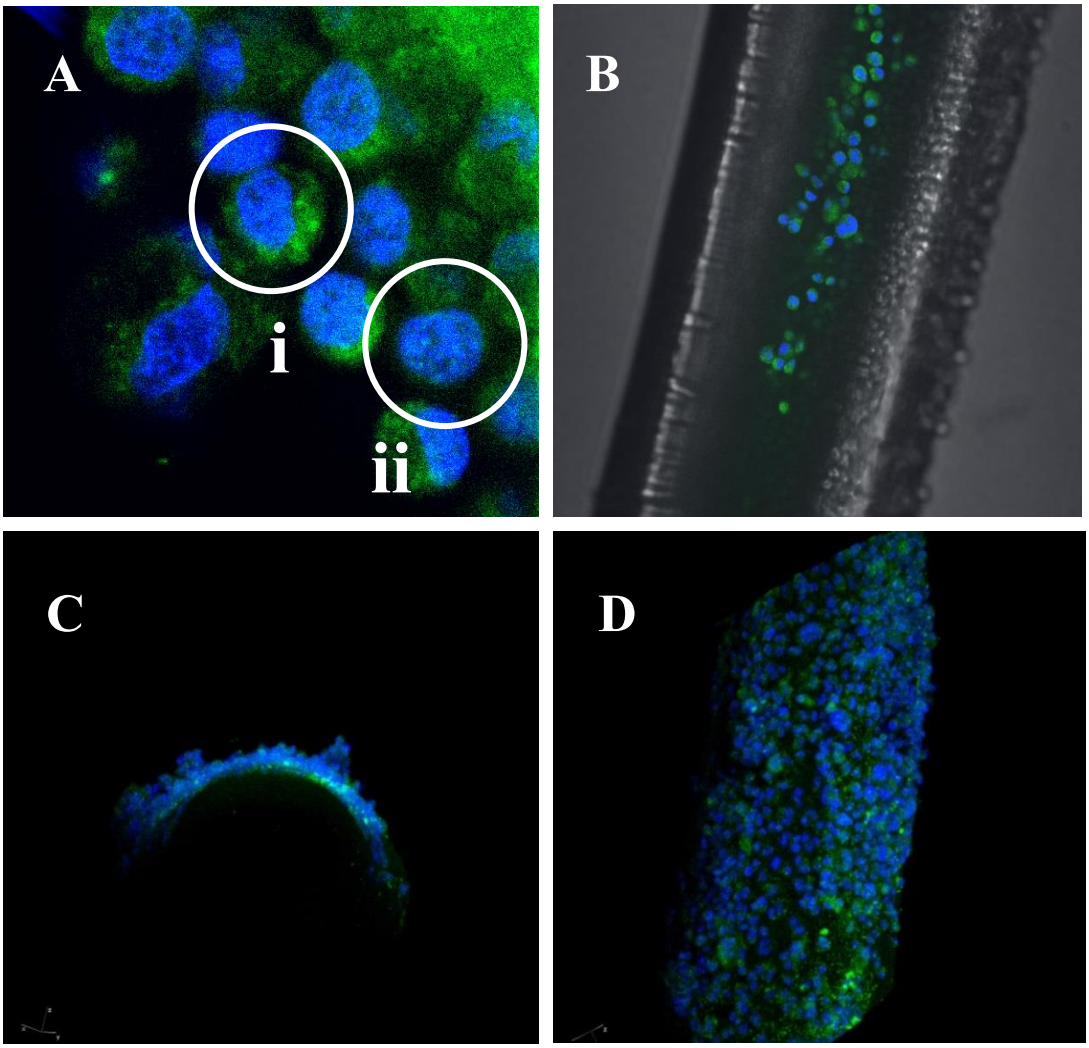

Figure 4.7. Fluorescent images of RBL-astrocyte co-culture after specific antibody labeling of cell nuclei with DAPI (blue, both cells) and GFAP (green, astrocyte-specific). Astrocytes are identified as areas where both green and blue fluorescence are co-localized (A.i) while RBLs are identified as areas where only a blue nucleus is seen without a surrounding green membrane (A.ii). Cells can be visualized on the probe by overlaying fluorescent and brightfield channels (B). The growth of cells along the curvature of the probe (C) and down the sampling region (D) are more clearly illustrated with 3D composites composed from z-stack images collected with a fluorescence confocal microscope.

4.4.3 Astrocyte/Neuron Co-Culture

The past decade has seen a burgeoning in the literature pertaining to astrocyte-mediated neuron function.[140-143] The ability of *in vitro*-microdialysis to monitor dynamic changes of non-electroactive analytes on a sub-minute time scale could provide insights to a variety of communication mechanisms between these two cells. For example, one of the mechanisms by which astrocytes have been shown to interact with neurons is through the efflux of astrocytic intracellular Ca^{2+} into gap junctions, where it is then taken up by neurons.[144-146] These junctions are believed to control the conduction of Ca^{2+} waves through astrocytes and neurons. Since elevated levels of extracellular Ca^{2+} are associated with increased transmitter release, it is believed that experiments employing gap junction blockers should result in a decrease in the relative abundance of transmitters from basal values.

Though this experiment is difficult to perform via traditional methods, the set-up would be quite simple for *in vitro*-microdialysis. A pharmacological blockage of gap junctions in the neuron-astrocyte co-culture could be performed by exposing the probe to a solution containing one of several gap junction inhibitors (octanol, sodium propionate, and halothane) previously been used for this purpose.[147] How the abundance of transmitters responds could then be monitored with high-speed capillary electrophoresis, offering temporal insights to this pathway which are currently unknown. Though the purpose of this work was not to answer these types of questions, it is offered to demonstrate the applicability of *in vitro*-microdialysis to biologically pertinent models and as a suggestion for future work.

The inability of mature neurons to divide and propagate makes them difficult to culture from immortalized lines. Typically, primary cell cultures are employed. However,

several immortalized neuron lines are available for purchase through the American Type Culture Collection (ATCC) which remain viable for approximately 2 passages after cryo-preservation. The HCN-1A neuron line has been frequently employed to model neuronal networks in immortalized culture and was employed in the described co-culture model.

The co-culture was initiated as a confluent monolayer of C8-D1A astrocyte cells, maintained as detailed in previous sections. When the HCN-1A neuron culture reached confluency, neurons were subsequently plated onto the astrocyte culture with the same seeding density used for passaging (1:3 split ratio, approximately 1×10^6 cells/25 cm^2). Astrocytes were selected as the base cell for a variety of reasons. First, they simply outnumber neurons by large numbers in brain tissue. Though the exact ratio can change depending on the brain region, it is most often estimated that astrocytes outnumber neurons by a 10:1 ratio.[15] Second, it has been demonstrated that astrocyte promote neuron survival, synapse formation, and plasticity.[20] Therefore, by having them as the base cell, astrocytes can better support neuron function once they are introduced.

When the culture reached maturity, fluorescence confocal microscopy was used to classify the cell types by morphology and immunoreactivity, as well as assess the coverage of confluent co-cultured monolayers in the flask and on a probe (Figure 4.8). The nuclei of both cells were stained with a DAPI nucleus stain (4.8 A) enabling identification of all cells across the sampling region. Astrocytes were labeled with an astrocyte-specific GFAP antibody label (green) while neurons were labeled with a neuron-specific neurofilament antibody label (red). Both labels were detected using fluorescence confocal microscopy (4.8 B), enabling identification of areas where neurons

adhered to the base layer of astrocytes. Cell coverage across the sampling region (4.8 C) and around the curvature of the membrane surface (4.8 D) was also visualized.

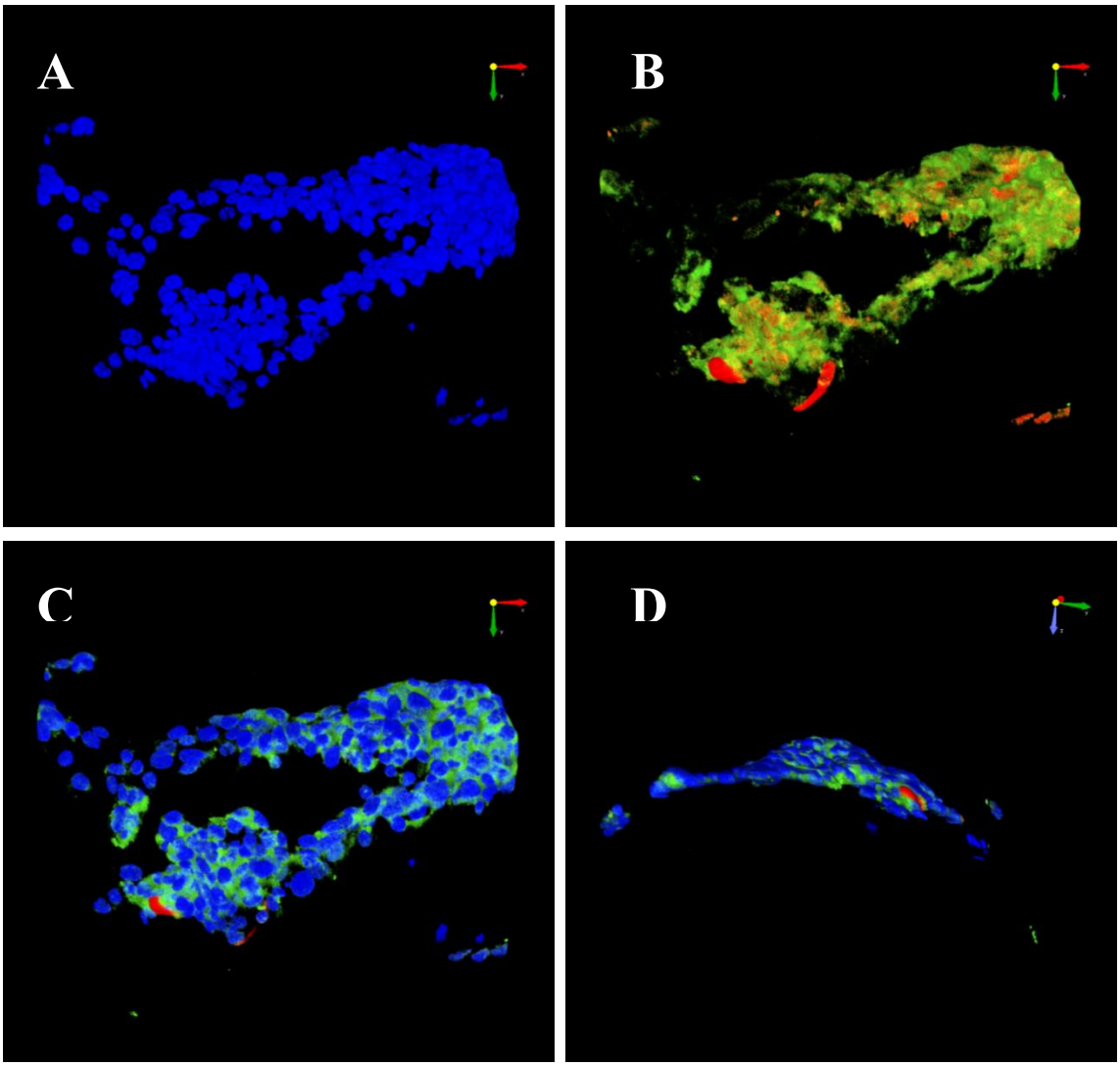

Figure 4.8. Fluorescent images of astrocyte-neuron co-culture after specific antibody labeling of cell nuclei with DAPI (blue, both cells), GFAP (green, astrocyte-specific), and neurofilament (red, neuron-specific). DAPI stained nuclei show cell coverage, regardless of cell type, across the sampling region (A). Using specific labels for both astrocytes and neurons enables identification of areas where both cells are co-localized (B). The growth of cells along down the sampling region (C) and around the curvature of the probe (D) are clearly illustrated with 3D composites composed from z-stack images collected with a fluorescence confocal microscope.

These images demonstrate, for the first time, that a co-culture of two cell types can be cultured and confirmed by specific antibody labeling on the surface of an *in vitro*-microdialysis probe. It is especially important that neurons, which are notoriously difficult to sustain in culture, were confirmed on the probe surface. This result represents not just the utility of *in vitro*-microdialysis for neuroscientific applications between astrocytes and neurons, but holds promise for many other co-culture models of adherent cell lines.

4.5 Conclusions

This work established the applicability of *in vitro*-microdialysis for a variety of alternative physiological models. Several different cell types were cultured as individual monolayers on the surface of the microdialysis membrane: 3T3 fibroblasts, RBL-2HC basophils, C8-D1A astrocytes. Adherence of viable cells was confirmed by labeling cells with FDA, an often employed viability assay, and imaging them under a microscope. The only cell type which failed to adhere was a primary line of human adipocytes. Failure of these cells to adhere to the probe was likely due to the large size of the adipocytes (cell bodies upwards of 100 μm, which is nearly half the outer diameter of the microdialysis membrane). To date, large cell body size is the only known attribute of an adherent cell line that limits compatibility with *in vitro*-microdialysis. Several co-culture models were also explored. Attempts to establish a physically blocked co-culture, by culturing cells on the interior and exterior of the membrane, were unsuccessful due to difficulties flowing and growing cells inside of the probe structure. Successful co-culture platforms were developed by culturing both cell types in contact with one another on the exterior surface

of the probe. This was done successfully for two different models: RBL-astrocyte and astrocyte-neuron, both of which were confirmed by specific antibody labeling.

4.6 Acknowledgements

I'd like to thank the lab of Dr. Christy Haynes for providing access to cell lines employed in their labs, Rachel Harstad for the work she did attempting to culture human adipocytes on microdialysis probes and for allowing the work to be discussed within the context of this chapter, and Audrey Meyer, a PhD recipient from Dr. Haynes' lab, for working with me to develop the physically blocked co-culture model between RBLs and astrocytes.

Chapter 5

Monitoring Glutamate and Aspartate Continuously Using Microdialysis and Micro Free Flow Electrophoresis (μFFE)

5.1 Summary

Microdialysis was coupled directly to a micro free flow electrophoresis (μFFE) device as a step towards continuously monitoring the dynamics of non-electroactive analytes release from cultured cells. Microdialysis and μFFE are continuous techniques, so direct coupling does not require segmentation of a continuous dialysate stream into discrete injections. A mismatch in common operating flow-rates of the two techniques led to serious backpressure issues within the separation device, hampering efforts to successfully apply this technique to *in vitro*-microdialysis probes. Here, traditional bare microdialysis probes were used with amino acid standards to optimize the separation conditions for aspartate and glutamate. Two separation modes were employed in the microfluidic device: zone electrophoresis (μFFZE, which will throughout this chapter be referred to simply as μFFE) and isoelectric focusing (μFFIEF). Both modes ultimately enabled separation of aspartate and glutamate from other amino acids and by-products of the labeling reaction, while achieving resolution between aspartate and glutamate. Though further optimization and characterization work is required, μFFIEF appears to offer better resolution of the analytes and it is suggested as the route for future *in vitro*-microdialysis work with micro free flow electrophoresis.

5.2 Introduction

The advantages of microdialysis have been well documented in the literature for decades.[4, 10, 100] The small size of the probe sampling region, relative ease and customizability of probe construction, continuous flow, and aqueous compatibility make it an almost ideal tool for *in vivo* and *in situ* measurements. However, microdialysis is still fundamentally limited by several physical constraints; one of the most often cited is the limited time resolution. Traditionally, the majority of microdialysis experiments were performed by collecting fractions of bulk fluid containing the desired analytes. This offline methodology results in temporal responses of upwards of 10 minutes.[108] Since *in vivo* dynamics occur on a significantly faster timescale than these measurements allow, efforts in the past decade have focused on improving the time limitations of microdialysis.

Temporal resolution can be dramatically improved by coupling probes directly with an online analytical separation.[11] When microdialysis is coupled directly to an analytical separation, the temporal resolution is primarily determined by the analysis time, sample volume requirements, and detection limits of the instrument as well as longitudinal diffusion through system tubing. The small sample volume requirement and fast analysis times of capillary electrophoresis (CE) make it an ideal analytical separation for online analysis with microdialysis sampling. Coupling to high-speed CE has brought analysis times down to the sub-minute timescale.[111] More recently, the development of flow-segmented plugs has brought temporal resolution down to 0.1-2 seconds.[148] This technique, however, depends on the difficult task of collecting and storing nanoliter sized fractions of aqueous sample.

Microdialysis is a continuous sampling technique, therefore, it's analysis by the majority of analytical techniques requires mechanisms to segment the continuous stream into discrete injection plugs. Though progress has been made, as demonstrated by the impressive achievement of sub-second temporal resolution using specialized flow-segmented plugs, they still result in the very challenging aspect of handling said fractions. This work describes an alternative route of fast analysis for microdialysis samples. A microdialysis probe is connected to a capillary that is fed directly into the inlet channel of a micro free flow electrophoresis (μFFE) device, a microfluidic chip which conducts electrophoretic separations continuously in a planar channel, allowing continuous analysis of microdialysis samples.

Free flow electrophoresis is separation technique in which analytes are separated continuously in an electric field applied perpendicular to a pressure-driven buffer flow.[149] The technique found widespread use for sample clean-up devices, separation of cells and subcellular particles, and preparative methods.[150-152] The first μFFE device was developed in 1994; made from silicon, the dimensions of separation channel are comparable to what is still used today (10 mm width × 50 mm length × 50 μm depth).[153, 154] The miniaturization of the device minimizes the high amounts of joule heating exhibited in other FFE devices, requires smaller amounts of reagent and sample, and decreases analyte residence time.[155] Another key advantage to this design is the integration of an online detection system, allowing separations to be monitored in real time.[156] By coupling the *in vitro*-microdialysis probe to a fabricated μFFE device, temporal response is limited to the exposure time of a charge-coupled device (CCD) camera, 100 ms.

5.3 Materials and Methods

5.3.1 Chemicals and Reagents

Reagents. Amino acid standards were purchased from Sigma-Aldrich (St. Louis, MO). Sodium tetraborate decahydrate was purchased from Fisher Scientific (Pittsburgh, PA). Carrier ampholytes (30% solution, pH range: 2.5-5.0) were purchased from GE Healthcare Life Sciences (Pittsburgh, PA).

Buffers and Solutions. All solutions were prepared in deionized water (Milli-Q, 18.2 MΩ; Millipore, Bedford, MA) and filtered (0.22 μm) unless otherwise described. Borate run buffer contained borate (100 mM) and was adjusted to pH 10.5. Acetate run buffer contained acetate (50 mM), Triton X-100 (300 μM), and was adjusted to pH 4.0. HEPES run buffer contained HEPES (25 mM), Triton X-100 (300 μM), and was adjusted to pH 7.0. CAPS run buffer contained CAPS (25 μM), either Triton X-100 (300 μM) or methanol (20%), and was adjusted to pH 10.0. Derivatization solution was prepared fresh daily by dissolving 40 mM NBD-F (TCI America, Portland, OR) in methanol and diluting 1:1 with 500 μM HCl yielding a final solution of 20 mM NBD-F/250 μM HCl in 50% methanol which was degassed under vacuum for 2 minutes. Artificial cerebral spinal fluid (aCSF) was prepared with NaCl (145 mM), KCl (2.7 mM), MgSO4 (1.0 mM), and CaCl2 (1.2 mM).

5.3.2 Device Fabrication

The design of this device was conceived by Dr. Nic Frost and all fabrication steps for this work were performed by Matthew Geiger, both colleagues in the lab of Dr. Michael Bowser. The fabrication process is similar to previously described devices[18, 157, 158], and is discussed here briefly. Photolithography was used in a three-step

succession to etch (1) an 85 µm capillary channel, (2) 30 µm deep electrode channels, and (3) a 10 µm deep separation bed into two 1.1 mm borofloat glass wafers (Precision Glass & Optics, Santa Ana, CA). When combined, these mirror-image wafers form a capillary channel (125 µm deep, ~250 µm wide), electrode channels (40 µm), and a separation channel (10 µm deep, 1 cm wide, 2.5 cm long). To make the electrodes, a Temescal electron beam evaporator was used to deposit a 150 nm thick layer of Ti then a 150 nm thick layer of Au to one of the wafers. Unwanted Ti and Au were removed with another photolithography step. Access holes (1 mm) were drilled into the second wafer and a 90 nm thick layer of amorphous silicon was deposited. A Karl Suss SB-6 wafer bonder (Munich, Germany) was used to align and anodically bond the wafers (900 V, 3 h, 450ºC, 5 µbar). Nanoports (Upchurch Scientific, Oak Harbor, WA) were attached over the access holes using epoxy rings. Lead wires were connected to the electrodes using a conductive silver epoxy. A fused silica capillary (20 µm i.d., 150 µm o.d., Polymicro Technologies, Phoenix, AZ) was inserted while the device was heated on a hot plate to ~150ºC and under vacuum. After insertion, the capillary was bonded in place by pulling Crystalbond 509 through the remaining space between the capillary and the channel. Residual amorphous silicon was removed from the channels by perfusing the chip with NaOH (1 M).

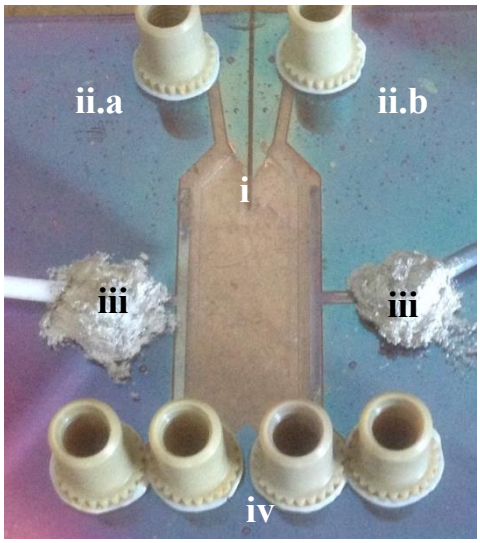

Figure 5.1. An image of a micro free flow electrophoresis device detailing the inlet capillary (i), run buffer inlets (ii.a-b), electrodes (iii), and buffer outlets (iv).

The image of a completed device is shown in Figure 5.1. The inlet capillary (i) is inserted into the device through a narrow capillary channel. Buffer inlets (ii.a-b) are attached at the top of the device in a slightly deeper section of the mask leading down to the electrodes (iii). At the bottom of the device, buffer exits through several outlet streams (iv).

5.3.3 Interfacing Microdialysis and µFFE

Offline. Amino acid standards ranging in concentration from 10-40 µM were reacted with NBD-F (5 mM) in a 1:1:1 solution of methanol, Borate (100 mM, pH 10.5), and aCSF. The solution was mixed for 1 minute on a vortex, degassed, and heated at 80ºC for 5 minutes. This offline derivatization solution was pumped at a rate of 25 µL/hr into a carrier capillary with a microsyringe pump (Harvard Apparatus Inc., Holliston, MA, USA). The carrier capillary (40 µm i.d. × 360 µm o.d.) transported the labelled amines to the inlet capillary (20 µm i.d. × 360 µm o.d.) of the µFFE device.

Online. A schematic diagram of *in vitro*-microdialysis coupled online to a µFFE device is presented in Figure 5.2. Briefly, microdialysis probes were perfused with aCSF at a rate of 25 µL/hr with a microsyringe pump. Dialysate was transported in a 40 µm i.d. × 360 µm o.d. fused silica capillary to a 250 µm i.d. stainless steel cross (Valco Instruments Co. Inc, Houston, TX) where it was mixed with a 5 µL/hr stream of borate buffer and a 5 µL/hr stream of derivitization solution. The labeling reaction progressed as it traveled through a 90 cm capillary of 75 µm i.d. × 360 µm o.d. dimensions. The rate of the reaction was accelerated by heating a 66 cm portion of this capillary to 80ºC by passing the capillary through tubing that was circulated with water from a heating bath (NESLAB EX-7 Digital one heating bath circulator, Thermo, Newington, NH). The

length of the reaction capillary and flow rates of solutions resulted in a 5 minute reaction time allowing the reaction to go to completion. The reaction capillary was connected to the μFFE inlet capillary via a home-built capillary connector (PTFE tubing, Grace Davison Discovery Science, Deerfield, IL).

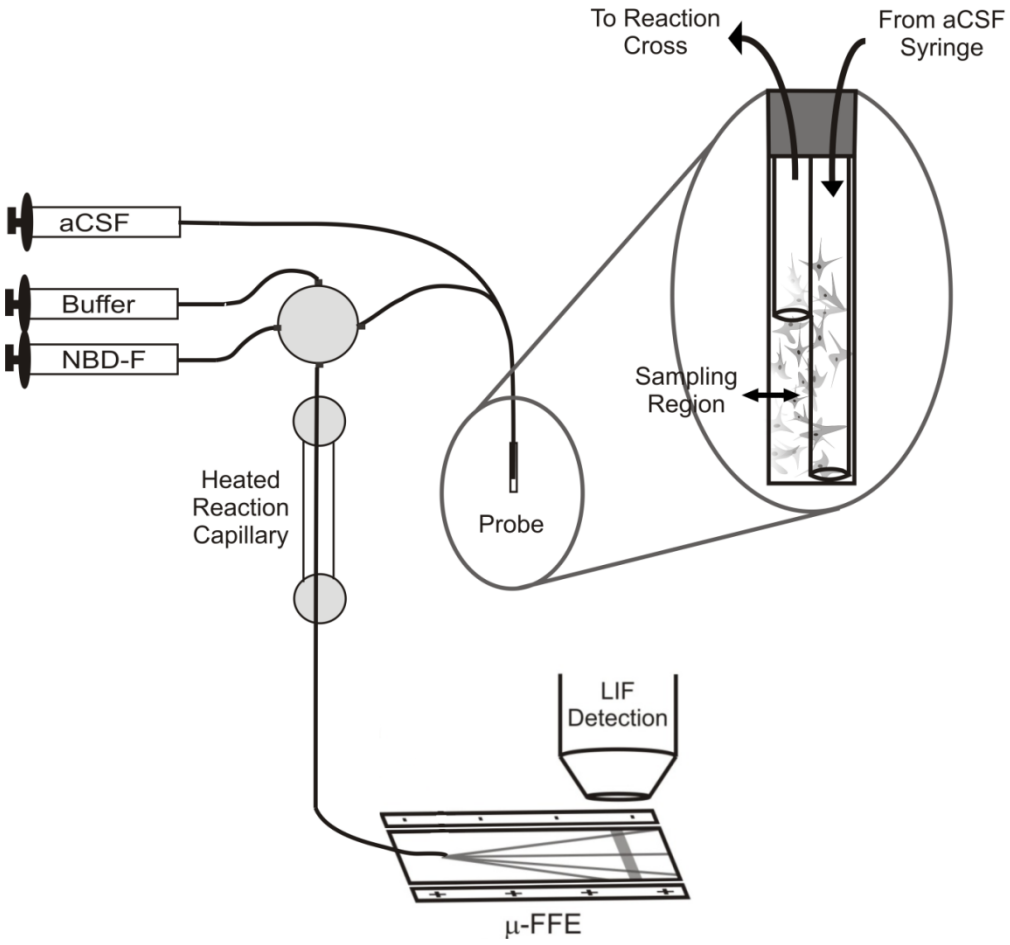

Figure 5.2. The schematic diagram of *in vitro*-microdialysis coupled online to a micro free flow electrophoresis (μFFE) device. Small molecules diffuse across the sampling region of the dialysis membrane and are transported to the reaction cross in the dialysate. 7-Fluoro-4-Nitrobenzo-2-Oxa-1,3-Diazole (NBD-F) is used to fluorescently label primary and secondary amines. The reaction takes place in a heated reaction capillary. Injections into the μFFE device are performed continuously by streaming the fluorescently labeled dialysate directly into inlet capillary of the device through a capillary connector. Laser induced fluorescence (LIF) detection is implemented at the near the bottom of the separation channel.

5.3.4 Device Operation

Micro Free Flow Zone Electrophoresis. Separation buffer was pumped into the μFFE device at a total rate of 0.5 mL/min, corresponding to a flow of 0.25 mL/min into each buffer inlet using a syringe pump (Harvard Apparatus, Holliston, MA). A voltage ranging from 50-200 V was applied to the left electrode (Figure 5.3 ii) during analysis, while the right electrode was held at ground. The production of an electric field across the separation bed deflected analytes laterally (Figure 5.3 iii) according to their size and charge. Both online and offline analysis were performed in this mode.

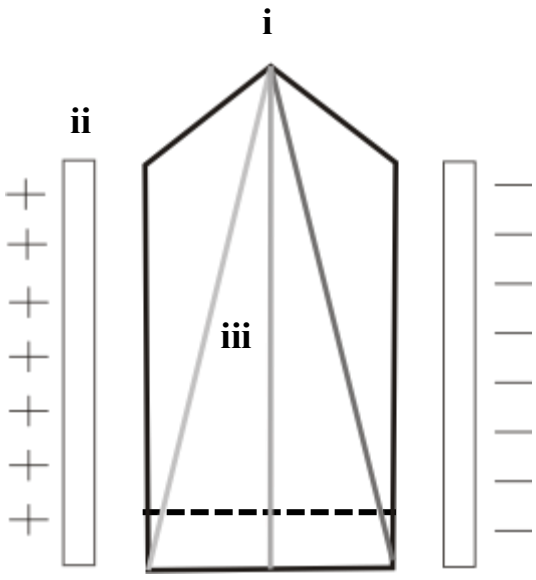

Figure 5.3. A separation schematic within a micro free flow electrophoresis device. Sample is introduced through the capillary inlet at point (i) located at the top of the separation channel. Application of a positive voltage on the left electrode (ii), while the right electrode is held at ground, produces an electric field across the separation channel. This causes lateral deflection of analytes by size and charge across the separation channel (iii). LIF detection is performed near the exit of the separation channel towards the bottom of the chip (dotted line).

Laser-induced fluorescence (LIF) detection and imaging was performed near the exit of the separation channel towards the base of the device. Analytes were excited with the 488 nm emission line of a 150 mW argon-ion laser (Melles Griot, Carlsbad, CA) expanded into a 2.5 cm × 150 μm line. Fluorescence was captured with an AZ100 stereromicroscope (Nikon Corp., Tokyo, Japan) mounted with a Cascade 512B CCD camera (Photometrics, Tucson, AZ)

and equipped with a GFP bandpass emission filter cube (Nikon Corp, ex. filter: 450-490 nm, em. filter: 500-550 nm, and dichroic mirror: 495 nm cut-off). Acquisition rate for detection was 500 ms. To minimize background signal, the entire instrument setup was enclosed in a black, rubberized fabric containment (Thorlabs, Newton, NJ). Cutter 5.0[99] was used to process line scans.

Micro Free Flow Isolelectric Focusing. Two different ampholyte-containing separation buffers were pumped into the μFFE device at a total rate of 0.5 mL/min, corresponding to a flow of 0.25 mL/min of each buffer into one of the two buffer inlets using a syringe pump (Harvard Apparatus, Holliston, MA). The ampholyte buffer pumping into inlet i.a was pH adjusted to 5.0, while the ampolyte buffer pumping into inlet i.b was pH adjusted to 2.5. A voltage ranging from 50-200 V was applied to the left electrode during analysis, while the right electrode was held at ground. The production of an electric field across the separation bed induced the formation of a pH gradient across the channel according to the isoelectric points of the ampholytes. Only offline analyses were performed. Detection set-up and collection was identical to that described for the zone electrophoresis mode.

5.4 Results and Discussion

5.4.1 Separation Optimization

A variety of separation conditions were evaluated in an attempt to optimize the separation of aspartate and glutamate. These analytes were selected because they are doubly negative at high pH's while other amino acids remain singly negative. It was hypothesized that the additional charge on these analytes would cause them to more

readily separate from other amino acids. To maintain consistency with high-speed CE results, the borate buffer used for previous studies (100 mM, pH 10.5) was employed. The high ionic concentration and pH of this buffer resulted in the generation of extremely high current (5 mA) in the μFFE device, preventing analysis at useful voltages. A series of other buffers spanning a variety of pH values were explored, and it was found that acetate buffer (pH 4.0) and CAPS buffer (pH 10.0) gave the most promising results. Figure 5.4 shows an electropherogram of two standard amino acid mixtures, one containing a glutamate spike (black; 20 μM glutamate, 10 μM aspartate, taurine, and serine) and the other an aspartate spike (gray; 20 μM aspartate, 10 μM glutamate, taurine, and serine) while using an acetate run buffer. Though there was enough resolution between the target analytes that peak identification could be made with spiked samples, the peaks were not baseline resolved from each other, other amino acids (taurine and serine), nor the reaction byproducts peak (observable 6-7 mm).

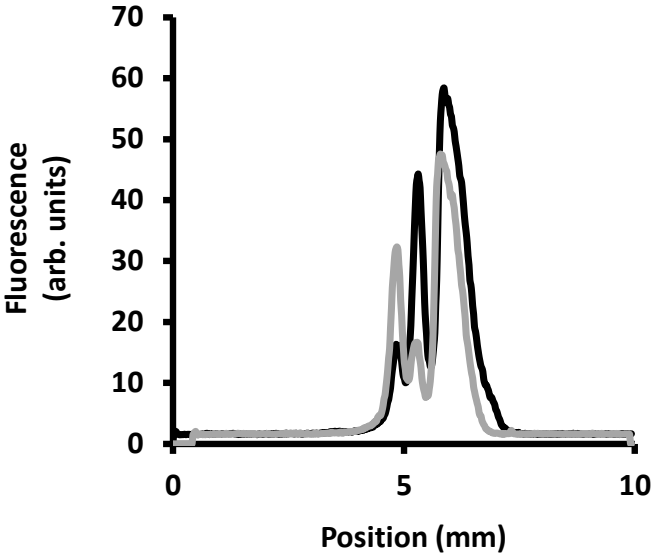

Figure 5.4. μFFE separation of glutamate spiked (black) and aspartate spiked (gray) amino acid standard solutions using acetate run buffer. These conditions resulted in a separation lacking baseline resolution from labeling reaction byproduct peak (large peak at 6-7 mm) and co-elution of target analytes with singly charged amino acids.

In an attempt to increase the resolution between glutamate, aspartate, and the other reaction products, a higher pH CAPS buffer (pH=10.0) was employed. At this pH

glutamate and aspartate are doubly negative while other amino acids are singly negative. This should encourage their resolution in the separation window. Figure 5.5 A shows the separation of an offline-reacted glutamate-spiked amino acid sample. Note that the sharp peak to the far right of the separation window is due to an imperfection in the microfluidic device. The large peak at around 8 mm is a combination of the labeling reaction byproduct and amino acids. It is believed that both aspartate and glutamate are present in the small shoulder to the right of the peak, though peak identification was difficult to achieve. Triton X-100 is an additive intended to reduce bubble formation within the device by lowering the surface tension of the separation buffer.[159] In this case, the lack of resolution exhibited in these conditions is likely attributed to the formation of Triton X-100 micelles in the run buffer, causing many of the analytes to migrate together. When an alternative CAPS buffer was made substituting methanol for Triton X-100, to

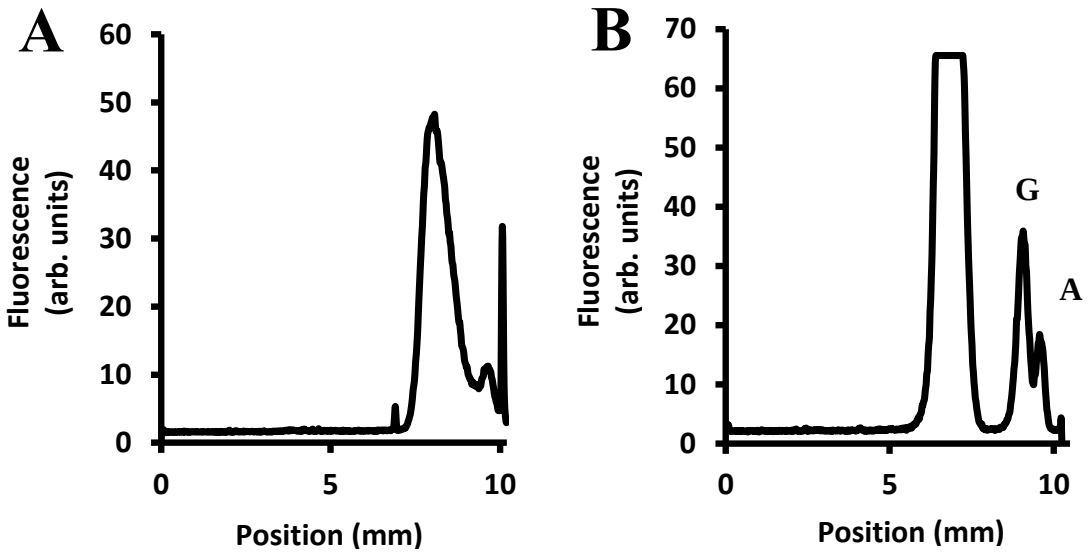

Figure 5.5. Glutamate spiked samples run with CAPS with Triton X-100 (A) and CAPS with Methanol. (B). The sharp peak at the far right of the window in (A) was due to an imperfection in the chip and is not representative of any legitimate signal. The lack of resolution between aspartate and glutamate in (A) was believed to have been due to the formation of micelles in the run buffer. By switching Triton X-100 for methanol, resolution between the analytes and byproduct peak was regained (B).

eliminate the possible presence of the micelles while still aiding in the production of smaller electrolysis bubbles, significantly better resolution was achieved (Figure 5.5 B). Glutamate and aspartate (9 mm) are baseline resolved from the labeling byproduct peak (6-7 mm). Other amino acids (taurine and serine) co-migrated with the labeling byproduct peak. Peaks were identified by running spiked variations of the offline-reacted amino acid mixture. Though the substitution of Triton X-100 for methanol in the CAPS buffer offered increased resolution between the target analytes and both the labelling byproduct peak and other amino acids, resolution between glutamate and aspartate was sacrificed. The inability to fully resolve glutamate and aspartate from both the labelling byproduct peak and other amino acids prevented further analysis with zone electrophoresis in the μFFE device.

5.4.2 Isoelectric Focusing

Isoelectric focusing (IEF) is an alternative mode of separation in which a pH gradient is established perpendicular to the buffer flow, achieved by the addition of ampholytes to the run buffer. Upon application of a voltage, the ampholytes migrate laterally in the separation channel according to their specific isoelectric point (pI) the point at which the net charge of the analyte is zero.[160] As opposed to zone electrophoresis, which separates analytes based on their size to charge ratio, IEF separates analytes based on their isoelectric points. Other studies performing IEF in a μFFE device empirically determined that analytes with a minimum difference in pI of 0.4 could be resolved, though the theoretical minimum difference in pI was calculated to be

even lower at 0.23.[161] Though the described device operated with a higher electric field (~200 V/cm) a significantly larger pH gradient (2.5-11.5) was also employed, suggesting that similar results could be achieved by performing IEF in our μFFE device. Specifically, IEF could be used to enhance the aspartate and glutamate separation from other amino acids, because the isoelectric points of aspartate and glutamate are more acidic than other amino acids (Table 5.1).

Amino Acid	pI
Aspartic Acid	2.77
Glutamic Acid	3.22
Cysteine	5.07
Serine	5.68
Valine	5.96
Glycine	5.97

Table 5.1. Isoelectric points for aspartic acid, glutamic acid, and several other amino acids. Previous reports have found that a minimum difference of 0.23 is necessary to theoretically separate two analytes using IEF in a μFFE device. Glutamic acid and aspartic acid are shown here to have a difference in pI of 0.45, implying their ability to resolve under these conditions. Furthermore, aspartic acid and glutamic acid are several pI units more acidic than other amino acid, suggesting that they should be resolved with significant ease.

To establish a pH gradient in the device, the ampholyte buffer pumping into one inlet (i.a in Figure 5.3) was pH adjusted to 5.0, while the ampholyte buffer pumping the other inlet (i.b in Figure 5.3) was pH adjusted to 2.5. Formation of a gradient was confirmed by a decrease in current, which dropped from 0.6-0.8 mA initially, to a minimum of 0.2 mA after a gradient was achieved. An electropherogram collected under IEF conditions is shown in Figure 5.6. With little optimization, glutamate (left) and aspartate (right) were nearly baseline resolved. The large labeling byproduct peak was not observed in the separation window and was likely carried off-chip, a significant

advantage to operating in this separation mode. To validate the utility of this method for *in vitro*-microdialysis applications, more characterization work needs to be done. Other amino acid standards should be run in conjunction with glutamate and aspartate to confirm separation. Separation conditions may also be adjusted to optimize the separation for baseline resolution of the analytes, enabling quantitation.

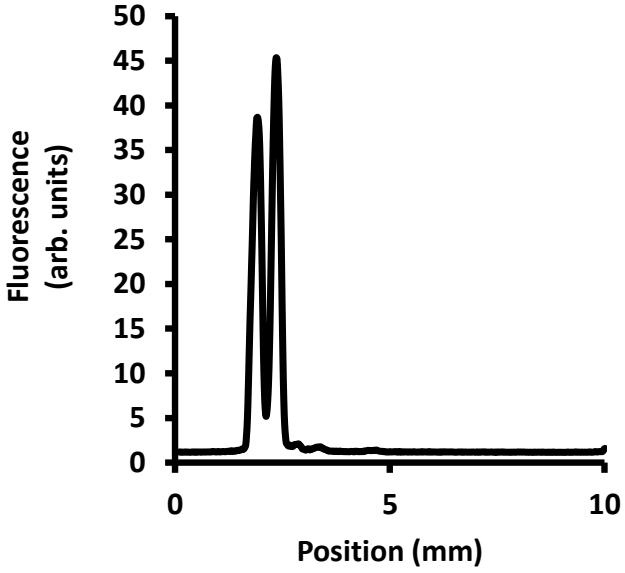

Figure 5.6. Electropherogram of offline-reacted glutamate and aspartate separated using IEF in a µFFE device. Glutamate (left) and aspartate (right) are nearly baseline resolved after little optimization.

5.4.3 Backpressure and Flow Regulation

The primary limitation in interfacing microdialysis with a continuous flow µFFE device is the production of excessive system backpressure. Closed electrophoretic systems inherently maintain some degree of internal pressure, however, inconsistent flow rates between microdialysis and µFFE platforms result in such a high backpressure that system components begin to fail. As the system was run, increasing internal pressure caused leaky fluidic connections and increased precipitate formation from the fluorescent labeling reaction. At times the severity backpressure became so significant that fluid was forced backwards through the capillary and microdialysis probe such that it was ultimately leaking out of the backside of the syringe. In these instances, the leak was physical evidence of the backpressure, though the signal was also indicating a problem.

During offline analysis the sample inlet stream was switched between the fluorescently labeled amines and non-fluorescent aCSF, a switch that should illicit an immediate drop-off in signal intensity. Figure 5.7A illustrates that when the system was experiencing a high degree of back pressure, the signal did demonstrate an initial drop (observable ~10 minutes), but instead of dropping to baseline levels the signal gradually dissipated for another 50 minutes. It is hypothesized that the signal didn't drop because the non-fluorescent solution was no longer being fully pumped into the chip. High system backpressure was causing issues with clogging, leaky fluidic connections, and backwards flow. As a result, the non-fluorescent solution was unable to reach the separation channel at full velocity and the fluorescent solution was never fully flushed out of the chip.

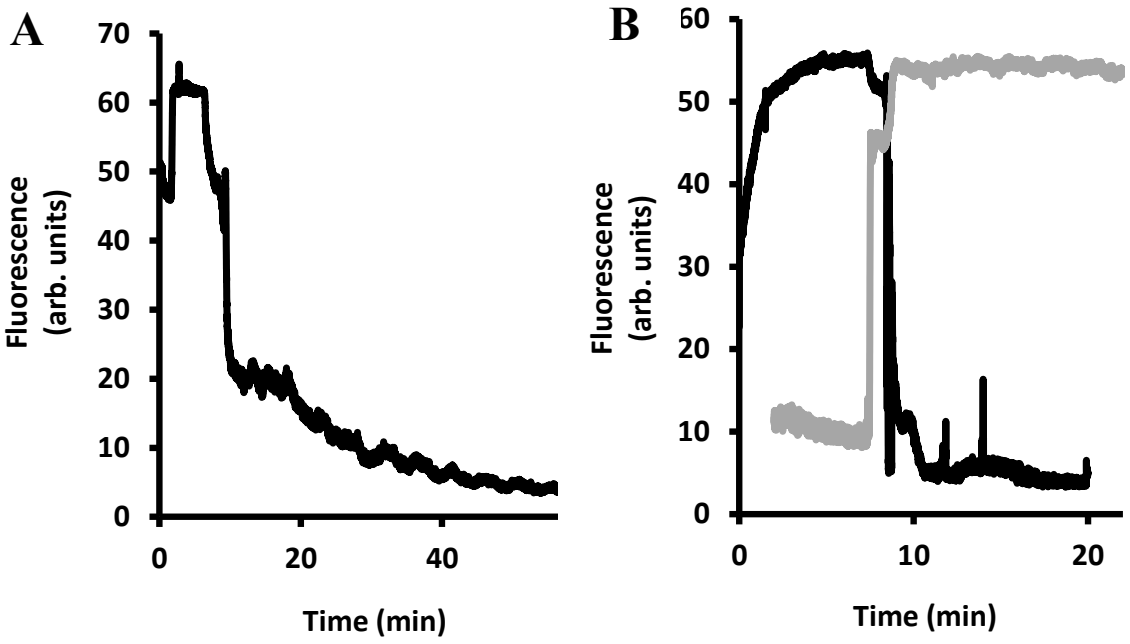

Figure 5.7. Fluorescence signal from offline derivatization syringe after being switched to borate (A) did not drop as immediately in fluorescence intensity as expected. This was the consequence of a faulty syringe and back-pressure issues in the instrument. Proper functioning of the instrument can be confirmed by immediate changes in signal intensity (B) when switching between fluorescent and non-fluorescent injection streams. This is observed both as a drop-off in signal intensity when switching from a fluorescent solution to aCSF (black) and as an increase in signal intensity when switching from aCSF to the injection of a fluorescent solution (gray).

Though the backpressure issue was never completely resolved, it was minimized by making several changes. First, only new and slightly used syringes were used. These syringes had significantly better contact between the plunger rod and internal syringe walls, limiting the ability of fluid to leak out in instances of high backpressure. Second, smaller inner diameter capillary (40 µm) was used to transport sample to the inlet capillary of the device. Though backpressure is typically increased by employing a narrower capillary, in this system it reduced backpressure by minimizing inconsistent flow rates between the microdialysis and µFFE platforms. The capillary channel etched into the µFFE device had an inner diameter of only 20 µm, while the carrier capillary transporting dialysate from the probe to the chip had an inner diameter of 75 µm. The decrease in inner diameter encountered at the junction of these two capillaries was compounded by the extra length of carrier capillary required to fluorescently label the dialysate and transport it into the chip. By switching to a smaller inner diameter carrier capillary (40 µm) the inconsistency between platforms was reduced and system backpressure lowered. It should be noted that formation of a byproduct precipitate in the labeling reaction prevented the routine use of capillaries with smaller inner diameters than 40 µm, simply because they would become clogged too quickly.

Taking these steps helped to reduce the backpressure, which was tested again by switching between fluorescent and non-fluorescent solutions. Figure 5.7B shows that after steps were taken to reduce back pressure, the signal demonstrated a nearly immediate drop, falling to basal levels (black) in 480 ms. Switching from a non-fluorescent to fluorescent solution, likewise exhibited an immediate change, causing an increase from basal levels to high fluorescence signal intensity (gray) in 150 ms.

Reducing backpressure enabled analysis of amino acid standards both offline and online, though the duration of experiments was limited to only 15-20 minutes, after which point either a capillary line became clogged or system backpressure became too severe. This window is too small to currently be compatible with *in vitro*-microdialysis experiments.

5.5 Conclusions

Microdialysis has been directly coupled to a µFFE device, enabling the continuous detection of glutamate and aspartate. Two separation modes were explored: zone electrophoresis and isoelectric focusing. While glutamate and aspartate could often be identified, they failed to ever be completely resolved from each other and other products of the labeling reaction in zone electrophoresis. Isoelectric focusing seems more promising. With little optimization, glutamate and aspartate were nearly baseline resolved from each other and the large labeling byproduct peak was carried off-chip. However, further characterization work needs to be done in this mode before application in *in vitro* studies. The primary limitation of this technique is currently system backpressure, the severity of which has limited analysis to 15-20 minute windows due to inconsistent flow streams. If system backpressure can be minimized, it is believed that µFFE will be capable of monitoring aspartate and glutamate with sub-second resolution as they are released from cultured cells.

5.6 Acknowledgements

Thank you to Matt Geiger for his work fabricating and operating the microfluidic device employed in this work.

Chapter 6

Summary and Future Outlook

6.1 Summary

Cell-based assays have long been used to obtain biochemical information while avoiding the inherent complications of *in vivo* systems including metabolism, obstructions, uptake/release mechanisms, and interferences.[162] Unfortunately, *in vitro* analysis is traditionally limited by several key factors. Fast analysis (sub-second resolution) is restricted to electroactive analytes, while analysis of non-electroactive analytes suffers from long temporal responses (5-10 minutes). Thus, *in vitro*-microdialysis offers a unique and novel approach offering insight that no existing model can provide. Non-electroactive analytes can be monitored on sub-minute (and possibly sub-second) timescales. Coupling this novel *in vitro* platform to an analytical method, capable of separating and quantitating the collected analytes simultaneously, has the ability to expose dynamics not previously attainable by existing methods. This work has described the development, characterization, and applications of *in vitro*-microdialysis.

In Chapter 2, we described the development of *in vitro*-microdialysis by culturing cells on the surface of a microdialysis probe. Analysis of the collected analytes was achieved by directly coupling the *in vitro*-microdialysis probe to a high-speed capillary electrophoresis (CE) instrument. Separation conditions were optimized resulting in an LOD ranging from 100-250 nM, depending on the analyte. Growth of cells was confirmed across the sampling region by collecting a series of fluorescent confocal images detailing the expansion of cells across the membrane surface over a period of 3 weeks. A potassium stimulation was administered to the cells by transferring the microdialysis probe from a solution of aCSF to a 100 mM K^+-spiked aCSF solution. The amino acid levels were within the detection limits of the system, allowing us to monitor

an increase in the relative abundance of these non-electroactive analytes with 20 second temporal resolution. This result was exciting and important because, to the best of our knowledge, simultaneous dynamic changes in an array of non-electroactive analyte release from cultured cells had never been previously recorded at this time scale. Our ability to make this measurement suggests the utility of *in vitro*-microdialysis in monitoring biological significant processes that are currently lost using other techniques.

In Chapter 3, further characterization efforts were made to better understand the influence of several parameters on the efficacy and accuracy of *in vitro*-microdialysis. We demonstrated that cell medium was cleared from the probe lumen after 10 minutes of perfusion. Therefore, it could be ruled out as having an influence on the intensity and duration of the observed signal. The composition of aCSF sustaining cells on an *in vitro* probe, after removal from culture flasks, was assessed by studying long-term viability of the cells in aCSF and buffered variants. Though several different buffered-aCSF systems were investigated, it was ultimately shown that cells survived as well in aCSF as they did in the buffered systems. Parameters influencing the microdialysis environment, specifically temperature and size of the containment, were also investigated. Both were found to have a substantial effect on signal intensity and release dynamics. When compared to basal and release levels collected at 37ºC, transferring a probe to a solution maintained at room temperature drastically lowered the signal intensity, demonstrating a need to perform experiments at biological temperatures. We also found that in smaller environments signal intensity was larger and release dynamics were prolonged, suggesting the occurrence of resampling. Understanding the effects of these variables will

be important when designing and analyzing future applications with *in vitro*-microdialysis.

In Chapter 4, we explored a variety of alternative physiological models for applications employing *in vitro*-microdialysis. Three types of individual cell lines were successfully cultured on the microdialysis probe: 3T3 fibroblasts, RBL-2HC fibroblasts, and C8-D1A astrocytes. Coverage and viability were assessed by imaging after exposing cells to fluorescein diacetate (FDA). Several co-cultures were also established on the probe. These included: 3T3-RBL, RBL-astrocyte, and astrocyte-neuron models. Presence of both cell types was confirmed using specific antibody labeling in conjunction with fluorescent confocal microscopy. The only cell type which failed to adhere was a primary line of human adipocytes. We believe that failure of these cells to adhere to the probe was due to the large size of the adipocytes (cell bodies upwards of 100 µm, which is nearly half the outer diameter of the microdialysis membrane). To date, large cell body size is the only known attribute of an adherent cell line that limits compatibility with *in vitro*-microdialysis. Identifying a variety of cell types and co-culture systems that are compatible with *in vitro*-microdialysis demonstrates the vast applicability of this sampling platform in biologically relevant studies.

In Chapter 5, we sought to further improve the speed at which we could monitor analytes by directly coupling the microdialysis probe to a micro free flow electrophoresis (µFFE) device. Both microdialysis and µFFE are continuous techniques, so direct coupling did not require any flow-segmenting mechanisms. We tried two different separation modes to tailor our separation for glutamate and aspartate: zone electrophoresis and isoelectric focusing. While glutamate and aspartate could often be

identified, they failed to ever be completely resolved from each other and other products of the labeling reaction in zone electrophoresis. Isoelectric focusing was more promising. With little optimization, glutamate and aspartate were nearly baseline resolved from each other and the large labeling byproduct peak was carried off-chip. However, difficulties with flow compatibility led to serious backpressure issues within the separation device. Our effectiveness in reducing the backpressure of the system was assessed by alternating between fluorescent and non-fluorescent sample inputs and observing the subsequent immediate and drastic change in signal intensity. Though we were successful in reducing the severity of backpressure, it continued to limit analysis times to 15-20 minutes. This time frame is too short to be currently compatible with *in vitro* studies. The prospect of monitoring non-electroactive analytes released from cells continuously is very exciting and holds undoubtable promise for providing new insights to biologically significant mechanisms.

6.2 Future Outlook

The future of *in vitro*-microdialysis is open to many possibilities, both technologically and towards application. The possibility of *in vitro*-microdialysis to provide new biological insights is incredibly promising. In Chapter 4, we demonstrated the compatibility of *in vitro*-microdialysis with a variety of different physiological models. Our findings show that any adherent immortalized cell line with cell bodies of approximately 50 µm and smaller, can be cultured on the surface of a microdialysis probe. In Chapter 4, we suggest how *in vitro*-microdialysis can be used with the employed cell line to offer new and physiological insights. Establishing a co-culture on

the exterior of the probe allows for investigation into the mechanisms of communication and activation between the employed cell types. This could be applied to mast cells and astrocytes, where the release of mediators from mast cells in the presence of astrocytes are believed to result in dual-activation of both cell types, leading to a cascade of inflammatory agents exchanged between the cells as they are involved in an inflammatory response. Or, it could be used to investigate whether one of the mechanisms by which astrocytes interact with neurons is through the efflux of astrocytic intracellular Ca^{2+} into gap junctions, where it is then taken up by neurons. Though this is a difficult question to answer with traditional techniques, *in vitro*-microdialysis offers a straight forward solution. Briefly, a pharmacological blockage of gap junctions in the neuron-astrocyte co-culture could be performed by exposing the probe to a solution containing one of several gap junction inhibitors (octanol, sodium propionate, and halothane), and the subsequent change in abundance of transmitters could be monitored with high-speed capillary electrophoresis, offering temporal insights to this previously elusive pathway.

The aforementioned applications are merely suggestions of how *in vitro*-microdialysis could be used with exterior co-culture models we know to be compatible with the probe. If a physically-blocked co-culture model is successfully developed, another area of applications could be unlocked. As an example, we suggest that such a model could be used to assess whether physical contact between airway smooth muscle (ASM) and mast cells is a necessary component of this interaction, or if chemical contact is all that is required for the interactions to take place. The applicability of *in vitro*-

microdialysis is not limited to these models; rather, they demonstrate the possibility of widespread application of this technique.

The other primary direction for the future of *in vitro*-microdialysis is with technical advancements. As analytical chemists, we are constantly pushing our techniques to run faster at smaller levels. Such a drive has led to a recent expansion of microfluidics. In Chapter 5, we demonstrated the utility of *in vitro*-microdialysis for monitoring glutamate and aspartate release continuously by coupling the probe to a μFFE device. Despite our advances in joining these techniques, difficulties with high system backpressure limited our ability to use the technique *in vitro*. We suggest that a new device be fabricated with a larger inlet capillary and separation channel. This can be achieved by etching deeper structures during the fabrication process, 40 μm instead of the previous depth of 20 μm. By increasing the size of the inlet capillary and separation channel, we can use a larger inner diameter capillary (40 μm) matching the diameter of the capillaries used on the microdialysis end; a change we believe would aid in the reduction of backpressure generated when a 40 μm capillary is connected to a 20 μm capillary leading into the device. Addressing system backpressure, in this manner or another, will be critical prior to the application of this technique towards *in vitro* samples.

Whether it is by pushing the capabilities of the technique or by using it to study biological mechanisms, it is my hope that the utility of *in vitro*-microdialysis continue to be recognized. As we hone the ability to monitor the elusive non-electroactive analytes on more meaningful timescales, the true nature of their role in regulatory and communicative pathways can be identified. I am thankful to have worked on a project that was so engaging, collaborative, and providing of many different directions.

References

1. Parsons, L. H.; Justice, J. B., *Crit. Rev. Neurobiol.* **1994,** *8* (3), 189-220.
2. Davies, M. I., *Anal. Chim. Acta* **1999,** *379* (3), 227-249.
3. Bal-Price, A. K.; Sunol, C.; Weiss, D. G.; van Vliet, E.; Westerink, R. H. S.; Costa, L. G., *Neurotoxicology* **2008,** *29* (3), 520-531.
4. Westerink, B. H. C.; Damsma, G.; Rollema, H.; Devries, J. B.; Horn, A. S., *Life Sci.* **1987,** *41* (15), 1763-1776.
5. Andren, P. E.; Caprioli, R. M., *J. Mass Spectrom.* **1995,** *30* (6), 817-824.
6. Lindekens, N.; Smolders, I.; Khan, G. M.; Bialer, M.; Ebinger, G.; Michotte, Y., *Pharm. Res.* **2000,** *17* (11), 1408-1413.
7. Smolders, I.; Khan, G. M.; Lindekens, H.; Prikken, S.; Marvin, C. A.; Manil, J.; Ebinger, G.; Michotte, Y., *J. Pharmacol. Exp. Ther.* **1997,** *283* (3), 1239-1248.
8. Church, J., *Journal of Physiology-London* **1992,** *455*, 51-71.
9. Westerink, R. H. S., *Neurotoxicology* **2013,** *39*, 169-172.
10. Khan, S. N. H.; Shuaib, A., *Methods* **2001,** *23* (1), 3-9.
11. Davies, M. I.; Lunte, C. E., *Chem. Soc. Rev.* **1997,** *26* (3), 215-222.
12. Kennedy, R. T.; Wang, M.; Slaney, T.; Mabrouk, O., *Journal of Neuroscience Methods* **2010,** *190* (1), 39-48.
13. Kennedy, R. T.; Bowser, M. T., *Electrophoresis* **2001,** *22* (17), 3668-3676.
14. Lada, M. W.; Vickroy, T. W.; Kennedy, R. T., *Anal. Chem.* **1997,** *69* (22), 4560-4565.
15. Kast, B., *Nature* **2001,** *412* (6848), 674-676.
16. Fonslow, B. R.; Barocas, V. H.; Bowser, M. T., *Anal. Chem.* **2006,** *78* (15), 5369-5374.
17. Walker, M. E.; Hatfield, J. K.; Brown, M. A., *Biochimica Et Biophysica Acta-Molecular Basis of Disease* **2012,** *1822* (1), 57-65.
18. Fonslow, B. R.; Bowser, M. T., *Anal. Chem.* **2008,** *80* (9), 3182-3189.
19. Fonslow, B. R.; Bowser, M. T., *Anal. Chem.* **2006,** *78* (24), 8236-8244.
20. Jones, E. V.; Cook, D.; Murai, K. K., *Astrocytes: Methods and Protocols* **2012,** *814*, 341-352.
21. Lunte, S. M.; Nandi, P., *Anal. Chim. Acta* **2009,** *651* (1), 1-14.
22. Ungerstedt, U., Marsden, C. A., Ed. John Wiley & Sons: New York, 1984; pp 81-105.
23. Bungay, P. M.; Morrison, P. F.; Dedrick, R. L., *Life Sci.* **1990,** *46* (2), 105-119.
24. Hsiao, J. K.; Ball, B. A.; Morrison, P. F.; Mefford, I. N.; Bungay, P. M., *J. Neurochem.* **1990,** *54* (4), 1449-1452.
25. Chaurasia, C. S., *Biomed. Chromatogr.* **1999,** *13* (5), 317-332.
26. Jennifer L. Peters, H. Y., Adrian C. Michael, *Anal. Chim. Acta* **2000,** *412*, 1-12.
27. Song, Y.; Lunte, C. E., *Anal. Chim. Acta* **1999,** *379* (3), 251-262.
28. Zhou, S. Y.; Zuo, H.; Stobaugh, J. F.; Lunte, C. E.; Lunte, S. M., *Anal. Chem.* **1995,** *67* (3), 594-599.
29. Hogan, B. L.; Lunte, S. M.; Stobaugh, J. F.; Lunte, C. E., *Anal. Chem.* **1994,** *66* (5), 596-602.
30. Jensen, S. M.; Hansen, H. S.; Johansen, T.; Malmlof, K., *J. Pharm. Biomed. Anal.* **2007,** *43* (5), 1751-1756.
31. Sato, N.; Takeda, S.; Ikimura, K.; Nishino, H.; Rakugi, H.; Morishita, R., *Neuroscience* **2011,** *186*, 110-119.
32. Lada, M. W.; Schaller, G.; Carriger, M. H.; Vickroy, T. W.; Kennedy, R. T., *Anal. Chim. Acta* **1995,** *307* (2-3), 217-225.
33. Cano-Cebrian, M. J.; Zornoza, T.; Polache, A.; Granero, L., *Curr. Drug Metab.* **2005,** *6* (2), 83-90.

34. Michael, A. C.; Yang, H.; Peters, J. L.; Allen, C.; Chern, S. S.; Coalson, R. D., *Anal. Chem.* **2000,** *72* (9), 2042-2049.
35. Stahle, L., *Adv. Drug Del. Rev.* **2000,** *45* (2-3), 149-167.
36. Lonnroth, P.; Jansson, P. A.; Smith, U., *Am. J. Physiol.* **1987,** *253* (2), E228-E231.
37. Stahle, L.; Arner, P.; Ungerstedt, U., *Life Sci.* **1991,** *49* (24), 1853-1858.
38. Brunner, M.; Derendorf, H., *Trac-Trends in Analytical Chemistry* **2006,** *25* (7), 674-680.
39. Connelly, C. A., *Journal of Physiology-London* **1999,** *514* (2), 303-303.
40. Wang, M.; Roman, G. T.; Perry, M. L.; Kennedy, R. T., *Anal. Chem.* **2009,** *81* (21), 9072-9078.
41. Wages, S. A.; Church, W. H.; Justice, J. B., *Anal. Chem.* **1986,** *58* (8), 1649-1656.
42. Chen, A. Q.; Lunte, C. E., *J. Chromatogr. A* **1995,** *691* (1-2), 29-35.
43. Caprioli, R. M.; Lin, S. N., *Proc. Natl. Acad. Sci. U. S. A.* **1990,** *87* (1), 240-243.
44. Lin, S. N.; Slopis, J. M.; Butler, I. J.; Caprioli, R. M., *J. Neurosci. Methods* **1995,** *62* (1-2), 199-205.
45. Mao, L. Q.; Zhang, M. N., *Front. Biosci.* **2005,** *10*, 345-352.
46. Berners, M. O. M.; Boutelle, M. G.; Fillenz, M., *Anal. Chem.* **1994,** *66* (13), 2017-2021.
47. Miele, M.; Berners, M.; Boutelle, M. G.; Kusakabe, H.; Fillenz, M., *Brain Res.* **1996,** *707* (1), 131-133.
48. Maidment, N. T.; Brumbaugh, D. R.; Rudolph, V. D.; Erdelyi, E.; Evans, C. J., *Neuroscience* **1989,** *33* (3), 549-557.
49. Lunte, S. M.; Huynh, B. H.; Fogarty, B. A.; Martin, R. S., *Anal. Chem.* **2004,** *76* (21), 6440-6447.
50. Kennedy, R. T.; Sandlin, Z. D.; Shou, M. S.; Shackman, J. G., *Anal. Chem.* **2005,** *77* (23), 7702-7708.
51. Oshea, T. J.; Teltingdiaz, M. W.; Lunte, S. M.; Lunte, C. E.; Smyth, M. R., *Electroanalysis* **1992,** *4* (4), 463-468.
52. Oshea, T. J.; Weber, P. L.; Bammel, B. P.; Lunte, C. E.; Lunte, S. M.; Smyth, M. R., *J. Chromatogr.* **1992,** *608* (1-2), 189-195.
53. Tellez, S.; Forges, N.; Roussin, A.; Hernandez, L., *Journal of Chromatography-Biomedical Applications* **1992,** *581* (2), 257-266.
54. Lemmo, A. V.; Jorgenson, J. W., *Anal. Chem.* **1993,** *65* (11), 1576-1581.
55. Hooker, T. F.; Jorgenson, J. W., *Anal. Chem.* **1997,** *69* (20), 4134-4142.
56. Lunte, S. M.; Zhou, J. X.; Heckert, D. M.; Zuo, H.; Lunte, C. E., *Anal. Chim. Acta* **1999,** *379* (3), 307-317.
57. Lada, M. W.; Kennedy, R. T., *J. Neurosci. Methods* **1997,** *72* (2), 153-159.
58. Kennedy, R. T.; Li, Q.; Zubieta, J. K., *Anal. Chem.* **2009,** *81* (6), 2242-2250.
59. Kennedy, R. T.; Wang, M.; Roman, G. T.; Perry, M. L., *Anal. Chem.* **2009,** *81* (21), 9072-9078.
60. Lada, M. W.; Kennedy, R. T., *Anal. Chem.* **1996,** *68* (17), 2790-2797.
61. Kennedy, R. T.; Lada, M. W.; Vickroy, T. W., *J. Neurochem.* **1998,** *70* (2), 617-625.
62. Ewing, A. G.; MacTaylor, C. E., *Electrophoresis* **1997,** *18* (12-13), 2279-2290.
63. Colyer, C., *Cell Biochem. Biophys.* **2000,** *33* (3), 323-337.
64. Lingeman, H.; Bardelmeijer, H. A.; de Ruiter, C.; Underberg, W. J. M., *J. Chromatogr. A* **1998,** *807* (1), 3-26.
65. Underberg, W. J. M.; Waterval, J. C. M., *Electrophoresis* **2002,** *23* (22-23), 3922-3933.
66. Molnar-Perl, I.; Vasanits, A., *J. Chromatogr. A* **1999,** *835* (1-2), 73-91.
67. Bowser, M. T.; Klinker, C. C., *Anal. Chem.* **2007,** *79* (22), 8747-8754.
68. Chen, D. Y.; Adelhelm, K.; Cheng, X. L.; Dovichi, N. J., *Analyst* **1994,** *119* (2), 349-352.

69. Dovichi, N. J.; Swerdlow, H.; Zhang, J. Z.; Chen, D. Y.; Harke, H. R.; Grey, R.; Wu, S. L.; Fuller, C., *Anal. Chem.* **1991,** *63* (24), 2835-2841.
70. Nimmerjahn, A., *Journal of Physiology-London* **2009,** *587* (8), 1639-1647.
71. Dienel, G. A.; Cruz, N. F.; Ball, K. K., *Asn Neuro* **2010,** *2* (4).
72. Kielian, T.; Karpuk, N.; Burkovetskaya, M.; Fritz, T.; Angle, A., *J. Neurosci.* **2011,** *31* (2), 414-425.
73. Matteoli, M.; Montana, V.; Malarkey, E. B.; Verderio, C.; Parpura, V., *Glia* **2006,** *54* (7), 700-715.
74. Bergles, D. E.; Tritsch, N. X., *Neuron* **2007,** *54* (4), 497-500.
75. Cornellbell, A. H.; Finkbeiner, S. M.; Cooper, M. S.; Smith, S. J., *Science* **1990,** *247* (4941), 470-473.
76. Parpura, V.; Basarsky, T. A.; Liu, F.; Jeftinija, K.; Jeftinija, S.; Haydon, P. G., *Nature* **1994,** *369* (6483), 744-747.
77. Porter, J. T.; McCarthy, K. D., *Prog. Neurobiol.* **1997,** *51* (4), 439-455.
78. Nedergaard, M.; Wang, X. H.; Lou, N. H.; Xu, Q. W.; Tian, G. F.; Peng, W. G.; Han, X. N.; Kang, J.; Takano, T., *Nat. Neurosci.* **2006,** *9* (6), 816-823.
79. Fiacco, T. A.; Agulhon, C.; McCarthy, K. D., *Annu. Rev. Pharmacol. Toxicol.* **2009,** *49*, 151-174.
80. Holy, T. E.; Holekamp, T. F.; Turaga, D., *Neuron* **2008,** *57* (5), 661-672.
81. Dienel, G. A.; Gandhi, G. K.; Cruz, N. F.; Ball, K. K.; Theus, S. A., *J. Neurochem.* **2009,** *110* (3), 857-869.
82. Oheim, M.; Li, D. D.; Herault, K.; Ropert, N., *Proc. Natl. Acad. Sci. U. S. A.* **2009,** *106* (51), 21960-21965.
83. Haydon, P. G.; Araque, A.; Parpura, V.; Sanzgiri, R. P., *Eur. J. Neurosci.* **1998,** *10* (6), 2129-2142.
84. Kawagoe, K. T.; Wightman, R. M., *Talanta* **1994,** *41* (6), 865-874.
85. Marszalek, P. E.; Markin, V. S.; Tanaka, T.; Kawaguchi, H.; Fernandez, J. M., *Biophys. J.* **1995,** *69* (4), 1218-1229.
86. Day, N. C.; Williams, T. L.; Ince, P. G.; Kamboj, R. K.; Lodge, D.; Shaw, P. J., *Mol. Brain Res.* **1995,** *31* (1-2), 17-32.
87. Spreafico, R.; Frassoni, C.; Arcelli, P.; Battaglia, G.; Wenthold, R. J.; Debiasi, S., *Dev. Brain Res.* **1994,** *82* (1-2), 231-244.
88. Weihong Tan, P. G. H., and Edward S. Yeung, *Appl. Spectrosc.* **1997,** *51* (8), 1139-1143.
89. Dmitri A. Rusakov, K. Z., and Christian Henneberger, *Neuroscientist* **2011,** *20* (10), 1-11.
90. Mothet, J. P.; Pollegioni, L.; Ouanounou, G.; Martineau, M.; Fossier, P.; Baux, G., *Proc. Natl. Acad. Sci. U. S. A.* **2005,** *102* (15), 5606-5611.
91. Tan, S. J.; Jana, N. R.; Gao, S. J.; Patra, P. K.; Ying, J. Y., *Chemistry of Materials* **2010,** *22* (7), 2239-2247.
92. Pasantesmorales, H.; Chacon, E.; Murray, R. A.; Moran, J., *J. Neurosci. Res.* **1994,** *37* (6), 720-727.
93. Huang, Y. X.; Cai, D.; Chen, P., *Analytical Chemistry* **2011,** *83* (12), 4393-4406.
94. Nedergaard, M.; Verkhratsky, A., *Glia* **2012,** *60* (7), 1013-1023.
95. McCarthy, K. D.; Agulhon, C.; Petravicz, J.; McMullen, A. B.; Sweger, E. J.; Minton, S. K.; Taves, S. R.; Casper, K. B.; Fiacco, T. A., *Neuron* **2008,** *59* (6), 932-946.
96. Hamilton, N. B.; Attwell, D., *Nature Reviews Neuroscience* **2010,** *11* (4), 227-238.
97. Bowser, M. T.; Ciriacks, C. M., *Anal. Chem.* **2004,** *76* (22), 6582-6587.
98. Alliot, F.; Pessac, B., *Brain Res.* **1984,** *106* (1-2), 283-291.
99. Kennedy, R. T.; Shackman, J. G.; Watson, C. J., *J. Chromatogr. A* **2004,** *1040* (2), 273-282.

100. Plock, N.; Kloft, C., *Eur. J. Pharm. Sci.* **2005,** *25* (1), 1-24.
101. Thomas, D. H.; Rob, A.; Rice, D. W., *Protein Eng* **1989,** *2* (6), 489-491.
102. Cambier, D.; Pessac, B., *J. Neurochem.* **1987,** *49* (3), 802-805.
103. Barcelo-Rico, F.; Bondia, J.; Diez, J. L.; Rossetti, P., *Diabetes Technol. Ther.* **2012,** *14* (1), 74-82.
104. Draberova, E.; D'Agostino, L.; Caracciolo, V.; Sladkova, V.; Sulimenko, T.; Sulimenko, V.; Sobol, M.; Maounis, N. F.; Tzelepis, E.; Mahera, E.; Kren, L.; Legido, A.; Giordano, A.; Mork, S.; Hozak, P.; Draber, P.; Katsetos, C. D., *J. Neuropathol. Exp. Neurol.* **2015,** *74* (7), 723-742.
105. Abdullaev, I. F.; Rudkouskaya, A.; Schools, G. P.; Kimelberg, H. K.; Mongin, A. A., *Journal of Physiology-London* **2006,** *572* (3), 677-689.
106. Kaul, A.; Toonen, J. A.; Cimino, P. J.; Gianino, S. M.; Gutmann, D. H., *Neuro Oncol.* **2015,** *17* (6), 843-853.
107. Esposito, E.; Paterniti, I.; Mazzon, E.; Genovese, T.; Di Paola, R.; Galuppo, M.; Cuzzocrea, S., *Brain Behavior and Immunity* **2011,** *25* (6), 1099-1112.
108. Nandi, P.; Lunte, S. M., *Anal. Chim. Acta* **2009,** *651* (1), 1-14.
109. Kalivas, P. W., *Behav. Pharmacol.* **1996,** *7* (7), 658-660.
110. DiChiara, G.; Tanda, G.; Carboni, E., *Behav. Pharmacol.* **1996,** *7* (7), 640-657.
111. Presti, M. F.; Watson, C. J.; Kennedy, R. T.; Yang, M.; Lewis, M. H., *Pharmacol. Biochem. Behav.* **2004,** *77* (3), 501-507.
112. Ash, K. D.; Schumann, R. L.; Bowser, G. C., *Weather Clim Soc* **2014,** *6* (1), 104-118.
113. Stenken, J. A.; Church, M. K.; Gill, C. A.; Clough, G. F., *Aaps J* **2010,** *12* (1), 73-78.
114. Chen, K. C.; Hoistad, M.; Kehr, J.; Fuxe, K.; Nicholson, C., *J. Neurochem.* **2002,** *81* (1), 108-121.
115. Kobayashi, S., *Prog. Neurobiol.* **1989,** *32* (2), 103-135.
116. Sgaragli, G. P.; Palmi, M., Oja, S. S.; Ahter, L.; Kontro, P.; Paasonen, M. K., Eds. Alan R. Liss: New York, 1985; pp 343-357.
117. Hruska, R. E.; Thut, P. D.; Huxtable, R. J.; Bressier, B. L., Huxtable, R.; Barbeau, A., Eds. Raven: New York, 1976; pp 347-356.
118. Molchanova, S. M.; Oja, S. S.; Sa, P., *Taurine 6* **2006**, 365-372.
119. Hanretta, A. T.; Lombardini, J. B., *The Biology of Taurine: Methods and Mechanisms* **1986**, 307-317.
120. Tigges, G. A.; Philibert, R. A.; Dutton, G. R., *Neurosci. Lett.* **1990,** *119*, 23-26.
121. Pasantesmorales, H.; Moran, J.; Schousboe, A., *Glia* **1990,** *3* (5), 427-432.
122. Price, P. B.; Sowers, T., *Proc. Natl. Acad. Sci. U. S. A.* **2004,** *101* (13), 4631-4636.
123. Clarke, A., *Funct. Ecol.* **2004,** *18* (2), 252-256.
124. Gillooly, J. F.; Brown, J. H.; West, G. B.; Savage, V. M.; Charnov, E. L., *Science* **2001,** *293* (5538), 2248-2251.
125. Chefer, V. I.; Thompson, A. C.; Zapata, A.; Shippenberg, T. S., *Curr. Protoc. Neurosci.* **2009,** *Chapter 7*, Unit7 1.
126. Sam, P. M.; Justice, J. B., *Anal. Chem.* **1996,** *68* (5), 724-728.
127. Theoharides, T. C.; Alysandratos, K. D.; Angelidou, A.; Delivanis, D. A.; Sismanopoulos, N.; Zhang, B.; Asadi, S.; Vasiadi, M.; Went, Z.; Miniati, A.; Kalogeromitros, D., *Molecular Basis of Disease* **2012,** *1822* (1), 21-33.
128. Passante, E.; Ehrhardt, C.; Sheridan, H.; Frankish, N., *Inflamm. Res.* **2009,** *58* (9), 611-618.
129. Davidson, M. W. *Optical Microscopy Primer: Human Cortical Neuronal Cells (HCN-1A Line)* [Online], 2004.

130. Zhang, Z. Y.; Drzewiecki, G. J.; Hom, J. T.; May, P. C.; Hyslop, P. A., *Neurosci. Lett.* **1994,** *177* (1-2), 162-164.
131. Pope, A., *Dynamic Properties of Glial Cells* **1978**, 13-20.
132. Shi, M. J.; Majumdar, D.; Gao, Y. D.; Brewer, B. M.; Goodwin, C. R.; McLean, J. A.; Lib, D.; Webb, D. J., *Lab Chip* **2013,** *13* (15), 3008-3021.
133. Brightling, C.; Bradding, P., *Clin. Exp. Allergy* **2003,** *33* (8), 1165-1165.
134. Bradding, P.; Cruse, G., *Eur. Respir. J.* **2005,** *26* (4), 745-746.
135. Page, S.; Ammit, A. J.; Black, J. L.; Armour, C. L., *American Journal of Physiology-Lung Cellular and Molecular Physiology* **2001,** *281* (6), L1313-L1323.
136. Brightling, C. E.; Bradding, P.; Symon, F. A.; Holgate, S. T.; Wardlaw, A. J.; Pavord, I. D., *N. Engl. J. Med.* **2002,** *346* (22), 1699-1705.
137. West, A. R.; Zaman, N.; Cole, D. J.; Walker, M. J.; Legant, W. R.; Boudou, T.; Chen, C. S.; Favreau, J. T.; Gaudette, G. R.; Cowley, E. A.; Maksym, G. N., *American Journal of Physiology-Lung Cellular and Molecular Physiology* **2013,** *304* (1), L4-L16.
138. Seeldrayers, P. A.; Levin, L. A.; Johnson, D., *J. Neuroimmunol.* **1992,** *36* (2-3), 239-243.
139. Kim, D. Y.; Jeoung, D.; Ro, J. Y., *J. Immunol.* **2010,** *185* (1), 273-283.
140. Belanger, M.; Allaman, I.; Magistretti, P. J., *Cell Metab* **2011,** *14* (6), 724-738.
141. Blackburn, D.; Sargsyan, S.; Monk, P. N.; Shaw, P. J., *Glia* **2009,** *57* (12), 1251-1264.
142. Ricci, G.; Volpi, L.; Pasquali, L.; Petrozzi, L.; Siciliano, G., *J. Biol. Phys.* **2009,** *35* (4), 317-336.
143. Kimelberg, H. K.; Nedergaard, M., *Neurotherapeutics* **2010,** *7* (4), 338-353.
144. Kimelberg, H. K.; Norenberg, M. D., *Sci. Am.* **1989,** *260* (4), 66-&.
145. Hassinger, T. D.; Guthrie, P. B.; Atkinson, P. B.; Bennett, M. V. L.; Kater, S. B., *Proc. Natl. Acad. Sci. U. S. A.* **1996,** *93* (23), 13268-13273.
146. Dani, J. W.; Chernjavsky, A.; Smith, S. J., *Neuron* **1992,** *8* (3), 429-440.
147. Fujita, K.; Nakanishi, K.; Sobue, K.; Ueki, T.; Asai, K.; Kato, T., *Neurochem. Int.* **1998,** *33* (1), 41-49.
148. Wang, M.; Hershey, N. D.; Mabrouk, O. S.; Kennedy, R. T., *Anal. Bioanal. Chem.* **2011,** *400* (7), 2013-2023.
149. Kohlheyer, D.; Eijkel, J. C. T.; van den Berg, A.; Schasfoort, R. B. M., *Electrophoresis* **2008,** *29* (5), 977-993.
150. Kuhn, R.; Wagner, H., *J. Chromatogr.* **1989,** *481*, 343-351.
151. Kuhn, R.; Wagner, H., *Electrophoresis* **1989,** *10* (3), 165-172.
152. Wagner, H., *Nature* **1989,** *341*, 669-670.
153. Raymond, D. E.; Manz, A.; Widmer, H. M., *Anal. Chem.* **1994,** *66* (18), 2858-2865.
154. Raymond, D. E.; Manz, A.; Widmer, H. M., *Anal. Chem.* **1996,** *68* (15), 2515-2522.
155. Manz, A.; Eijkel, J. C. T., *Pure Appl. Chem.* **2001,** *73* (10), 1555-1561.
156. Turgeon, R. T.; Bowser, M. T., *Anal. Bioanal. Chem.* **2009,** *394* (1), 187-198.
157. Fonslow, B. R.; Bowser, M. T., *Anal. Chem.* **2005,** *77* (17), 5706-5710.
158. Geiger, M.; Frost, N. W.; Bowser, M. T., *Anal. Chem.* **2014,** *86* (10), 5136-5142.
159. Frost, N. W.; Bowser, M. T., *Lab Chip* **2010,** *10* (10), 1231-1236.
160. Horka, M.; Willimann, T.; Blum, M.; Nording, P.; Friedl, Z.; Slais, K., *J. Chromatogr. A* **2001,** *916* (1-2), 65-71.
161. Kohlheyer, D.; Eijkel, J. C. T.; Schlautmann, S.; van den Berg, A.; Schasfoort, R. B. M., *Anal. Chem.* **2007,** *79* (21), 8190-8198.
162. Siegel, G. J., *Basic Neurochemistry: Molecular, Cellular, and Medical Aspects*. Seventh ed.; Elsevier Academic Press Canada, 2006.